Microtubules tune mechanosensitive cell responses

Shailaja Seetharaman, Benoit Vianay, Vanessa Roca, Aaron Farrugia, Chiara de Pascalis, Batiste Boëda, Florent Dingli, Damarys Loew, Stepĥane Vassilopoulos, Alexander Bershadsky, et al.

Microtubules tune mechanosensitive cell responses

Shailaja Seetharaman[1, 2], Benoit Vianay[3], Vanessa Roca[1], Aaron Farrugia[4], Chiara De Pascalis[1], Batiste Boëda[1], Florent Dingli[5], Damarys Loew[5], Stéphane Vassilopoulos[6], Alexander Bershadsky[4], Manuel Théry[3], Sandrine Etienne-Manneville[1*]

[1] Cell Polarity, Migration and Cancer Unit, Institut Pasteur, UMR3691 CNRS, Equipe Labellisée Ligue Contre le Cancer, F-75015, Paris, France.

[2] Université Paris Descartes, Sorbonne Paris Cité, 12 Rue de l'École de Médecine, 75006 Paris, France.

[3] Paris University, INSERM, CEA, Hôpital Saint Louis, Institut Universitaire d'Hematologie, Paris, France.

[4] Mechanobiology Institute, National University of Singapore, T-lab, 5A Engineering Drive 1, Singapore, 117411, Singapore.

[5] Institut Curie, PSL Research University, Centre de Recherche, Laboratoire de Spectrométrie de Masse Protéomique, 26 rue d'Ulm, Paris 75248 Cedex 05, France.

[6] Sorbonne Université, INSERM UMRS 974, Institute of Myology, Paris, France.

*Correspondence: setienne@pasteur.fr

Abstract

Mechanotransduction is a process by which cells sense the mechanical properties of their surrounding environment, and adapt accordingly to perform cellular functions such as adhesion, migration and differentiation. Integrin-mediated focal adhesions are major sites of mechanotransduction, and their connection with the actomyosin network is crucial for mechanosensing as well as the generation and transmission of forces onto the substrate. Despite having emerged as major regulators of cell adhesion and migration, the contribution of microtubules to mechanotransduction still remains elusive. Here, we show that Talin- and actomyosin-dependent mechanosensing of substrate rigidity controls microtubule acetylation (a tubulin post-translational modification) by promoting the recruitment of alpha-tubulin acetyl transferase (αTAT1) to focal adhesions. Microtubule acetylation tunes mechanosensitivity of focal adhesions and YAP translocation, and in turn, promotes GEF-H1-mediated RhoA activation, actomyosin contractility, and traction forces. Our results reveal a fundamental crosstalk between microtubules and actin in mechanotransduction that contributes to mechanosensitive cell adhesion and migration.

Main

Cells sense the physical properties of their environment, translate them into biochemical signals and adapt their behaviour accordingly. This process known as mechanotransduction is crucial during development and in the adult, during physiological and pathological conditions such as cell migration, wound healing and cancer[1,2]. Integrin-mediated focal adhesions (FAs) sense the matrix rigidity, control the generation of actomyosin-dependent forces and the transmission of these traction forces onto the substrate as well as contribute to mechanosensitive cell responses such as migration[3,4]. In addition to the actin cytoskeleton, microtubules are also key regulators of 2D and 3D cell migration[5-8]. Several studies have demonstrated the role of the actomyosin cytoskeleton and FAs in mechanotransduction;

however, very little is known about microtubules in this context. In this study, we used primary rat astrocytes and primary human umbilical vein endothelial cells (HUVECs) (both types of cells are dependent on efficient microtubule dynamics for migration or invasion[9-13]), to address the role of microtubules in rigidity sensing and mechanosensitive migration.

The crucial factors affecting the functions of the microtubule network are post-translational modifications (PTMs) of tubulin such as acetylation, which occurs at the K40 residue of α-tubulin. The enzyme responsible for microtubule acetylation, αTAT1 (α-tubulin acetyltransferase 1, also called as MEC-17), is present in the lumen of microtubules[14] and is highly specific to α-tubulin K40. On the other hand, the enzymes involved in deacetylation at K40 are histone deacetylase family member 6 (HDAC6) and sirtuin type 2 (Sirt2), both of which target other substrates as well[15]. In this study, we used previously characterized siRNAs targeting αTAT1[13] (set 1: siαTAT1-1 and set 2: siαTAT1-2; Extended Data Fig. 1a, 1b and 1c) to decrease acetylation, and Tubacin (Extended Data Fig. 1a and 1c), a drug which increases microtubule acetylation by inhibiting HDAC6 without modifying the acetylation of other HDAC6 substrates such as histones[16,17].

Substrate rigidity promotes microtubule acetylation through integrin β_1 signalling

We have previously shown that microtubules come in close proximity to FAs, and that microtubule acetylation promotes FA turnover during migration[13]. Since FAs are major mechanosensitive structures[18], we investigated whether the extracellular matrix rigidity affects microtubule acetylation. Astrocytes were plated sparsely on polyacrylamide hydrogels of different rigidities: 1.26 kPa, 2 kPa, 9 kPa and 48 kPa (Fig. 1a and 1b). Astrocytes on soft substrates exhibited lower levels of acetylated tubulin than cells on stiff substrates (Fig. 1a and 1b). Tubulin acetylation levels showed a two fold increase with increasing rigidity (1.26 kPa to 48 kPa), a strongly significant change in comparison to the

maximal 3.8 fold increase obtained after Tubacin treatment (Extended Data Fig. 1d). Subsequently, to determine whether microtubule acetylation may be indirectly caused by a mechanism involving differential cell spreading, we plated astrocytes on adhesive micropatterns (area 2500 μm^2) printed on 2 kPa and 40 kPa hydrogels (Extended Data Fig. 1e). Similar to stiff substrates, astrocytes on soft substrates adopted a crossbow shape and identical spread area, and yet, microtubule acetylation was increased on stiff substrates as compared to softer substrates (Extended Data Fig. 1e). In contrast to tubulin acetylation, tubulin detyrosination (another tubulin PTM), remained unaffected by increased substrate rigidity in astrocytes (Extended Data Fig. 1f and 1g), and had no effect on astrocyte adhesion and migration[13], suggesting that rigidity sensing specifically affects microtubule acetylation.

Integrin-based FAs sense the matrix rigidity and trigger mechanosensitive signalling pathways[19]. To determine the role of integrin signalling in controlling microtubule acetylation, we first used a scratch-induced migration assay to trigger integrin activation at the wound edge[11]. Addition of cyclic RGD (cRGD) peptide, to prevent the binding of integrins to the RGD motif of extracellular matrix proteins, reduced tubulin acetylation (Extended Data Fig. 2a). Furthermore, integrin activation using $MnCl_2$ [20] led to an increase in microtubule acetylation as compared to control cells (Extended Data Fig. 2b). Finally, depletion of β_1 integrin using a siRNA (Extended Data Fig. 2c) also resulted in a significant decrease in tubulin acetylation as compared to control cells (Extended Data Fig. 2c and 2d), suggesting that β_1 integrins are major players in the control of microtubule acetylation. We then investigated the involvement of two central players in integrin signalling; the proto-oncogene c-Src and the Focal Adhesion Kinase (FAK). In migrating astrocytes, inhibition of Src (using Src kinase inhibitor 1 – referred to as Src kin 1) and FAK (using PF-562271) drastically reduced the levels of acetylated tubulin (Extended Data Fig. 2e). In addition, following Src and FAK inhibition, microtubule acetylation induced by cell spreading on 48 kPa substrates was decreased to a level similar to that observed on soft substrates (Fig.

1C and Extended Data Fig. 2f), indicating that Src and FAK are required for the rigidity-dependent increase in acetylation. Altogether, these results strongly suggest that β_1 integrin-mediated signalling promotes substrate rigidity-induced acetylation of microtubules.

αTAT1 interacts with Talin in mechanosensitive manner

Microtubule acetylation is mediated by αTAT1; however, the recruitment and/or activation of αTAT1 remains unknown[21]. Therefore, we carried out a quantitative mass spectrometry screen to identify interacting partners of αTAT1 using HEK293 cells. The mass spectrometry data (data available via ProteomeXchange with identifier PXD015871; check methods for details; Extended Data Fig. 2g) revealed interesting potential interactors, amongst which the proteins enriched in the gene ontology for focal adhesions depicted in red in Extended Data Fig. 2g. One of the significant interactors on the mass spectrometry screen was Talin (Extended Data Fig. 2g), a mechanosensitive partner of integrins[19]. We confirmed the interaction of αTAT1 with Talin using pulldown experiments. GST-αTAT1, but not GST alone, associated with endogenous Talin from astrocyte lysates (Fig. 1d and Extended Data Fig. 2h). The interaction was further confirmed by immunoprecipitation using GFP-αTAT1-transfected astrocytes. Talin co-immunoprecipitated with GFP-αTAT1 but not with GFP alone (Fig. 1e and Extended Data Fig. 2i). In addition, using TIRF microscopy, we observed that GFP-αTAT1 strongly localised at mCherry-vinculin-positive FAs (Fig. 1f)[13]. We then investigated whether Talin played a role in the recruitment of αTAT1 to FAs and the acetylation of microtubules. Therefore, we used specific siRNAs to reduce Talin expression in primary astrocytes (Extended Data Fig. 2j). Talin depletion reduced GFP-αTAT1 recruitment to FAs (Fig. 1f). In addition, Talin-depleted astrocytes plated on 48 kPa substrates exhibited decreased levels of tubulin acetylation as compared to the control cells (Fig. 1g).

Since αTAT1 is also present within microtubules (Extended Data Fig. 2k)[13,14], we tested whether the recruitment of αTAT1 to FAs was dependent on microtubules. To address this, GFP-αTAT1 and mCherry-vinculin expressing astrocytes were treated with Nocodazole to depolymerize all microtubules. Nocodazole-treated astrocytes displayed larger adhesions and increased stress fibres as observed in other cell types (Extended Data Fig. 2l, Supplementary Video 1)[22,23], and increased αTAT1 at FAs (Extended Data Fig. 2l, Supplementary Video 1), suggesting that microtubules are not required to localise αTAT1 at FAs, and that increased actomyosin contractility might facilitate αTAT1 concentration at FAs. Since actomyosin contractility is required for Talin-mediated mechanosensing[24,25], we used the ROCK inhibitor, Y-27632 (which strongly reduces actomyosin contractility[26]) to assess its role in the mechanosensitive acetylation of microtubules. By GST-αTAT1 pulldown as well as TIRF microscopy, we observed that Y-27632 treatment decreased αTAT1 interaction with Talin (Fig. 1h and 1i, Supplementary Video 2) and tubulin acetylation (Fig. 1j and 1k) confirming that actomyosin contractility and mechanosensing at FAs influence microtubule acetylation. Altogether, these results suggest that Talin- and actomyosin-dependent mechanosensing triggers the recruitment of αTAT1 to FAs, and is required for rigidity-dependent microtubule acetylation.

Microtubule acetylation influences mechanotransduction at focal adhesions

We then tested whether microtubule acetylation may be involved in mechanosensitive cell functions. Astrocytes were sparsely plated on soft (2 kPa) and stiff (48 kPa) polyacrylamide hydrogels and stained for Yes-associated protein (YAP), an actomyosin- and RhoGTPase-dependent transcriptional activator whose nuclear translocation is mechanosensitive[27]. Like in several cell types[28], quantification of nuclear-to-cytoplasmic ratio of YAP indicated that YAP nuclear localisation increased when astrocytes were plated on stiff substrates compared to soft substrates (Fig. 2a and 2b). In αTAT1-depleted

143 astrocytes, the nuclear recruitment of YAP in cells plated on 48 kPa substrates was strongly inhibited
144 and YAP localisation was similar in cells plated on soft and rigid substrates (Fig. 2a). Conversely,
145 increasing microtubule acetylation by Tubacin treatment led to a strong nuclear recruitment of YAP in
146 cells plated on 2 kPa substrates, recapitulating a phenotype of cells on stiff substrates (Fig. 2b). To
147 determine whether the effects of microtubule acetylation on YAP were specific to astrocytes, we
148 performed similar experiments on HUVECs. HUVECs exhibit low level of acetylated tubulin, even when
149 plated on stiff substrates (Extended Data Fig. 3b, 3c). Hence, to test the effects of microtubule
150 acetylation on YAP translocation in HUVECs, cells were treated with Tubacin to increase microtubule
151 acetylation (Extended Data Fig. 3c). Similar to astrocytes, increasing microtubule acetylation in HUVECs
152 plated on 2 kPa substrates resulted in an increased nuclear recruitment of YAP, mimicking the
153 phenotype of cells plated on stiff substrates (Fig. 2c). Altogether, this demonstrates that the
154 manipulation of microtubule acetylation tunes YAP mechanosensitive nuclear-cytoplasmic shuttling
155 (summary cartoon shown in Fig. 2g).
156
157 FAs are crucial mechanosensitive structures which sense and adapt to the matrix rigidity[29]. Thus, we
158 investigated the effects of substrate rigidity on FAs in astrocytes plated on polyacrylamide hydrogels of
159 different rigidities: 1.26 kPa, 2 kPa, 9 kPa and 48 kPa (Fig. 2d), by immunostaining of the FA-associated
160 protein, Paxillin[4,30]. Quantification of the density of FAs (Extended Data Fig. 3d) indicates that astrocytes
161 plated on soft substrates display FAs throughout the cell surface, whereas, FAs are predominantly at the
162 periphery of cells adhering to stiffer substrates (Fig. 2d). Thus, changes in substrate rigidity alter FA
163 distribution in astrocytes, allowing us to assess the impact of microtubule acetylation in this
164 phenomenon. Following αTAT1 depletion, FAs were distributed throughout the cell surface
165 independently of the rigidity of the substrate, i.e., αTAT1-depleted cells on stiff substrates showed a
166 distribution of FAs similar as that of control/siαTAT1 cells plated on soft substrates (Fig. 2e, Extended

Data Fig. 3e-3h). To confirm that the changes in FA distribution act through tubulin acetylation, we treated cells plated on different rigidities with Tubacin. Tubacin had no effect on FA distribution in cells plated on 48 kPa substrates (Fig. 2f, Extended Data Fig. 3e and 3f). In contrast, Tubacin treatment of cells plated on 1.26 kPa substrates mimicked the phenotype (FAs at the cell periphery) observed in control/Tubacin-treated cells plated on stiff matrices (Fig. 2f, Extended Data Fig. 3e and 3f). Since cell spreading on different substrate rigidities can affect the distribution of FAs, we plated αTAT1-depleted cells on micropatterned hydrogels to observe FAs in cells of similar spread area. In line with our prior results, cells on soft substrates or αTAT1-depleted cells on stiffer substrates displayed FAs throughout the cell spreading area (Extended Data Fig. 3i). Together with previous findings that microtubule acetylation controls membrane vesicle delivery at FAs and FA dynamics[13,31], these results show that the rigidity-dependent microtubule acetylation controls the mechanosensitive distribution of FAs (Fig. 2g).

Microtubule acetylation controls cytoskeletal organization at focal adhesions

Next, we investigated the impact of αTAT1 depletion on the FA-associated cytoskeleton. In migrating astrocytes, the actin network comprises of longitudinal stress fibres connected to FAs at the front of the leader cells as well as inter-junctional transverse arcs connecting neighbouring cells at adherens junctions (Fig. 3a and Extended Data Fig. 4a)[26,32]. In αTAT1-depleted cells, the transverse arcs of actin were dramatically reduced and the longitudinal fibres did not extend to the front of migrating cells (Fig. 3a, Extended Data Fig. 4a). Associated with these longitudinal fibres, FAs were located further back within the protrusion rather than at the front of leader cells (Fig. 3a and Extended Data Fig. 4a)[13]. Myosin light chain phosphorylation (pMLC) is predominantly seen at the leading edge of migrating control cells; however, in αTAT1-depleted cells, pMLC was barely visible at the leading edge of cells and was only associated with the remaining actin fibres at the cell centre, similar to Myosin IIa distribution

(Fig. 3a, 3b and Extended Data Fig. 4a). Moreover, intermediate filaments (visualised using Vimentin), which play a major role in regulating FAs and collective migration of astrocytes[32] and normally extend from the perinuclear region to the cell periphery close to FAs[32,33], were absent from the front of αTAT1-depleted cells and frequently appeared fragmented (Fig. 3c). We then looked closely at the effect of αTAT1 on the cytoskeletal organisation at FAs by using platinum-replica transmission electron microscopy (EM) on unroofed migrating astrocytes located at the wound edge. As by light microscopy, EM images showed that FAs connected to actin bundles were distributed further within the protrusion in case of siαTAT1 cells as compared to a highly organised and parallel set of FAs at the leading edge of control cells (Fig. 3d). From the high magnification views of FAs in the control cells, microtubules were often seen along actin cables reaching FAs (Fig. 3d, marked with white arrows in i.1). Intermediate filaments were also clearly visible, intertwined with the actin filaments at FAs (Fig. 3d, marked with yellow arrows in i. 2 and i. 3). In siαTAT1 cells, the actin bundles near FAs were strikingly thinner than those in controls (Fig. 3d). We consistently observed a lack of microtubules and intermediate filaments associated with FAs in αTAT1-depleted cells (Fig. 3d). All these results strongly support a role for αTAT1 in the cytoskeletal organisation at FAs in astrocytes. We then tested the effects of microtubule acetylation on the cytoskeletal organisation by treating HUVECs and astrocytes plated on soft substrates with Tubacin to increase microtubule acetylation. In Tubacin-treated cells, we observed prominently larger actin cables, increased Myosin-IIa filaments, together with larger and more peripheral FAs (Fig. 3e and Extended Data Fig. 3b), reminiscent of the phenotype observed in astrocytes plates on stiff substrates (Fig. 3f), confirming that microtubule acetylation regulates actomyosin organization.

Microtubule acetylation increases actomyosin contractility via GEF-H1 and Rho

One major impact of mechanosensing is the adaptation of traction forces to the rigidity of the substrate[34]. We thus investigated whether microtubule acetylation might affect traction forces by plating control or αTAT1-depleted astrocytes on crossbow-shaped micropatterned hydrogels. By traction force microscopy, we observed that αTAT1 depletion resulted in lower traction force production on 40 kPa substrates (Fig. 4a and 4b). In contrast, overexpression of GFP-αTAT1 increased traction energies and forces and also rescued the effect observed on αTAT1 knockdown (siαTAT1 + GFP-αTAT1; Fig. 4a and 4b) when astrocytes were plated on 40 kPa. In addition, Tubacin-treated astrocytes on soft 2 kPa hydrogels showed increased traction energies and forces, comparable to control astrocytes plated on 40 kPa (Fig. 4c). We also studied the effects of microtubule acetylation on traction forces in Tubacin-treated HUVECs plated on soft 2 kPa substrates. Similar to astrocytes, increased microtubule acetylation using Tubacin resulted in higher traction energies and forces in HUVECs (Fig. 4d). Thus, the level of microtubule acetylation dictates traction forces exerted on the substrate through FAs. This further illustrates the essential role of the mechanosensitive regulation of microtubules in force transmission.

The crucial role of microtubule acetylation in the controlling cytoskeletal organisation and traction forces led us to further investigate the molecular mechanisms involved in this process. We focused on RhoA, a small G protein of the Rho family, well-known for promoting stress fibre formation and actomyosin contractility, via its effector ROCK and MLC phosphorylation. Pulldown of GTP-bound active RhoA using GST-Rhotekin beads showed that αTAT1 depletion reduced RhoA activity (Fig. 4e), suggesting that microtubule acetylation may promote actomyosin contractility by activating RhoA. RhoA activation is mediated by Guanine nucleotide exchange factors (GEFs)[35]. Amongst these GEFs, GEF-H1 (also known as ARHGEF2) is a microtubule-bound RhoGEF which, when released from microtubules triggers the Rho-ROCK signalling cascade and cell contractility[36,37]. Previously, substrate stiffness was suggested to correlate with GEF-H1 activity and actomyosin contractility[38]. In addition, GEF-H1 was

239 recently shown to be controlled by the interaction of microtubules with integrin-mediated adhesions[39],
240 leading us to investigate whether integrin-mediated microtubule acetylation could affect the association
241 of GEF-H1 with microtubules. In control astrocytes plated on rigid glass coverslips, GEF-H1 localised
242 partially (approximately 42%) on microtubules but also in the cytosol, a localisation that corresponds to
243 the active/released GEF- H1 (Fig. 5a and Extended Data Fig. 5a)[40]. In contrast, in αTAT1-depleted cells,
244 GEF-H1 was predominantly localised on microtubules (approximately 60%; Fig. 5a and Extended Data
245 Fig. 5a). Tubacin treatment of αTAT1-depleted cells led to the release of GEF-H1 into the cytosol,
246 rescuing the effect of αTAT1 depletion and confirming the role of microtubule acetylation in the GEF-H1
247 localisation (Fig. 5a and Extended Data Fig. 5a). In control HUVECs (which exhibit relatively low levels of
248 acetylated tubulin) GEF-H1 was mostly bound to microtubules (approximately 50%; Fig. 5b). Like in
249 astrocytes, the treatment of HUVECs with Tubacin resulted in the release of GEF-H1 into the cytoplasm,
250 with only 38% of GEF-H1 colocalising with microtubules (approximately 38%; Fig. 5b). GEF-H1
251 association with microtubules was confirmed using GFP-immunoprecipitation experiments using HEK
252 cells transfected with GFP-Ctl or GFP-GEF-H1 (Fig. 5c). Like Nocodazole treatment which leads to the
253 depolymerisation of microtubules, Tubacin treatment (which increases microtubule acetylation)
254 abolished the binding of GEF-H1 to microtubules (Fig. 5c). Altogether, these results show that
255 microtubule acetylation promotes the release of GEF-H1 from microtubules into the cytoplasm.
256
257 We then tested whether substrate rigidity and αTAT1 play a role in the association of GEF-H1 with
258 microtubules. Astrocytes plated soft 2 kPa substrates exhibit a higher microtubule-bound portion of
259 GEF-H1 as compared to cells on stiff 48 kPa gels (Fig. 5d and Extended Data Fig. 5b). In αTAT1-depleted
260 cells plated on stiff substrates, GEF-H1 was found predominantly bound to microtubules, mimicking the
261 phenotype observed in cells plated on soft substrates (Fig. 5d and Extended Data Fig. 5b). These results

strongly suggest that rigidity-dependent microtubule acetylation contributes to mechanotransduction by enabling RhoA activation and actomyosin contractility.

Microtubule acetylation modulates mechanosensitive cell migration by tuning mechanotransduction at focal adhesions

The involvement of microtubule acetylation in mechanotransduction and in the mechanosensitive regulation of FAs and actomyosin contractility led us to investigate its influence on cell migration, which has often been described as a mechanosensitive cellular response[2,41]. To this end, we developed a collective migration assay on hydrogels, where microdropping a small amount of a chemical (sodium hydroxide) induced a circular wound in the cell monolayer (Fig. 6A, Supplementary Video 3). Sodium hydroxide treatment did not noticeably alter the hydrogel properties (see Methods). Wild-type astrocytes migrated significantly slower on 2 kPa gels than on 48 kPa gels (Fig. 6B, Supplementary Video 4), implying that astrocyte migration speed is affected by substrate rigidity. Most importantly, αTAT1 depletion abolished the increase of cell speed observed on stiff 48 kPa gels (Fig. 6C, Supplementary Video 5), so that the migration speed of αTAT1-depleted cells plated on 48 kPa was similar to that of control and αTAT1-depleted cells on 2 kPa substrates. In addition, the effects of αTAT1 depletion in cells plated on 48 kPa gels is in line with our previous results described on the role of αTAT1 during collective migration on glass coverslips[13]. Thus, we demonstrate that microtubule acetylation is required for the mechanosensitive regulation of astrocyte collective migration.

Discussion

Our results show that microtubules are regulated in response to substrate rigidity sensing and in turn, play a key role in mechanotransduction by participating in mechanosensitive cellular responses,

287 including translocation of the transcriptional coactivator YAP, focal adhesion distribution, actomyosin
288 contractility, generation of traction forces and cell migration (Fig. 6d). Our results point to a mechanism
289 by which Talin-mediated mechanosensing downstream of integrin-mediated signalling (Fig. 6d-i)
290 controls the recruitment of αTAT1 to FAs (Fig. 6d-ii) and induces microtubule acetylation (Fig. 6d-iii). We
291 show that αTAT1 interacts with Talin and that, on rigid substrates, Talin is required for the recruitment
292 of αTAT1 to FAs, and for the acetylation of microtubules (Fig. 6d-ii). Although we do not have any clear
293 evidence of a direct interaction of Talin with αTAT1, the β_1-integrin- and actomyosin-dependent
294 association of αTAT1 with Talin suggest that tension-induced changes in Talin conformation may be
295 involved in inducing αTAT1 recruitment to FAs and microtubule acetylation.
296
297 How αTAT1 enters the lumen of microtubules still remains unclear although one can speculate that
298 αTAT1 accesses the lumen through microtubule lattice defects or through the open ends[21]. Growing
299 microtubule ends are often seen in close proximity to FAs at the leading edge of migrating cells[8]
300 (Extended Data Fig. 5C). It is very likely that, like other FA-associated proteins, a large proportion of
301 talin-associate αTAT1 rapidly exchange with a cytosolic pool[42]. This lead us to propose a model in which
302 the increased interaction of αTAT1 with talin increases the local concentration of αTAT1 and facilitates
303 its entry in the microtubule lumen through microtubule open ends in the vicinity of adhesions (Fig. 6D-
304 iii; Extended Data Fig. 5C).
305
306 We show that microtubule acetylation reorganises the actomyosin network and promotes traction
307 forces. Therefore, we propose a feedback mechanism involving a crosstalk between microtubules and
308 actin wherein, actomyosin-dependent mechanosensing promotes microtubule acetylation which, in
309 turn, facilitates the release of GEF-H1 from microtubules into the cytosol (Fig. 6D-iv) to increase RhoA
310 activity (Fig. 6D-v), cell contractility (Fig. 6D-vi) and traction forces (Fig. 6D-vii). It was recently shown

311 that uncoupling microtubules from FAs results in a similar release of microtubule-bound GEF-H1 into the
312 cytosol[39], which then triggers myosin IIA assembly and increased cell contractility through RhoA.
313 Suppression of RhoA activity in the absence of αTAT1 might be due to the sequestering of GEF-H1 by
314 non-acetylated microtubules. Whether microtubule acetylation directly or indirectly induces the release
315 of GEF-H1 remains unclear. One can speculate that acetylation of Lysine 40 changes the conformation of
316 α-tubulin and modifies the binding site for GEF-H1, thereby, inducing its release from microtubules.
317 Alternatively, acetylation might change the mechanical properties of the microtubule lattice and affect
318 its curvature[41,42], which would in turn facilitate the release of GEF-H1 from microtubules. It is also
319 possible that any of the previous mechanisms affect a binding of a partner of GEF-H1, which alters GEF-
320 H1 conformation (via phosphorylation for instance) and promote its release into the cytosol.
321 Interestingly, microtubule acetylation also affects the association of intermediate filaments with actin
322 bundles at FAs. Since intermediate filaments have also been involved in the control of FA dynamics,
323 actomyosin contractility as well as GEF-H1 activity[32,40], the microtubule-actin interplay described here
324 may also involve intermediate filaments, whose role in mechanotransduction is still elusive.
325
326 In response to substrate rigidity sensing, cells adapt essential functions such as migration[43]. In the
327 absence of αTAT1, cells plated on stiff substrates produce less traction forces and migrate slower (Fig.
328 6d-viii). The relationship between forces and migration can be considered counter-intuitive for single
329 cell migration where traction forces appear to correlate with migration speed; and contractile forces are
330 required for migration but exaggerated traction forces tend to slow or even stop migration[44]. In fact,
331 measurements of traction forces exerted by astrocytes plated on substrates of various rigidities shows
332 that there is a rigidity optimum (around 50 kPa), at which the forces are maximal (Extended Data Fig.
333 5d). When looking at microtubule acetylation, actomyosin contractility, or cell migration, it is clear that
334 all of them increase up to about 48kPa but then reach a plateau or even decrease when cells are plated

on glass, indicative of a non-monotonous response. In collective cell migration, the distribution of forces within the migrating monolayer, more than the intensity itself, is crucial for the efficient control of collective cell migration. Also, collective cell migration relies on the transmission of forces between the leaders and followers. Cell-cell junctions not only transmit forces between cells but help maintain the integrity of the monolayer[26,45], which improves collective and directed cell migration. Alteration of microtubule acetylation did not induce any detachment of leader cells from followers and did not affect directionality or persistence of migration[13]. Therefore, we propose a model in which, on stiff substrates, increased microtubule acetylation would trigger higher traction forces in leader cells, which would transmit these pulling forces to followers and increase collective migration speed. Microtubule acetylation may also affect cell migration by controlling FA dynamics. We have previously demonstrated that microtubule acetylation promotes the fusion of Rab6-dependent post-Golgi carriers at FAs and increases FA turnover[13], such that they are continuously renewed at the front of leader cells. Depletion of αTAT1 (as that of Rab6) alters the distribution of FAs in migrating cells[13]. The change in FA distribution between the cell center and the cell periphery suggests that rigidity-induced acetylation of microtubules may promote FA turnover during cell spreading, thereby, excluding them from the cell center. We speculate that the increase in FA turnover together with the increase in cell contractility participate in strengthening the traction forces exerted on FAs concentrated at the leader cell wound edge and improve astrocyte collective migration (Fig. 6d-viii).

In conclusion, our results depict a crosstalk between the actin and microtubule cytoskeletal networks (Fig. 6d), whereby microtubule acetylation, downstream of rigidity-dependent integrin-mediated signalling, alters actomyosin contractility as well as focal adhesion distribution and dynamics to promote mechanosensitive migration of astrocytes, thus closing a crucial feedback loop governing mechanotransduction at FAs (Fig. 6d).

Methods

Cell culture

Primary astrocytes were obtained from E17 rat embryos[12]. Use of these animals is in compliance with ethical regulations and has been approved from the Prefecture de Police and Direction départementale des services vétérinaires de Paris. Astrocytes were grown in 1g/L glucose DMEM supplemented with 10% FBS (Invitrogen, Carlsbad, CA), 1% penicillin-streptomycin (Gibco) and 1% Amphotericin B (Gibco) at 5% CO_2 and 37°C. Human umbilical vein endothelial cells (HUVECs) were cultured in EGM-2 BulletKit media (Lonza, catalogue no. CC-3162).

Cell nucleofection

Astrocytes were transfected with Lonza glial transfection solution and electroporated with a Nucleofector machine (Lonza). Cells were then plated on appropriate supports previously coated with poly-L-Ornithine (Sigma). Experiments are carried out 3 or 4 days post-transfection and comparable protein silencing was observed. siRNAs were used at 1 nmol and DNA was used at 5 µg. siRNA sequences used were:

Luciferase (control) UAAGGCUAUGAAGAGAUAC; αTAT1 rat (siαTAT1-1): 5'-ACCGACACGUUAUUUAUGU-3' and 5'-UUCGAAACCUGCAGGAACG-3'; αTAT1 rat (siαTAT1-2): 5'-UAAUGGAUGUACUCAUUCA-3' and 5'-UCAUGACUAUUGUAGAUGA-3'; Talin-1 rat (siTalin1): 5'-GGGACACCAUGGAGUACAGAA-3', 5'-GACCCCCACUUCCAGGAUAUU-3', 5'-GCUGGAAGCUGUGGAUAACCU-3', and 5'-GACCUCCACCCCUGAAGAUUU-3'; β_1 integrin (AUUGCCAGAUGGAGUAACA).

Constructs used were: GFP-αTAT1 and GST-αTAT1 (gift from Philippe Chavrier, Institut Curie and Guillaume Montagnac, Institut Gustave Roussy) and mCherry-vinculin. siαTAT1-1 and siαTAT1-2 are

pools of two siRNAs each. For all experiments, siαTAT1-2 has been used due to better knockdown efficiency as seen in Extended Fig. 1a and previously characterized in [13]. A few major experiments have been carried out with siαTAT1-1 and the results are shown in the respective extended data figures.

Cell treatment

Cells were treated with 5-10 μM Tubacin (Sigma SMLOO65) or 10 μM Niltubacin (negative control for Tubacin; Enzo Life Sciences) or DMSO (control) were added cells (3 h treatment for HUVECs; 6 h treatment for astrocytes). Similarly, RGD peptide (Enzo Life Sciences) and RGE Control peptide (Enzo Life Sciences) were added prior to wounding. ROCK inhibitor, Y-27632, and $MnCl_2$ (1 μM) were added 6 h after wounding and 2 h before fixation. For TIRF experiments, 10 μM Nocodazole or Y-27632 were added after 10 min of acquisition. For pull-downs, 10 μM Nocodazole or Y-27632 were added 1 h before cell lysis.

Preparation of homogenously coated polyacrylamide hydrogels

Protocol to prepare polyacrylamide hydrogels was adapted from[41,46,47]. Coverslips were plasma cleaned for 3 min and silanised for 10 min using a solution of 1% (v/v) 3-(trimethoxysilyl)propyl methacrylate and 1% (v/v) acetic acid in ethanol. Coverslips were then washed twice with absolute ethanol and dried. A solution of polyacrylamide (proportions of acrylamide and bisacrylamide in the solution define the rigidity of the hydrogel) was prepared. 2.5 μl 10% APS and 0.25 μl TEMED was added and mixed well with the solution. A 50 μl drop of the solution was added over each coverslip (20x20 mm) and immediately, an 18x18 mm coverslip was placed gently over the solution. The solution was allowed to polymerise for 1 h at room temperature. HEPES was added over the coverslips to detach the top glass. The polymerised gel was then activated under UV for 5 min using Sulpho-SANPAH and washed with HEPES twice. The hydrogels were then coated with 100 μg/ml of rat tail collagen I overnight at 4^{o}C. The excess collagen was washed once with PBS and approximately 5 x 10^4 cells/ml were plated on hydrogels.

Micropatterning

Coverslips were plasma-cleaned for 45 s and incubated with 0.1 mg/ml poly-l-lysine/polyethylene glycol (PLL-PEG) diluted in 10 mM HEPES for 30 min at room temperature. Excess of PLL-PEG was allowed to slide down by gravity, and the coverslips were dried and stored at $4^{o}C$ overnight before printing. Micropatterns were printed on previously prepared PLL-PEG coverslips for 3 min with specifically designed chrome masks and coated with 50:50 v/v fibronectin/fibrinogen mixture (20 µg/ml each) diluted in fresh $NaHCO_3$, pH 8.3, 100 mM, for 30 min at room temperature. Micropatterned coverslips were washed thrice in $NaHCO_3$ and used immediately for transfer on hydrogels. Plated cells (approximately 6 x 10^4 cells/ml) were allowed to adhere for 16 h before imaging/fixation. Crossbow patterns have an area of ~2500 μm^2.

Traction force experiments on micropatterned substrates

After printing and coating micropatterned coverslips, gel mixtures were prepared as follows: 40.4 kPa – 100 µl 40% acrylamide, 120 µl 2% bisacrylamide, 280 µl water (final concentration of 8% acrylamide and 0.48% bisacrylamide in water); 2.61 kPa – 50 µl 40% acrylamide, 25 µl 2% bisacrylamide, 425 µl water (final concentration of 8% acrylamide and 0.048% bisacrylamide in water). 5 µl of fluorescent microbeads (FluoSpheres; Molecular Probes) were incubated with 0.1 mg/ml PLL-PEG on a rotator for 1 h at 4°C prior to mixing with the gel mixture. The PLL-PEG coated beads were washed and centrifuged thrice at 1000 rpm for 10 min with 10 mM HEPES. These beads were then mixed with 165 µl of the gel mixture. After adding 1 µl APS and 1 µl TEMED, the solution was added as a 25 µl drop on a silanised 20x20 mm coverslip. The protein-coated micropatterned coverslip was then gently placed on the gel mixture. The solution was allowed to polymerize for 25 min at room temperature. After detaching the micropatterned glass from the polymerized gel, 6 x 10^4 cells/ml were plated on the gels and allowed to adhere and spread for 16 h before TFM experiments. Stacks of single micropatterned cells were acquired before and after trypsin treatment. Acquisitions were performed with a Nikon Eclipse Ti-E epifluorescence inverted microscope, with a 40× 1.49 NA air objective equipped with a pco.edge sCMOS

camera and Metamorph software. Cells were maintained at 5% CO_2 and 37°C in normal astrocyte medium during acquisition.

Migration assays

In vitro wound healing assays: cells were plated on appropriate supports (dishes, plates, coverslips or glass-bottom MatTek) and grown to confluence. The cell monolayer was scratched with a p200 pipette tip to induce migration and imaged during 8h.

Migration on soft substrates: cells were plated on hydrogels of different rigidities in 6-well glass bottom plates (MatTek) and allowed to grow for 72 h after transfection before creating a chemical wound. 0.05 M NaOH was gently dropped on the cells using a microinjector. NaOH is used to instantly kill and detach cells localized in a region of a few hundred microns. The NaOH is added with a microinjector which delivers a fraction of a nanoliter of NaOH (0.05M) on a cell monolayer, which immediately mixes with 2 ml of culture medium that is present in the culture dish. The dead cells and debris were gently washed away using PBS. Fresh medium was added to the cells. Cells were placed on the microscope for live imaging. In these conditions, the hydrogel is only very locally and briefly exposed to the chemical. As cells migrate into this space (wounded area of the monolayer), the fibronectin coating and the surface of the hydrogel remains intact with negligible and unnoticeable changes. NaOH treatment did not affect the weight of the gel -indicative of gel swelling-; it did not induce any detectable bead movements – indicative of gel contraction or expansion of the gel-, nor did it affect the traction forces of cells, indicating that cells did not sense any difference in substrate rigidity. Acquisition was started 30 min after wounding. Supplementary Videos were acquired with a Zeiss Axiovert 200M or a Nikon Eclipse Ti-E epifluorescence inverted microscope with cells maintained at 5% CO_2 and 37°C. All images were acquired with dry objective 10X 0.45 NA and an EMCCD camera/pco.edge sCMOS camera and Metamorph software. Images were acquired every 15 min for 24 h. Nuclei of leader cells were manually tracked with Fiji software (Manual Tracking plugin).

Immunostaining

Cells were fixed with cold methanol for 3 min at -20°C, or 4% warm PFA, or 4% PFA + 0.2% glutaraldehyde + 0.25% Triton X-100 for 10 min at 37°C. After fixation with PFA, glutaraldehyde and triton, free aldehyde groups were quenched with a solution of 1 mg/ml sodium borohydride (Sigma-Aldrich) freshly added to cytoskeletal buffer (10 mM MES or MOPS, 150 mM NaCl, 5 mM EGTA, 5 mM $MgCl_2$, 5 mM glucose, pH 6.1) for 10 min on ice. Cells were permeabilised for 5 min with 0.1% Triton in case of PFA fixation. Coverslips were blocked for 1 h with 5% BSA in PBS. The same solution was used for primary and secondary antibody incubation for 1 h. Nuclei were stained for DAPI and coverslips were mounted with Prolong Gold.

Antibody anti-Acetylated Tubulin (1:10000; clone 6-11B-1, mouse monoclonal, T-6793 Sigma Aldrich or 1:200; clone 6-11B-1, ab24610, Abcam), anti-Poly-Glu Tubulin (1:1000; AbC0101, ValBiotech), anti-α-Tubulin (1:1000; MCA77G, rat, Biorad), anti-Paxillin (1:500; 610051, mouse monoclonal, lot 5246880; BD; and ab32084, rabbit monoclonal, clone Y133 and lot GR215998-1; Abcam), anti-Talin (1:1000; T3287, mouse monoclonal, clone 8D4, lot 035M4805V; Sigma-Aldrich), anti-GEF-H1 (1:100; ab155785, Abcam), Alexa fluor 647 Phalloidin (1:2000; 176759, lot GR278180-3; Abcam or 1:300; Thermo Fisher Scientific), anti-Vimentin (1:200; V6630, mouse monoclonal lot 10M4831; Sigma-Aldrich), anti-pMLC (1:1000; 3675S, S19, mouse, Cell signalling), anti-Myosin IIA (1:1000; non-muscle, M8064, rabbit polyclonal, Sigma-Aldrich), anti-Vinculin (1:400; V9131, Sigma-Aldrich). Secondary antibodies were Alexa Fluor 488 donkey anti–rabbit (711-545-152), Rhodamine (TRITC) donkey anti–rabbit (711-025-152), Alexa Fluor 647 donkey anti–rabbit (711-695-152), Alexa Fluor 488 donkey anti–mouse (715-545-151), Rhodamine (TRITC) donkey anti–mouse (715-025-151), Alexa Fluor 647 donkey anti-rat (711-605-152), and Alexa Fluor 488 donkey anti–rat (712-545-153); all from Jackson ImmunoResearch. Images were acquired with a Leica DM6000 microscope equipped with 40X 1.25 NA or 63X 1.4 NA objectives and

recorded on a CCD camera with a Leica software, or imaged at the basal plane using Yokogawa CSU-W1, Nikon TiE Spinning disk confocal microscope, at 100x magnification.

TIRF microscopy

Acquisitions were performed with a Nikon Eclipse Ti-E epifluorescence inverted microscope, with a 60× 1.49 NA oil objective equipped with a pco.edge sCMOS camera with Metamorph software. Cells were maintained at 5% CO_2 and 37°C in normal astrocyte medium. After acquiring a 15 min movie of GFP-αTAT1 and mCherry-vinculin, Nocodazole or Y27 were added and images were acquired every 2 min for 1 h.

Transmission electron microscopy

Adherent migrating astrocytes plated on glass coverslips were disrupted by sonication as described previously[48]. Coverslips were unroofed by scanning the coverslip with rapid sonicator pulses in KHMgE buffer (70 mM KCl, 30 mM HEPES, 5 mM $MgCl_2$, 3 mM EGTA, pH 7.2). Paraformaldehyde 2%/glutaraldehyde 2%-fixed cells were further sequentially treated with 0.5% OsO_4, 1% tannic acid and 1% uranyl acetate prior to graded ethanol dehydration and Hexamethyldisilazane substitution (HMDS, Sigma-Aldrich). Dried samples were then rotary-shadowed with 2 nm of platinum and 5-8 nm of carbon using an ACE600 high vacuum metal coater (Leica Microsystems). Platinum replicas were floated off the glass by 5% hydrofluoric acid, washed several times by floatation on distilled water, and picked up on 200 mesh formvar/carbon-coated EM grids. The grids were mounted in a eucentric side-entry goniometer stage of a transmission electron microscope operated at 80 kV (Philips, model CM120) and images were recorded with a Morada digital camera (Olympus). Images were processed in Adobe Photoshop to adjust brightness and contrast and presented in inverted contrast.

Image analysis

Normalised mean intensity levels of acetylated and detyrosinated tubulin for immunofluorescence images were calculated as shown in equation 1:

504 *1*

$$Ratio\ of\ acetyl\ or\ detyr\ tubulin\ level\ = \frac{Acetyl/detyr\ tubulin\ intensity}{Total\ tubulin\ intensity}$$

505 YAP nuclear/cytoplasmic ratio was calculated as shown in equation 2:

506 *2*

$$YAP\ nuclear\ to\ cytoplasmic\ ratio\ = \frac{Intensity\ of\ YAP\ in\ the\ nucleus}{Intensity\ of\ YAP\ in\ the\ cytoplasm}$$

507 FA density was calculated as shown in equation 3:

508 *3*

$$FA\ density = \frac{Number\ of\ FAs\ in\ the\ region}{Area\ of\ the\ region}$$

509 Different regions of cells (entire cell, cell periphery-8 µm, 8 µm-16 µm, 16 µm-cell center) were analysed
510 as depicted in Extended Data Fig. 2d.

511 For migration assays, nuclei of cells were manually tracked to determine the speed directionality and
512 persistence of migration using the following formulae:

513 Mean velocity (v), persistance (p) and directionality (d) of cell migration are calculated shown in
514 equations 4-6: for a given (x, y) coordinate of leading cell nucleus,

515 *4*

$$v = \frac{\sum \vartheta}{n}$$

516 *5*

$$p = \frac{\sqrt{[(x_{24} - x_0)^2 + (y_{24} - y_0)^2]}}{\sum \sqrt{[(x_n - x_{n-1})^2 + (y_n - y_{n-1})^2]}}$$

517 *6*

$$d = \frac{|(x_0 - x_{24})|}{\sum \vartheta \sqrt{[(x_n - x_{n-1})^2 + (y_n - y_{n-1})^2]}}$$

where n is the number of time points acquired and ϑ is cell velocity.

Analysis of TFM on micropatterns was performed with a custom-designed macro in Fiji based on work by [49]. The topmost planes of beads before and after trypsinisation were selected and aligned using a normalized cross-correlation algorithm (Align Slices in Stack plugin). The displacement field was computed from bead movements using particle image velocimetry (PIV). Parameters for the PIV were three interrogation windows of 128, 64, and 32 pixels with a correlation of 0.60. Traction forces were calculated from the displacement field using Fourier transform traction cytometry and a Young's modulus of 40 kPa or 2 kPa, a regularization factor of 10^{-9}, and a Poisson ratio of 0.5.

For the localisation of GEF-H1 on microtubules, the percentage GEF-H1 on microtubules was calculated as shown in equation 7:

$$Percentage\ intensity\ of\ GEFH1\ localisation\ on\ MT = \frac{Intensity\ of\ GEFH1\ on\ microtubules}{Intensity\ of\ GEFH1\ outside\ microtubules} \times 100 \quad (7)$$

Immunoprecipitations and pulldown assays

Cell lysates were prepared by scraping cells in 1X lysis buffer (10X buffer recipe: 50 mM Tris pH 7.5, triton 20%, NP40 10%, 2 M NaCl with Complete protease inhibitor tablet (Roche, Indianapolis, IN)) and centrifuged for 30 min at 13,000 rpm 4°C to pellet cell debris. Soluble detergent extracts were incubated with GFP-Trap agarose beads (Chromotek, GTP-20) for immunoprecipitation and with GST or GST-αTAT1 beads for 2 hr at 4°c prior to washing three times with wash buffer (50 mM ris pH 7.5, 150 mM NaCl, 0.1% triton , 1 mM EDTA, 2.5 mM $MgCl_2$). The resin was then mixed with Laemmli buffer and used for western blot and mass spectrometry analysis. HEK293 cells were used for mass spectrometry analysis in order to have enough amount of protein from cells expressing αTAT1.

Mass spectrometry

539 Proteins on beads were washed twice with 100 µL of 25 mM NH_4HCO_3 and we performed on-beads
540 digestion with 0.2 µg of trypsine/LysC (Promega) for 1 h in 100 µL of 25 mM NH_4HCO_3. Sample were
541 then loaded onto a homemade C18 StageTips for desalting. Peptides were eluted using 40/60
542 MeCN/H_2O + 0.1% formic acid and vacuum concentrated to dryness. Online chromatography was
543 performed with an RSLCnano system (Ultimate 3000, Thermo Scientific) coupled to an Orbitrap Fusion
544 Tribrid mass spectrometer (Thermo Scientific). Peptides were trapped on a C18 column (75 µm inner
545 diameter × 2 cm; nanoViper Acclaim PepMapTM 100, Thermo Scientific) with buffer A (2/98 MeCN/H_2O
546 in 0.1% formic acid) at a flow rate of 4.0 µL/min over 4 min. Separation was performed on a 50 cm x 75
547 µm C18 column (nanoViper Acclaim PepMapTM RSLC, 2 µm, 100Å, Thermo Scientific) regulated to a
548 temperature of 55°C with a linear gradient of 5% to 25% buffer B (100% MeCN in 0.1% formic acid) at a
549 flow rate of 300 nL/min over 100 min. Full-scan MS was acquired in the Orbitrap analyzer with a
550 resolution set to 120,000 and ions from each full scan were HCD fragmented and analyzed in the linear
551 ion trap.
552 For identification, the data was searched against the Homo sapiens (UP000005640) SwissProt database
553 using Sequest^{HF} through proteome discoverer (version 2.2). Enzyme specificity was set to trypsin and a
554 maximum of two missed cleavage site were allowed. Oxidized methionine, N-terminal acetylation, and
555 carbamidomethyl cysteine were set as variable modifications. Maximum allowed mass deviation was set
556 to 10 ppm for monoisotopic precursor ions and 0.6 Da for MS/MS peaks. The resulting files were further
557 processed using myProMS [50] v3.6 (work in progress). FDR calculation used Percolator and was set to 1%
558 at the peptide level for the whole study. The label free quantification was performed by peptide
559 Extracted Ion Chromatograms (XICs) computed with MassChroQ version 2.2 [51]. For protein
560 quantification, XICs from proteotypic peptides shared between compared conditions (TopN matching)
561 with no missed cleavages were used. Median and scale normalization was applied on the total signal to
562 correct the XICs for each biological replicate. To estimate the significance of the change in protein

abundance, a linear model (adjusted on peptides and biological replicates) was performed and p-values were adjusted with a Benjamini–Hochberg FDR procedure with a control threshold set to 0.05. Up-regulated proteins with at least 3 proteotypic peptides (fold change > 1.5 and p-value < 0.05) and the unique proteins identified only in the GFP-αTAT1 were used for gene ontology (GO) enrichment analysis by using GO::TermFinder tools (10.1093/bioinformatics/bth456) through myProMS.

The mass spectrometry proteomics data have been deposited to the ProteomeXchange Consortium via the PRIDE[52,53] partner repository with the dataset identifier PXD015871 (username: reviewer89842@ebi.ac.uk; password: EC4DSdRf; project name: Potential interactors of alpha-tubulin acetyltransferase 1 (αTAT1/MEC17).

Rho activation assay

Rho activation assay was performed using a RhoA Pull-down Activation Assay Biochem Kit from Cytoskeleton Inc (BK036-S). In short, cells were lysed in ice-cold Cell Lysis Buffer plus 1x protease inhibitor cocktail. Cells were centrifuged at 10,000 g at 4°C for 10 min to pellet cell membranes and insoluble material. Part of the supernatant was stored as input for western blot. The remaining supernatant was divided equally into two parts (300-800 µg protein/tube). $1/15^{th}$ the volume of Loading Buffer was added to each tube (final conc. 15 mM). Then, $1/100^{th}$ the volume of GTPγS was added to one of the tubes and used as positive control (final conc. 0.2 mM). All tubes were incubated at room temperature for 15 min. The reaction was stopped by adding $1/10^{th}$ the volume of STOP Buffer to all tubes (final conc. 60 mM).

Rhotekin-RBD (50 µg) beads were resuspended and added to the tubes. Tubes were rotated at 4^{o}C for 1 h and centrifuged at 5000 g at 4^{o}C for 3 min. Beads were washed with 500 µl each of Wash Buffer. 10-20 ul of Laemmli sample buffer was added to each tube.

Western blot

Cells lysates were obtained with Laemmli buffer composed of 60 mM Tris-HCl pH6.8, 10% glycerol, 2% SDS and 50 mM DTT with the addition of anti-protease (cOmplete cocktail, Roche 11 873 588 001). Samples were boiled 5 min at 95°C before loading on polyacrylamide gels. Transfer occurred at 100V for 1 h on nitrocellulose membranes. Membranes were blotted with TBST (0.2% Tween) and 5% milk and incubated 1 h with the primary antibody and 1 h with HRP-conjugated secondary antibody. Bands were revealed with ECL chemoluminescent substrate (Biorad).

Primary antibodies used: Antibody anti-Acetylated Tubulin (1:10000; clone 6-11B-1, mouse monoclonal, T-6793 Sigma Aldrich), anti-αTAT1 (1:400; HPA046816, rabbit, Atlas Antibodies), anti-Poly-Glu Tubulin (1:1000; AbC0101, ValBiotech), anti-α-Tubulin (1:1000; MCA77G, rat, Biorad), anti-β_1 integrin (ab52971, Abcam), anti-Talin (1:1000; T3287, mouse monoclonal, clone 8D4, lot 035M4805V; Sigma-Aldrich), anti-GEF-H1 (1:100; ab155785, Abcam), anti-GAPDH (MAB374, lot 2689153 Millipore). Secondary HRP antibodies were all purchased from Jackson ImmunoResearch. Unmodified western blots of Figures 1, 4 and 5, as well as Extended Data Figures 1, 2 and 3 can be found in the corresponding source data files.

Graphs and statistics

All graphs and statistics were done using Graphpad Prism.

Data availability

The data supporting the findings of this study are available within the manuscript. The mass spectrometry proteomics data have been deposited to the ProteomeXchange Consortium via the PRIDE[52,53] partner repository with the dataset identifier PXD015871 (username: reviewer89842@ebi.ac.uk; password: EC4DSdRf; project name: Potential interactors of alpha-tubulin acetyltransferase 1 (αTAT1/MEC17). Unmodified western blots of Figures 1, 4 and 5, as well as Extended

609 Data Figures 1, 2 and 3 can be found in the corresponding source data files. Other raw data generated
610 during this study are available on reasonable request.
611

612 ## Code availability
613

614 Codes for focal adhesion distribution and traction forces are available from the authors upon request.
615

References

1 Jaalouk, D. E. & Lammerding, J. Mechanotransduction gone awry. *Nat Rev Mol Cell Biol* **10**, 63-73, doi:10.1038/nrm2597 (2009).

2 Sun, Z., Guo, S. S. & Fässler, R. Integrin-mediated mechanotransduction. *The Journal of Cell Biology* **215**, 445-456, doi:10.1083/jcb.201609037 (2016).

3 Elosegui-Artola, A. *et al.* Rigidity sensing and adaptation through regulation of integrin types. *Nat Mater* **13**, 631-637 (2014).

4 Ladoux, B., Mège, R.-M. & Trepat, X. Front-Rear Polarization by Mechanical Cues: From Single Cells to Tissues. *Trends Cell Biol.* **26**, 420-433, doi:10.1016/j.tcb.2016.02.002 (2016).

5 Etienne-Manneville, S. Microtubules in cell migration. *Annu Rev Cell Dev Biol* **29**, 471-499, doi:10.1146/annurev-cellbio-101011-155711 (2013).

6 Bouchet, B. P. & Akhmanova, A. Microtubules in 3D cell motility. *J. Cell Sci.* **130**, 39-50, doi:10.1242/jcs.189431 (2017).

7 Martins, G. G. & Kolega, J. A role for microtubules in endothelial cell protrusion in three-dimensional matrices. *Biol. Cell* **104**, 271-286 (2012).

8 Seetharaman, S. & Etienne-Manneville, S. Microtubules at focal adhesions – a double-edged sword. *J. Cell Sci.* **132**, jcs232843, doi:10.1242/jcs.232843 (2019).

9 Lyle, K. S., Corleto, J. A. & Wittmann, T. Microtubule dynamics regulation contributes to endothelial morphogenesis. *Bioarchitecture* **2**, 220-227, doi:10.4161/bioa.22335 (2012).

10 Myers, K. A., Applegate, K. T., Danuser, G., Fischer, R. S. & Waterman, C. M. Distinct ECM mechanosensing pathways regulate microtubule dynamics to control endothelial cell branching morphogenesis. *J. Cell Biol.* **192**, 321-334, doi:10.1083/jcb.201006009 (2011).

11 Etienne-Manneville, S. & Hall, A. Integrin-mediated activation of Cdc42 controls cell polarity in migrating astrocytes through PKCzeta. *Cell* **106**, 489-498 (2001).

12 Etienne-Manneville, S. In vitro assay of primary astrocyte migration as a tool to study Rho GTPase function in cell polarization. *Methods Enzymol* **406**, 565-578, doi:10.1016/S0076-6879(06)06044-7 (2006).

13 Bance, B., Seetharaman, S., Leduc, C., Boëda, B. & Etienne-Manneville, S. Microtubule acetylation but not detyrosination promotes focal adhesion dynamics and astrocyte migration. *Journal of Cell Science* **132**, jcs.225805, doi:10.1242/jcs.225805 (2019).

14 Coombes, C. *et al.* Mechanism of microtubule lumen entry for the α-tubulin acetyltransferase enzyme αTAT1. *Proceedings of the National Academy of Sciences* **113**, E7176-E7184, doi:10.1073/pnas.1605397113 (2016).

15 Valenzuela-Fernandez, A., Cabrero, J. R., Serrador, J. M. & Sánchez-Madrid, F. HDAC6: a key regulator of cytoskeleton, cell migration and cell–cell interactions. *Trends Cell Biol.* **18**, 291-297 (2008).

16 Haggarty, S. J., Koeller, K. M., Wong, J. C., Butcher, R. A. & Schreiber, S. L. Multidimensional Chemical Genetic Analysis of Diversity-Oriented Synthesis-Derived Deacetylase Inhibitors Using Cell-Based Assays. *Chem. Biol.* **10**, 383-396, doi:10.1016/S1074-5521(03)00095-4 (2003).

17 Haggarty, S. J., Koeller, K. M., Wong, J. C., Grozinger, C. M. & Schreiber, S. L. Domain-selective small-molecule inhibitor of histone deacetylase 6 (HDAC6)-mediated tubulin deacetylation. *Proceedings of the National Academy of Sciences* **100**, 4389-4394, doi:10.1073/pnas.0430973100 (2003).

18 De Pascalis, C. & Etienne-Manneville, S. Single and collective cell migration: the mechanics of adhesions. *Mol Biol Cell* **28**, 1833-1846, doi:10.1091/mbc.E17-03-0134 (2017).

19 Seetharaman, S. & Etienne-Manneville, S. Integrin diversity brings specificity in mechanotransduction. *Biol. Cell* **110**, 49-64, doi:10.1111/boc.201700060 (2018).

20 Cluzel, C. *et al.* The mechanisms and dynamics of αvβ3 integrin clustering in living cells. *J. Cell Biol.* **171**, 383-392, doi:10.1083/jcb.200503017 (2005).
21 Janke, C. & Montagnac, G. Causes and Consequences of Microtubule Acetylation. *Curr. Biol.* **27**, R1287-R1292 (2017).
22 Enomoto, T. Microtubule disruption induces the formation of actin stress fibers and focal adhesions in cultured cells: possible involvement of the rho signal cascade. *Cell Struct Funct* **21**, 317-326 (1996).
23 Bershadsky, A., Chausovsky, A., Becker, E., Lyubimova, A. & Geiger, B. Involvement of microtubules in the control of adhesion-dependent signal transduction. *Curr. Biol.* **6**, 1279-1289, doi:https://doi.org/10.1016/S0960-9822(02)70714-8 (1996).
24 Choquet, D., Felsenfeld, D. P. & Sheetz, M. P. Extracellular matrix rigidity causes strengthening of integrin-cytoskeleton linkages. *Cell* **88**, 39-48 (1997).
25 Wolfenson, H. *et al.* Tropomyosin controls sarcomere-like contractions for rigidity sensing and suppressing growth on soft matrices. *Nat. Cell Biol.* **18**, 33-42, doi:10.1038/ncb3277 (2016).
26 Peglion, F., Llense, F. & Etienne-Manneville, S. Adherens junction treadmilling during collective migration. *Nat. Cell Biol.* **16**, 639 (2014).
27 Dupont, S. *et al.* Role of YAP/TAZ in mechanotransduction. *Nature* **474**, 179-183, doi:10.1038/nature10137 (2011).
28 Panciera, T., Azzolin, L., Cordenonsi, M. & Piccolo, S. Mechanobiology of YAP and TAZ in physiology and disease. *Nature Reviews Molecular Cell Biology* **18**, 758-770, doi:10.1038/nrm.2017.87 (2017).
29 Jansen, K. A., Atherton, P. & Ballestrem, C. Mechanotransduction at the cell-matrix interface. *Semin. Cell Dev. Biol.* **71**, 75-83, doi:https://doi.org/10.1016/j.semcdb.2017.07.027 (2017).
30 Prager-Khoutorsky, M. *et al.* Fibroblast polarization is a matrix-rigidity-dependent process controlled by focal adhesion mechanosensing. *Nat. Cell Biol.* **13**, 1457, doi:10.1038/ncb2370 https://www.nature.com/articles/ncb2370#supplementary-information (2011).
31 Tran, A. D.-A. *et al.* HDAC6 deacetylation of tubulin modulates dynamics of cellular adhesions. *Journal of cell science* **120**, 1469-1479 (2007).
32 De Pascalis, C. *et al.* Intermediate filaments control collective migration by restricting traction forces and sustaining cell–cell contacts. *J. Cell Biol.* **217**, 3031-3044, doi:10.1083/jcb.201801162 (2018).
33 Sakamoto, Y., Boëda, B. & Etienne-Manneville, S. APC binds intermediate filaments and is required for their reorganization during cell migration. *J. Cell Biol.* **200**, 249-258 (2013).
34 Schiller, H. B. *et al.* beta1- and alphav-class integrins cooperate to regulate myosin II during rigidity sensing of fibronectin-based microenvironments. *Nat. Cell Biol.* **15**, 625-636, doi:10.1038/ncb2747 (2013).
35 Lawson, C. D. & Ridley, A. J. Rho GTPase signaling complexes in cell migration and invasion. *J. Cell Biol.* **217**, 447-457, doi:10.1083/jcb.201612069 (2018).
36 Krendel, M., Zenke, F. T. & Bokoch, G. M. Nucleotide exchange factor GEF-H1 mediates cross-talk between microtubules and the actin cytoskeleton. *Nat Cell Biol* **4**, 294-301 (2002).
37 Ren, Y., Li, R., Zheng, Y. & Busch, H. Cloning and characterization of GEF-H1, a microtubule-associated guanine nucleotide exchange factor for Rac and Rho GTPases. *J Biol Chem* **273**, 34954-34960 (1998).
38 Heck, J. N. *et al.* Microtubules regulate GEF-H1 in response to extracellular matrix stiffness. *Mol. Biol. Cell* **23**, 2583-2592, doi:10.1091/mbc.E11-10-0876 (2012).
39 Rafiq, N. B. M. *et al.* A mechano-signalling network linking microtubules, myosin IIA filaments and integrin-based adhesions. *Nature materials* **18**, 638-649, doi:10.1038/s41563-019-0371-y (2019).

40 Jiu, Y. *et al.* Vimentin intermediate filaments control actin stress fiber assembly through GEF-H1 and RhoA. **130**, 892-902, doi:10.1242/jcs.196881 (2017).
41 Trepat, X. *et al.* Physical forces during collective cell migration. *Nature Physics* **5**, 426-430, doi:10.1038/nphys1269 (2009).
42 Legerstee, K., Geverts, B., Slotman, J. A. & Houtsmuller, A. B. Dynamics and distribution of paxillin, vinculin, zyxin and VASP depend on focal adhesion location and orientation. *Scientific reports* **9**, 10460, doi:10.1038/s41598-019-46905-2 (2019).
43 Barriga, E. H., Franze, K., Charras, G. & Mayor, R. Tissue stiffening coordinates morphogenesis by triggering collective cell migration in vivo. *Nature* **554**, 523-527, doi:10.1038/nature25742 (2018).
44 Leal-Egaña, A. *et al.* The size-speed-force relationship governs migratory cell response to tumorigenic factors. *Mol. Biol. Cell* **28**, 1612-1621, doi:10.1091/mbc.E16-10-0694 (2017).
45 Sunyer, R. *et al.* Collective cell durotaxis emerges from long-range intercellular force transmission. *Science* **353**, 1157-1161, doi:10.1126/science.aaf7119 (2016).
46 Serra-Picamal, X., Conte, V., Sunyer, R., Muñoz, J. J. & Trepat, X. in *Methods Cell Biol.* Vol. 125 309-330 (Elsevier, 2015).
47 Tambe, D. T. *et al.* Collective cell guidance by cooperative intercellular forces. *Nat. Mater.* **10**, 469 (2011).
48 Heuser, J. The production of 'cell cortices' for light and electron microscopy. *Traffic* **1**, 545-552, doi:10.1034/j.1600-0854.2000.010704.x (2000).
49 Martiel, J. L. *et al.* Measurement of cell traction forces with ImageJ. *Methods Cell Biol* **125**, 269-287, doi:10.1016/bs.mcb.2014.10.008 (2015).
50 Poullet, P., Carpentier, S. & Barillot, E. myProMS, a web server for management and validation of mass spectrometry-based proteomic data. *Proteomics* **7**, 2553-2556, doi:10.1002/pmic.200600784 (2007).
51 Valot, B., Langella, O., Nano, E. & Zivy, M. MassChroQ: a versatile tool for mass spectrometry quantification. *Proteomics* **11**, 3572-3577, doi:10.1002/pmic.201100120 (2011).
52 Vizcaino, J. A. *et al.* 2016 update of the PRIDE database and its related tools. *Nucleic Acids Res* **44**, D447-456, doi:10.1093/nar/gkv1145 (2016).
53 Perez-Riverol, Y. *et al.* The PRIDE database and related tools and resources in 2019: improving support for quantification data. *Nucleic Acids Res.* **47**, D442-d450, doi:10.1093/nar/gky1106 (2019).

Acknowledgements

This work was supported by the La Ligue contre le cancer (S-CR17017), Centre National de la Recherche Scientifique and Institut Pasteur. SS is funded by the ITN PolarNet Marie Curie grant and Fondation pour la Recherche Médicale (FDT201904007930) and was enrolled at the Ecole Doctorale FIRE Frontières de l'Innovation en Recherche et Éducation (Frontières du Vivant FdV – Programme Bettencourt), CRI and the Université de Paris. We would like to thank Anna Akhmanova for providing GFP-Talin construct, Cécile Leduc for FA distribution macro, Bertille Bance and Franck Coumailleau for discussions, Nisha Mohd Rafiq for fixation protocols and discussions, Emma van Bodegraven for critical reading of the manuscript and discussions.

Author contributions

S.S. designed, performed experiments, analysed and interpreted the results, and wrote the paper; B.V. assisted in the setup of TFM experiments and analysis, helped with data interpretation and discussions; V.R. performed immunoprecipitation and pull down experiments; A. F. carried out a part of the experiments using HUVECs; C. D-P helped with experimental techniques and discussions; B. B optimised the GFP-nanobody and IP conditions used for mass spectrometry sample preparation and set up the chemical wound assay; F. D. carried out the MS experimental work; D. L. supervised the MS experiments and data analysis; S.V. performed EM experiments; A. B. helped with data interpretation and discussions; M.T. provided ideas, helped with data interpretation and discussions; S. E-M. supervised the project, interpreted the results, and wrote the paper.

Competing interests

Authors declare no competing interests.

Main figure legends

Figure 1: Integrin-mediated signalling and substrate rigidity regulate microtubule acetylation. **a, b, c**. Astrocytes (WT) or treated with **c (i, ii).** Ctl, Src kin 1 or PF-562271, plated on PAA gels; **(a. i, c. i)** images showing Acetylated tubulin and α-tubulin; **(b. i, b. ii)** western blots showing normalised ratio of acetylated tubulin over GAPDH. **(a)** n = 77 for 1.26 kPa, 88 for 2 kPa, 67 for 9 kPa and 81 for 48 kPa; **(c)** n = 30 for Ctl, 43 for Src kin1, 43 for PF-562271. **d, e.** Astrocyte lysate pulldown (PD; WT cells) and immunoprecipitations (cells transfected with GFP-Ctl or GFP-αTAT1), using (d) GST-αTAT1 and (e) GFP-αTAT1 resin respectively. Westerns showing Talin and Acetylated tubulin. **f.** Images of GFP-αTAT1 and mCherry-vinculin astrocytes transfected along with siCtl or siTalin1. **g.** Astrocytes on 48 kPa PAA gels showing **(g. i)** Acetylated tubulin and α-tubulin; **(g. ii)** ratio of the intensities of Acetylated tubulin over total Tubulin intensity; n = 51 for siCtl and 56 for siTalin1. **h.** Pulldown (PD; Ctl or Y-27632 treated cells) using GST-αTAT1 resin; **(h. i)** Westerns showing Talin and Ponceau staining; **(h. ii)** normalised Talin in DMSO (Ctl) and Y-27632 treated cells. **i.** Images showing GFP-αTAT1 and mCherry-vinculin expressing astrocytes treated with DMSO (Ctl) or Y-27632. **j, k.** Migrating astrocytes, treated with DMSO (Ctl) or ROCK inhibitor Y-27632 for 2 h; **(j)** Western blot showing the levels of Acetylated tubulin and GAPDH in Ctl or Y-27632 treated cells; **(k. i, ii)** ratio of the intensities of Acetylated tubulin over total Tubulin intensity; n = 98 for Ctl, 79 for Y-27632 treated cells respectively. **Scale bar** (a, c, g): 10 µm, (f, k): 20 µm. **Number of independent experiments** = 4 (for a, h), 5 (for b, i), 2 (for c), 3 (for d-g, j, k). In box-and-whisker plots, box extends from the 25^{th} to 75^{th} percentile, whiskers show minimum and maximum values, and the line within the box represents the median. **Statistical tests**: One-way ANOVA followed by Tukey's multiple comparison's test (for a, b, g), Paired t-test (for h), Unpaired Student's t-test (two-tailed; for k).

Figure 2: Microtubule acetylation tunes cell mechanosensitivity. **a, b.** Astrocytes transfected with siCtl and siαTAT1-2, or treated with NilTubacin and Tubacin, or **c.** HUVECs treated with NilTubacin and Tubacin plated on PAA gels of different rigidities; **(a-c. i)** stained for YAP and α-tubulin (not shown) to mark the cell boundary (marked by dotted lines); **(a-c. ii)** ratio of the YAP intensity in the nucleus over cytoplasm; (a) n = 49 for 2 kPa siCtl, 44 for 2 kPa siαTAT1-2, 68 for 48 kPa siCtl, 74 for 48 kPa siαTAT1-2; (b) n = 49 for 2 kPa Niltubacin, 53 for 2 kPa Tubacin, 51 for 48 kPa Niltubacin and 51 for 48 kPa Tubacin; (c) n = 26 for 2 kPa Niltubacin, 25 for 2 kPa Tubacin, 32 for 48 kPa Niltubacin and 26 for 48 kPa Tubacin. **d.** Astrocytes (WT) plated on PAA gels of different rigidities, **(d. i)** stained for α-tubulin and Talin. Images shown correspond to the same cells depicted in Fig. 1A; **(d. ii)** FA density in different regions of the cells; n = 40 for 1.26 kPa, 51 for 2 kPa, 94 for 9 kPa, 77 for 48 kPa. **e, f.** Astrocytes transfected with siCtl and siαTAT1-2, or treated with Niltubacin and Tubacin, plated on PAA gels of different substrate rigidities, and **(e. i, f. i)** stained for Paxillin; **(e. ii, f. ii)** FA density (number of FAs/μm^2) in the central region (16 µm-cell center) of cells depicted in panels e and f; n = 60 for 1.26 kPa siCtl, 36 for 1.26 kPa siαTAT1-2, 54 for 48 kPa siCtl and 47 for 48 kPa siαTAT1-2; n = 59 for 1.26 kPa Niltubacin, 55 for 1.26 kPa Tubacin, 46 for 48 kPa Niltubacin and 37 for 48 kPa Tubacin. **g.** Schematic (summarising a-f) showing focal adhesion distribution upon manipulation of microtubule acetylation. **Scale bar** (a-f): 10 µm; **Number of independent experiments** = 3 (for a, b, d-f), 2 (for c); In box-and-whisker plots, box extends from the 25^{th} to 75^{th} percentile, whiskers show minimum and maximum values, and the line within the box represents the median; **Statistical tests:** one-way ANOVA followed by Tukey's multiple comparison's test (for a, b, e, f), two-way ANOVA followed by Tukey's multiple comparison's test (for d).

Figure 3: Microtubule acetylation reorganises the actomyosin and intermediate filament networks. **a, b, c.** Astrocytes transfected with siCtl or siαTAT1, and stained for **(a. i)** Actin, pMLC and Paxillin; **(b)** Myosin IIa, Acetylated tubulin and α-tubulin; **(c)** Vimentin and α-tubulin; **(a. ii)** percentage of cells with

826 inter-junctional transverse arcs; n = 199 for siCtl and 159 siαTAT1-2. **d.** Ultrastructural organization of
827 focal adhesion-associated cytoskeleton in siCtl or siαTAT1-2 depleted cells; **d (i)** Platinum replica
828 electron microscopy (PREM) survey view of the cytoplasmic surface of the leading edge in siCtl unroofed
829 cells. Boxed regions correspond to focal adhesions. Extracellular space is pseudo-coloured in purple. (1,
830 2) High magnification views corresponding to the boxed regions in panel (i). White arrows indicate
831 microtubules and yellow arrowheads denote intermediate filaments. (3) Zoom-in region corresponding
832 to the boxed region in marked in region (2). Scale bar: 1 µm. White arrows indicate microtubules and
833 yellow arrowheads denote intermediate filaments. Scale bar: 2 µm and 1 µm. **d (ii, iii)** PREM survey view
834 of the cytoplasmic surface of the leading edge in αTAT1-depleted cells. Extracellular space is pseudo-
835 coloured in purple. Scale bars: 10 µm, 1 µm (inset). (4, 5) High magnification views corresponding to the
836 boxed regions in panel ii and iii respectively. Scale bar: 1 µm. **e.** HUVECs treated with DMSO or Tubacin,
837 stained for Actin, Vinculin and Myosin IIA. **f.** Astrocytes treated with Niltubacin or Tubacin, stained for
838 Actin and Paxillin. **Scale bar** (a-c): 20 µm, (e, f): 10 µm. In box-and-whisker plots, box extends from the
839 25^{th} to 75^{th} percentile, whiskers show minimum and maximum values, and the line within the box
840 represents the median. **Number of independent experiments** = 3 (for a-c); **Statistical tests**: Paired
841 Student's t-test (two-tailed; for a).

842

843 ***Figure 4: Microtubule acetylation promotes traction force generation and Rho activation.*** **a, b, c, d. (a-**
844 **d. i)** Stress-field maps of astrocytes on crossbow-shaped micropatterned PAA gels of different rigidities,
845 transfected with (a) siCtl and siαTAT1-2, (b) siCtl + GFP-αTAT1 and siαTAT1-2 + GFP-αTAT1, or treated
846 with (c) Niltubacin and Tubacin; or (d) HUVECs treated with Niltubacin and Tubacin; **(a, b, c. ii, d. ii)**
847 corresponding stored energies (in Joules, J; within the range of 0 and 5 x 10^{-13} J) of cells in the above
848 mentioned conditions; (a) n = 163 for siCtl and 141 for siαTAT1-2, (b) n = 74 for siCtl + GFP-αTAT1, and
849 70 for siαTAT1-2 + GFP-αTAT1, (c) n = 136 for Niltubacin and 141 for Tubacin, (d) n = 83 for Niltubacin

and 82 for Tubacin. **e.** GST-Rhotekin pulldowns were performed using siCtl or siαTAT1-transfected astrocytes. Western blots showing Red Ponceau and immunoblotted for RhoA. **Scale bar** (a-d): 10 µm; **Number of independent experiments** = 3 (for a-e). In box-and-whisker plots, the box extends from the 25^{th} to the 75^{th} percentile, the whiskers show the minimum and maximum values, and the line within the box represents the median. **Statistical tests**: one-way ANOVA followed by Tukey's multiple comparison's test (for a, b), unpaired Student's t-test (two-tailed; for c, d).

Figure 5: Microtubule acetylation promotes the release of GEF-H1 into the cytosol. **a.** Migrating astrocytes transfected with siCtl, siαTAT1-2, and siαTAT1-2 followed by treatment with Tubacin, **(a. i)** stained for Acetylated tubulin, α-tubulin and GEF-H1; **(a. ii)** percentage of GEF-H1 colocalised with microtubules; n = 99 for siCtl, 89 for siαTAT1-2, 72 for siαTAT1-2 + Tubacin; **b.** HUVECs treated with DMSO Ctl or Tubacin, **(b. i)** stained for α-tubulin and GEF-H1; **(b. ii)** percentage of GEF-H1 colocalised with microtubules; n = 78 for DMSO Ctl and 84 for Tubacin. **c.** Immunoprecipitations using anti-GFP nanobodies were performed with lysates from HEK293 cells transfected with GFP-Ctl or GFP-GEF-H1, and treated with Nocodazole or Tubacin. Samples were analysed by immunoblotting using α-tubulin, Acetylated tubulin, GEF-H1, GAPDH and GFP antibodies. **d.** Astrocytes transfected with siCtl and siαTAT1-2, and plated on 48 kPa PAA gels, **(d. i)** stained for GEF-H1 and α-tubulin; **(d. ii)** percentage of GEF-H1 colocalised with microtubules; n = 100 for 48 kPa siCtl, 112 for 48 kPa siαTAT1-2, 97 for 2 kPa siCtl, 86 for 2 kPa αTAT1-2 (1-2 regions per cell). **Scale bar** (a): 20 µm, (b, d): 10 µm. In box-and-whisker plots, the box extends from the 25^{th} to the 75^{th} percentile, the whiskers show the minimum and maximum values, and the line within the box represents the median. **Number of independent experiments** = 3 (for a-d); **Statistical tests:** Ordinary one-way ANOVA followed by Tukey's multiple comparison's test (for a, d); Unpaired Student's t-test followed by Mann-Whitney test (for b).

Figure 6: Microtubule acetylation is required for mechanosensitive migration. **a, b, c.** Phase contrast images of **(a, b. i)** Astrocytes (WT) or **(c. i)** transfected with siCtl or siαTAT1 migrating in a chemical wound assay on PAA gels of different rigidities for 24 h (pink and orange dotted lines show initial and final wound edge); **(b. ii, c. ii)** migration speed (in µm/min) of cells at the wound edge; n = 123 for 2 kPa WT, 117 for 9 kPa WT, 115 for 48 kPa WT, 91 for 2 kPa siCtl, 95 for 2 kPa siαTAT1-2, 93 for 48 kPa siCtl, 93 for 48 kPa siαTAT1-2. **Scale bar** (a): 200 µm, (b, c): 100 µm. **Number of independent experiments** = 3 (for b, c); **Statistical tests:** one-way ANOVA followed by Tukey's multiple comparison's test. In box-and-whisker plots, the box extends from the 25^{th} to the 75^{th} percentile, the whiskers show the minimum and maximum values, and the line within the box represents the median. **d. Proposed working model**: Cells sensing a soft substrate (d. i), with altered integrin-signalling (d. ii) exhibit less MT acetylation (d. iii). This results in GEF-H1 being bound to MTs (d. iv) and is therefore, unable to activate RhoA (d. v), which renders the cell less contractile (d. vi). In such conditions, cells generate a low amount of traction forces (d. vii) and migrate slower (d. viii). On the other hand, on stiff substrates, integrin- and talin-mediated rigidity sensing (d. i) promotes the tension-dependent recruitment of αTAT1 to FAs (d. ii) and increased microtubule acetylation (d. iii). How αTAT1 enters the lumen of microtubules still remains unclear although one can speculate that the recruitment of αTAT1 at FAs increases the local cytosolic pool of the protein which can then enter microtubules through microtubule lattice defects or through the open ends of microtubules in close proximity to FAs (Extended Data Fig. 5C). Microtubule acetylation triggers the release of GEF-H1 from MTs (d. iv), which activates the RhoA-ROCK-myosin II pathway (d. v) to promote actomyosin contractility (d. vi), traction forces (d. vii) and cell migration (d. viii). Active GEF-H1, RhoA and ROCK are depicted in bold.

Extended data figure legends

Extended Data Figure 1: **a, b. (a. i)** Schematic and **(a. ii, b. i)** western blots showing **(a)** acetylation and **(b)** αTAT1 levels using two distinct sets of siRNAs targeting αTAT1 (siαTAT1-1 and siαTAT1-2), and Tubacin (an inhibitor of HDAC6 (deacetylase)); **(a. iii, a. iv)** ratio of the acetylated tubulin or **(b. ii)** αTAT1 intensity over GAPDH intensity, normalised to the values observed for the respective controls. **c.** Migrating astrocytes transfected with siCtl, **(c. i)** siαTAT1-1 and **(c. ii)** siαTAT1-2, or treated with Tubacin prior to wounding, showing acetylated tubulin and α-tubulin. **d.** Astrocytes plated on PAA gels of different rigidities and treated with Tubacin; ratio of the intensities of Acetylated tubulin over total Tubulin of each cell; n = 49 for 1.26 kPa WT, 51 for 1.26 kPa Tubacin, 72 for 48 kPa WT, 66 for 48 kPa Tubacin. **e.** siCtl or WT astrocytes plated on crossbow-shaped micropatterned hydrogels of different rigidities, **(e. i)** showing Acetylated tubulin and α-tubulin; **(e. ii)** ratio of the intensities of Acetylated tubulin over total Tubulin of each cell; n = 86 for 2 kPa and 103 for 48 kPa. **f.** Astrocytes plated on PAA gels of different rigidities, **(f. i)** stained with Detyrosinated tubulin and α-tubulin; **(f. ii)** ratio of Detyrosinated tubulin over total tubulin intensities in each cell; n = 39 for 2 kPa, 31 for 9 kPa and 40 for 48 kPa. **g. (g. i)** Western blots showing the levels of Detyrosinated tubulin and GAPDH in astrocytes plated on PAA gels of different substrate rigidities; **(g. ii)** ratio of the intensities of Detyrosinated tubulin over GAPDH normalised to the values observed for 2 kPa. **Scale bar** (c, e, f): 10 µm; **Number of independent experiments** = 4 (for a - siαTAT1), 6 (for a - Tubacin, c, g), 3 (for b), 5 (for e), 2 (for f). In box-and-whisker plots, box extends from the 25^{th} to 75^{th} percentile, whiskers show minimum and maximum values, and the line within the box represents the median; **Statistical tests:** one-way ANOVA followed by Tukey's multiple comparison's test or Holm-Šídák's multiple comparisons test (a - siαTAT1, b, d, e, g) or Paired Student's t-test (for a - Tubacin).

Extended Data Figure 2: **a, b.** Astrocytes were treated with (a) RGD control or RGD peptides, (b) solvant (Ctl) or $MnCl_2$, and **(a. i, b. i)** stained for acetylated tubulin, α-tubulin, paxillin or DAPI; **(a. ii, b. ii)** ratio of the intensities of Acetylated tubulin over total Tubulin; n = 146 for RGD control, 99 for RGD peptide, 116 for Ctl and 105 for $MnCl_2$. **c, d.** Astrocytes were transfected with siCtl or siβ_1 integrin; **(c. i)** Western blots showing levels of β_1 integrin, Acetylated tubulin and GAPDH; **(c. ii, iii)** ratio of intensities of β_1 integrin or Acetylated tubulin over GAPDH, normalised to the levels in siCtl respectively; **(d. i)** stained for Acetylated tubulin, α-tubulin and DAPI; **(d. ii)** ratio of the intensities of Acetylated tubulin over total Tubulin; n = 122 for siCtl and 117 for siβ_1 integrin. **e.** Astrocytes were treated with Ctl, Src kin 1 or PF-562271; **(e. i)** stained for Acetylated tubulin, α-tubulin and Paxillin; **(e. ii)** ratio of the intensities of Acetylated tubulin over total Tubulin intensity; n = 78 for Ctl, 70 for Src kin 1, 79 for PF-562271. **f.** Astrocytes were plated on 48 kPa gels and treated with Ctl or Src kin 1. **(f. i)** Western blots showing the levels of Acetylated tubulin and GAPDH; **(f. ii)** ratio of the intensities of Acetylated tubulin over GAPDH normalised to the Ctl. **g.** Volcano plot analysis showing fold changes (GFP-αTAT1/GFP-Ctl) of the quantified proteins with threshold of >3 peptides, minimum absolute fold change of 1.5 (green lines) and maximum adjusted p-value of 0.05 (red line). Enriched protein interactors related to GO:0005925 focal adhesion (red boxes; ratio = 1.98 and p = 7.89×10^{-5}). External plots show proteins with peptides identified only in one sample type (left in GFP-Ctl and right in GFP-αTAT1). **h, i.** Normalised Talin interaction in (h) GST-pulldown and (i) GFP-immunoprecipitations. **j.** Western blots **(j. i)** showing the levels of Talin and GAPDH in astrocytes transfected with siCtl and siTalin; **(j. ii)** ratio of the intensities of Talin over GAPDH normalised to the Ctl. **k, l.** Astrocytes showing **(k)** GFP-αTAT1 localisation by epifluorescence, on microtubules, **(l)** by TIRF, at FAs, in cells treated with or without nocodazole. **Scale bar** (a, b, d, e, k, l): 10 µm; **Number of independent experiments** = 3 (for a-d, h-j), 2 (for e), 4 (for f, g), 5 (for l). In box-and-whisker plots, the box extends from the 25th to the 75th percentile, whiskers show the

minimum and maximum values, and the line within the box represents the median; **Statistical tests:** Student's t-test (for a-j).

Extended Data Figure 3: **a.** HUVECs plated on different substrate rigidities and **(a. i)** stained for Acetylated tubulin (insets shown) and α-Tubulin; **(a. ii)** ratio of the intensities of Acetylated tubulin over total Tubulin of each cell; n = 46 for 2 kPa WT and 70 for 48 kPa. **b.** HUVECs treated with Niltubacin (Ctl) or Tubacin, and stained for Acetylated tubulin (insets shown), α-tubulin and Paxillin. **c.** Western blots showing **(c. i)** Acetylated and α-tubulin levels in HUVECs treated with DMSO (Ctl) and Tubacin; **(c. ii)** ratio of intensities of Acetylated tubulin over α-tubulin. **d.** Schematic representation of the different cell regions used to quantify FA density (Fig. 2D-F). **e, f.** Graphs show FA density (number of FAs/μm^2) in different regions of astrocytes transfected with siCtl or siαTAT1-2, or treated with Niltubacin or Tubacin, and plated on 1.26 kPa or 48 kPa substrates. **g, h.** Graphs show FA density (number of FAs/μm^2) in different regions of astrocytes transfected with siCtl or siαTAT1-1, and plated on 1.26 kPa or 48 kPa substrates. **i.** siCtl or siαTAT1-2-transfected astrocytes plated on crossbow-shaped micropatterned polyacrylamide gels of 40 kPa or 2 kPa, **(i. i)** stained with Paxillin and α-tubulin; **(i. ii)** FA density (number of FAs/μm^2) within 8-16 µm layer of the cell, or **(i. iii)** in different regions of astrocytes transfected with siCtl or siαTAT1-2, and plated on 2 kPa or 40 kPa substrates. **Scale bar** (a, b, i): 10 µm. **Number of independent experiments** = 2 (for a), 3 (for b, e-i). In box-and-whisker plots, the box extends from the 25^{th} to the 75^{th} percentile, the whiskers show the minimum and maximum values, and the line within the box represents the median. **Statistical tests:** Paired Student's t-test (for c), one-way ANOVA followed by Tukey's multiple comparisons test (for e-i).

Extended Data Figure 4: **a.** Astrocytes transfected with siCtl or siαTAT1-1, and **(a. i)** stained for Actin, Paxillin and Myosin IIa; **(a. ii)** percentage of siCtl or siαTAT1-transfected astrocytes with transverse interjunctional actin arcs; n = 191 for siCtl and 125 for siαTAT1-1; **Scale bar**: 10 μm. **Number of independent experiments** = 3; **Statistical test:** Paired Student's t-test (two-tailed).

Extended Data Figure 5: **a.** Migrating astrocytes transfected with siCtl, siαTAT1-1 and siαTAT1-1 treated with Tubacin, **(a. i)** stained for Acetylated tubulin, α-tubulin and GEF-H1; **(a. ii)** percentage of GEF-H1 colocalised with microtubules; n = 119 for siCtl, 131 for siαTAT1-1, 103 for siαTAT1-1 + Tubacin. **b.** Astrocytes transfected with siCtl and siαTAT1-2, and plated on 2 kPa PAA gels, stained for GEF-H1 and α-tubulin. **c.** Ultrastructural organization of a focal adhesion at the leading edge of a control astrocyte. Platinum replica electron microscopy (PREM) high magnification view of a focal adhesion on the cytoplasmic surface of the leading edge in siCtl unroofed astrocytes. Microtubules are both coloured in purple and indicated by white arrowheads. **d.** Traction forces in astrocytes plated on micropatterned polyacrylamide gels of different rigidities; traction forces for cells on different rigidities; Values for 2 kPa and 48 kPa are from experiments shown in Fig. 4a and 4b, pooled along with the values for 50 kPa, 91.8 kPa and 121 kPa; n = 136 for 2 kPa Niltubacin, 163 for 48 kPa siCtl, 31 for 50 kPa WT, 33 for 91.8 kPa WT and 30 for 121 kPa WT. In box-and-whisker plots, the box extends from the 25^{th} to the 75^{th} percentile, the whiskers show the minimum and maximum values, and the line within the box represents the median. **Scale bar** (a, b): 10 μm, (c): 200 nm; **Number of independent experiments** = 3 (for a, b, d - 2 kPa Niltubacin and 48 kPa siCtl), 2 (for d - 50 kPa, 91.8 kPa and 121 kPa). **Statistical tests:** One-way ANOVA followed by Tukey's multiple comparison's test (for a).

985

986

Figure 1

a (i)

1.26 kPa

Acetyl tub

Tub

48 kPa

Acetyl tub

Tub

Astrocytes

a (ii)

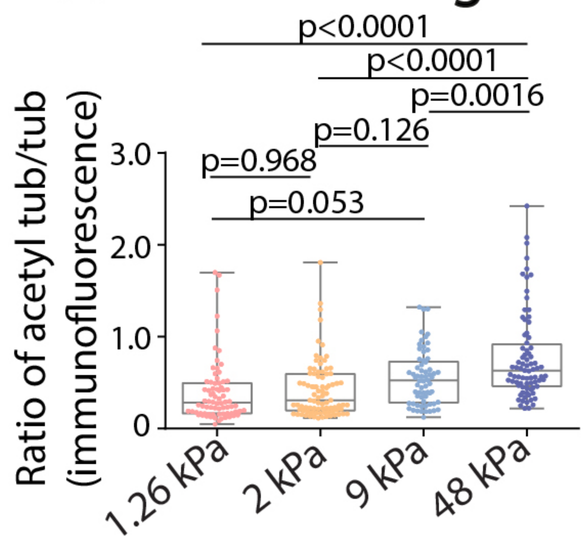

b (i)

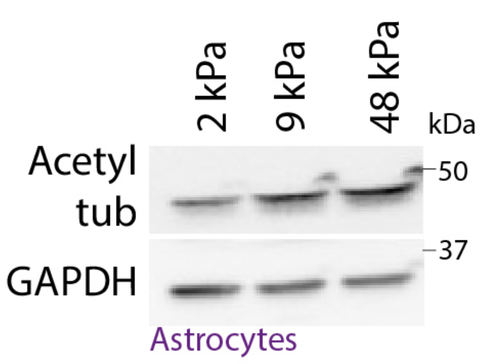

Astrocytes

b (ii)

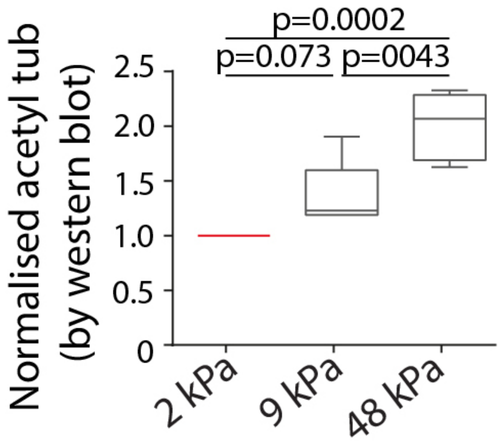

c (i)

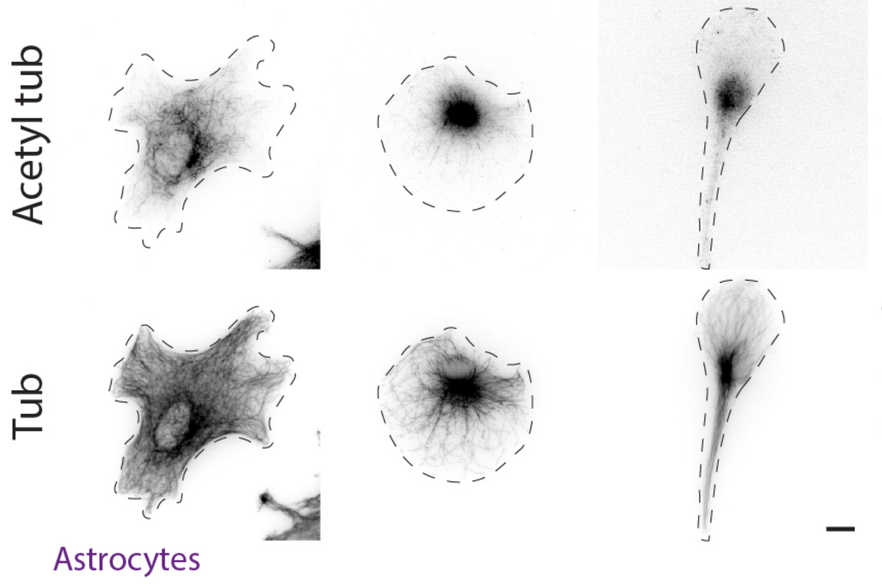

Astrocytes

c (ii)

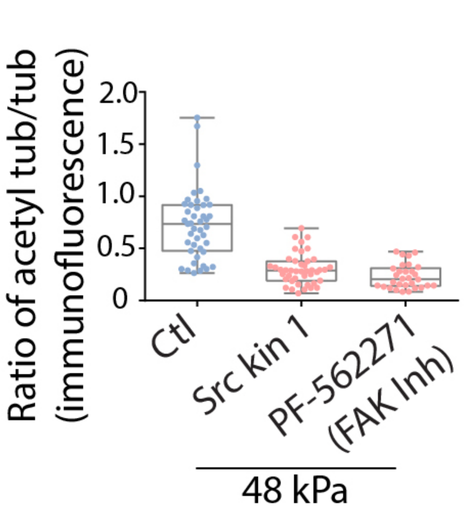

d

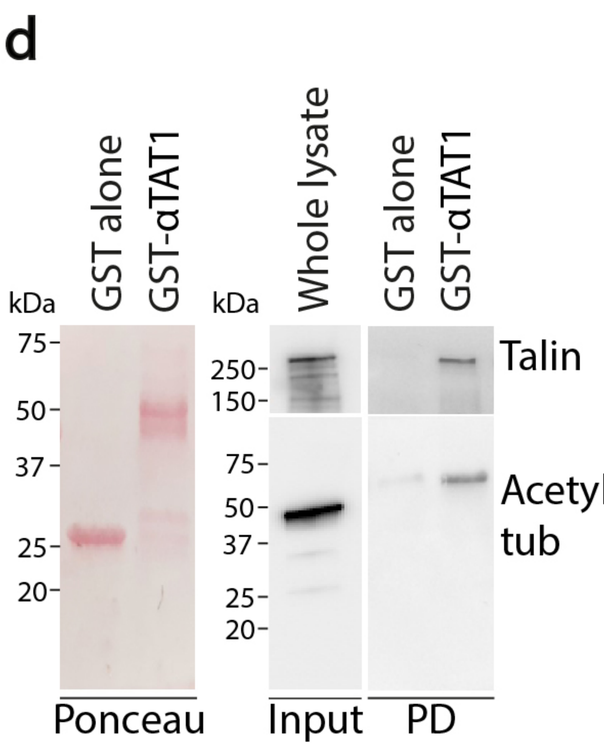

Astrocytes

e

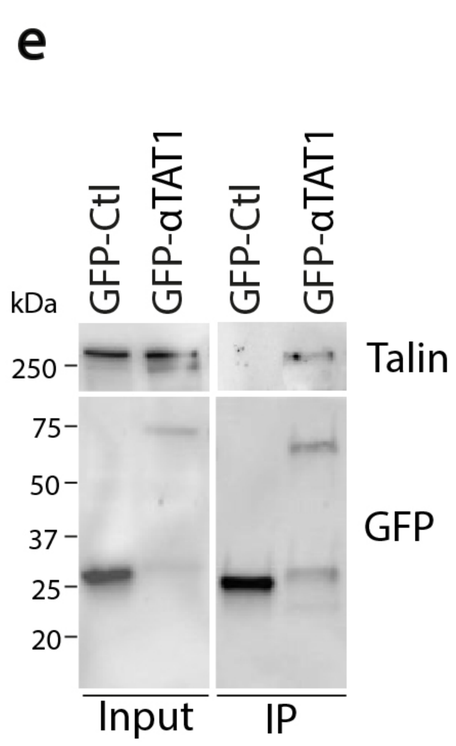

Astrocytes

f

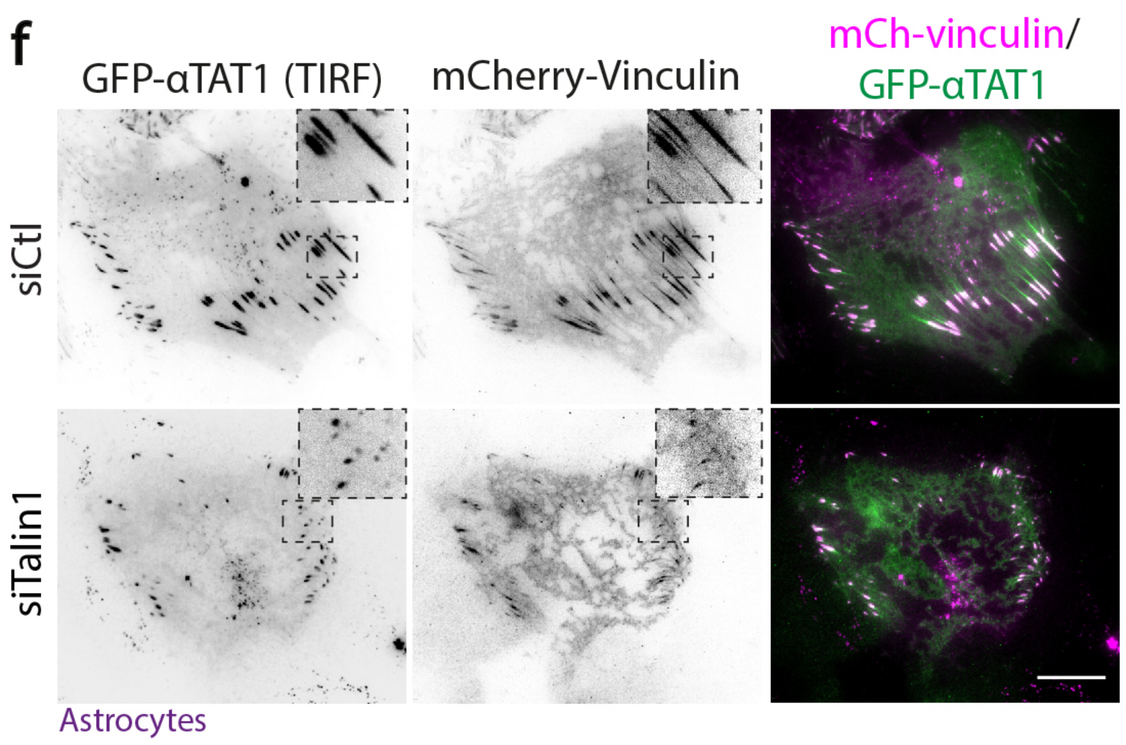

Astrocytes

g (i)

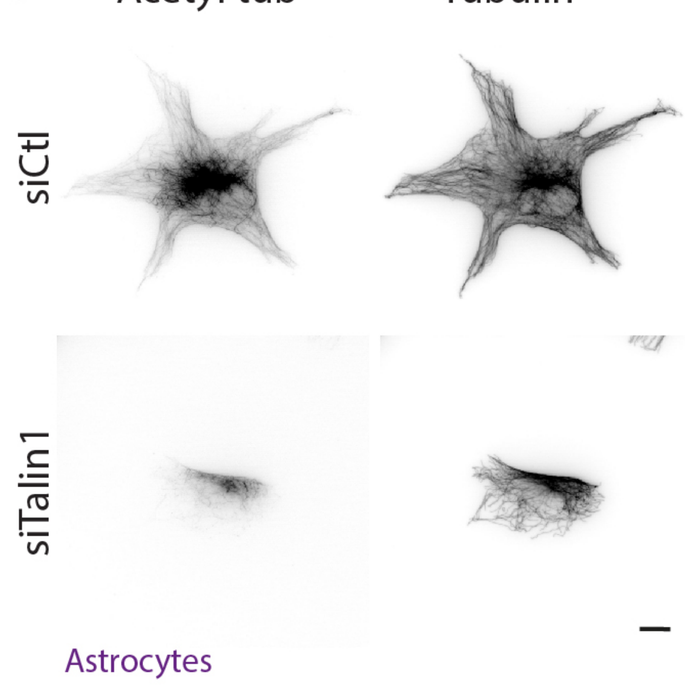

Astrocytes

g (ii)

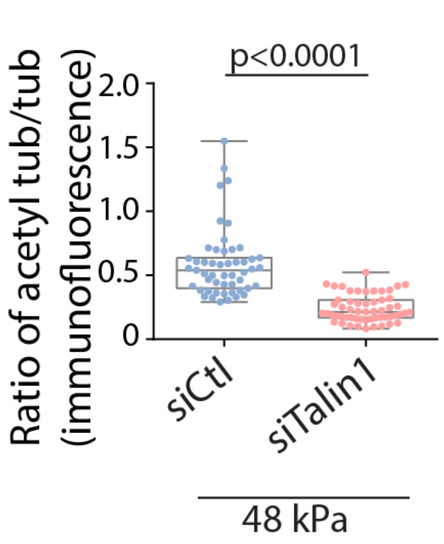

h (i)

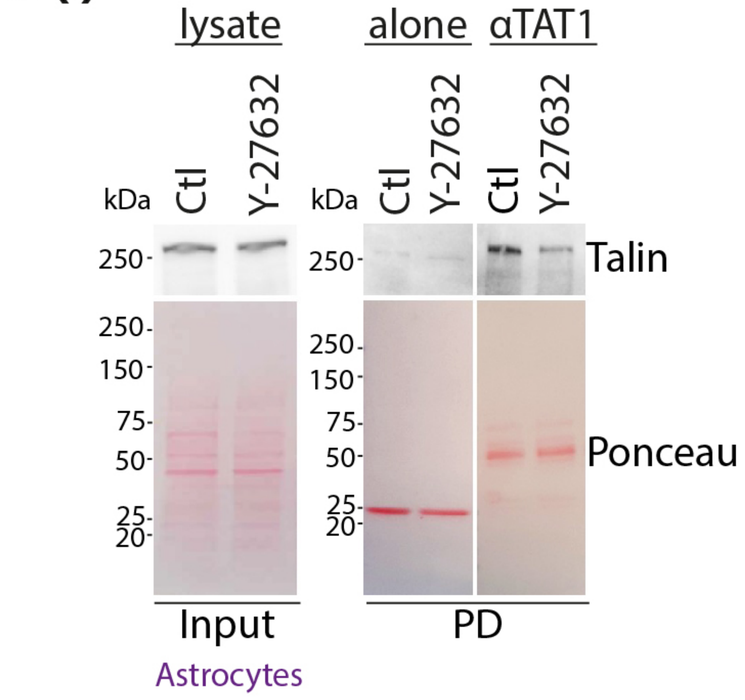

Astrocytes

h (ii)

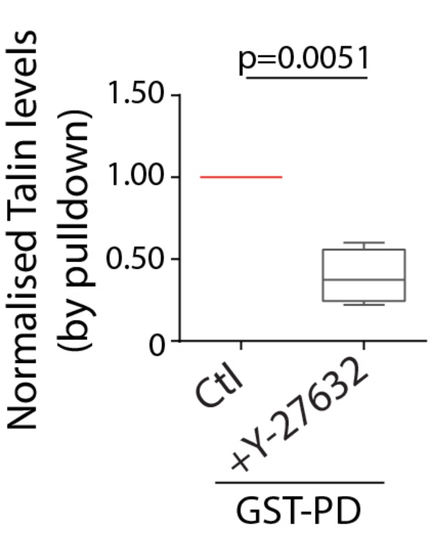

i

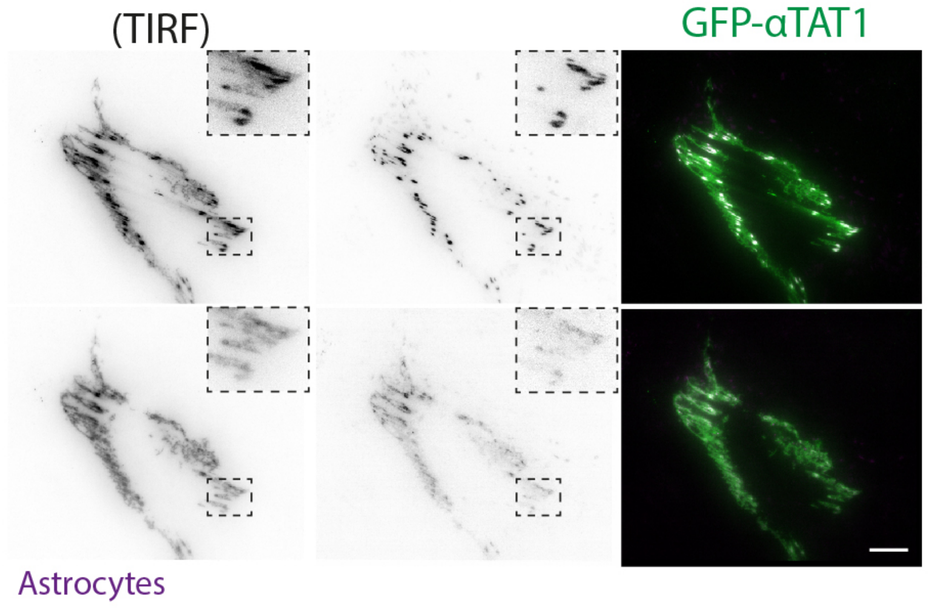

Astrocytes

j

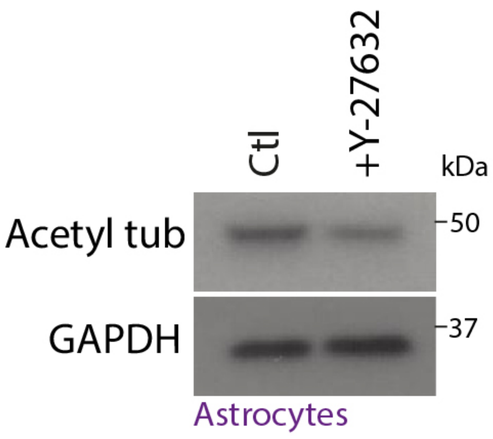

Astrocytes

k (i)

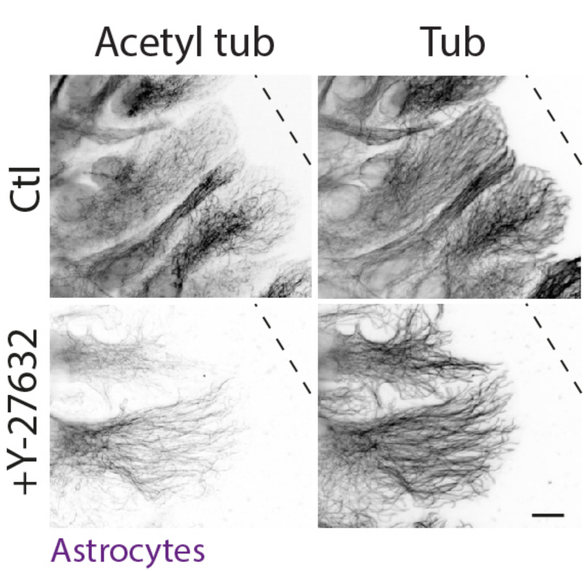

Astrocytes

k (ii)

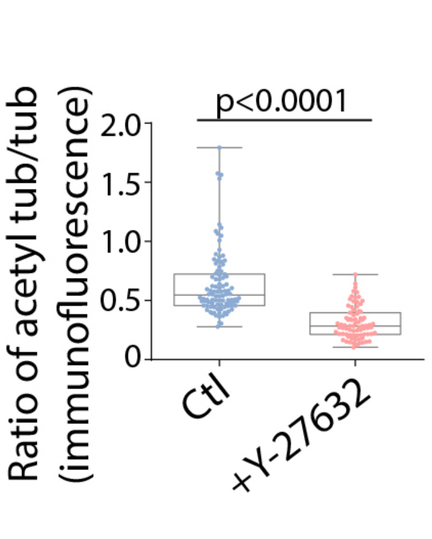

Figure 2

a (i)

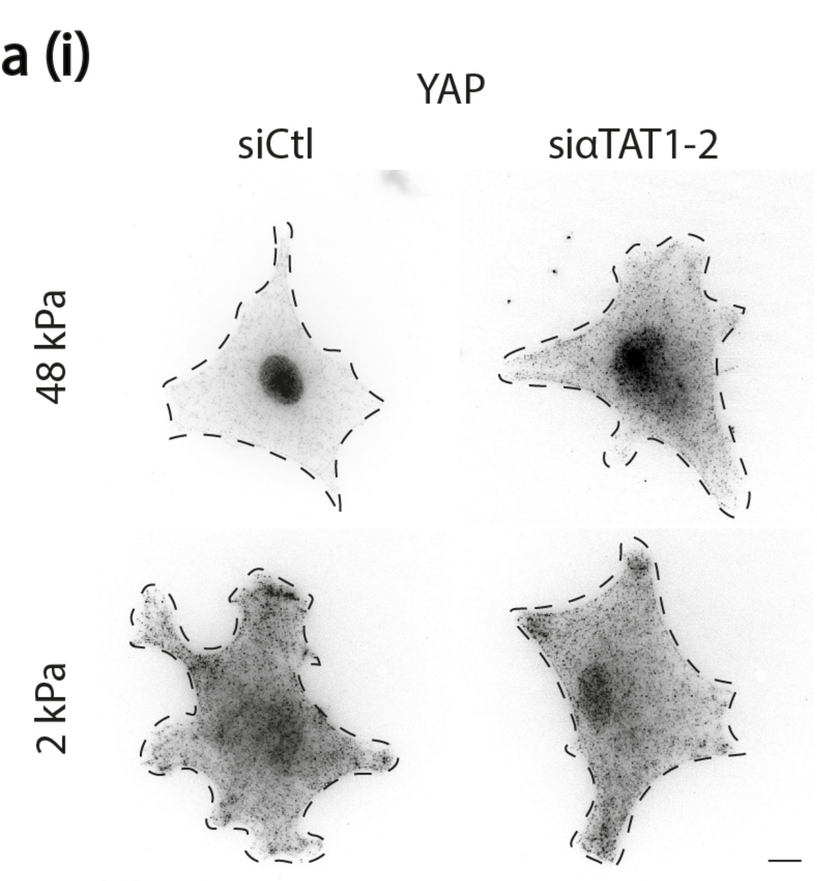

b (i)

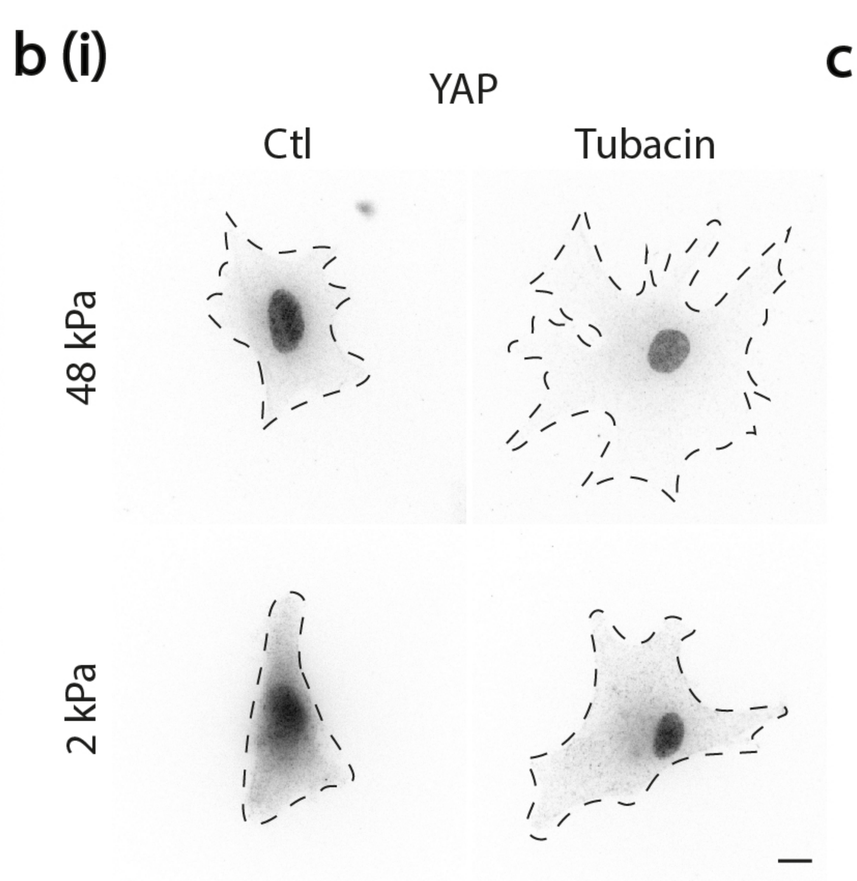

c (i)

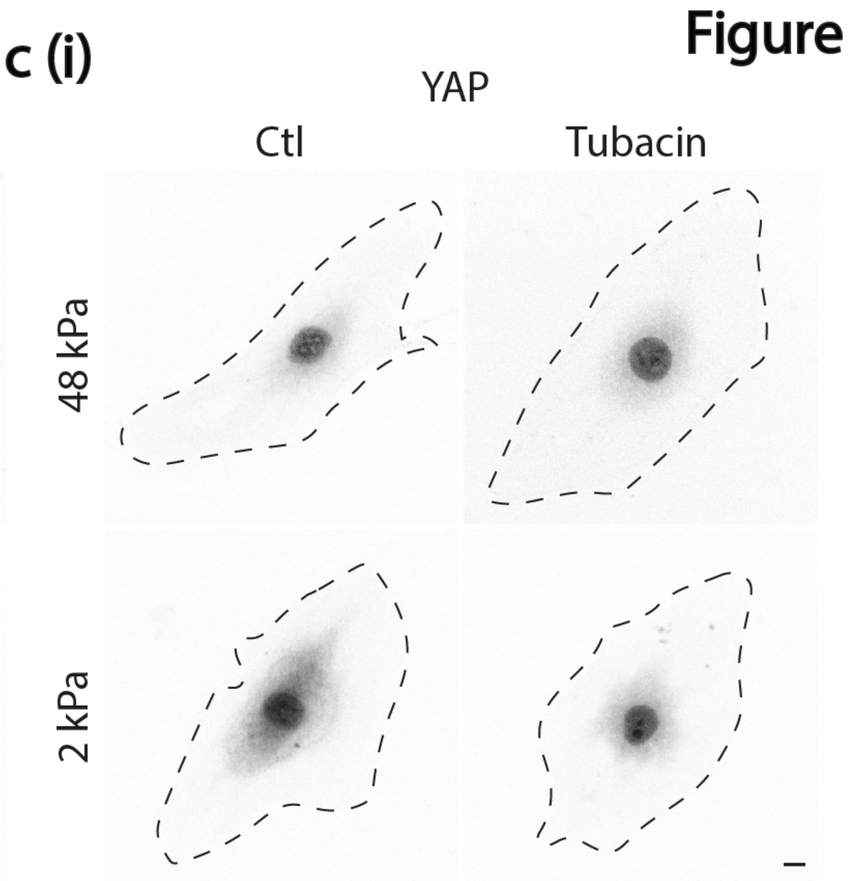

Astrocytes

a (ii)

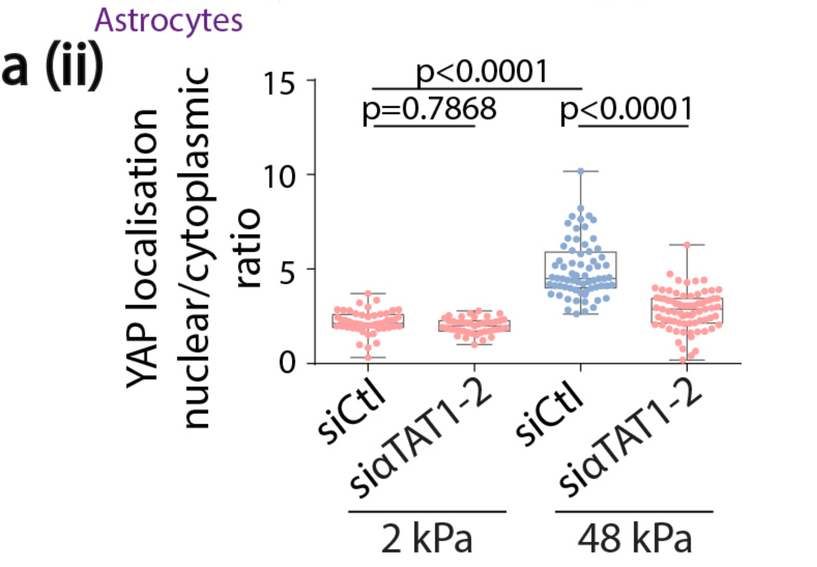

Astrocytes

b (ii)

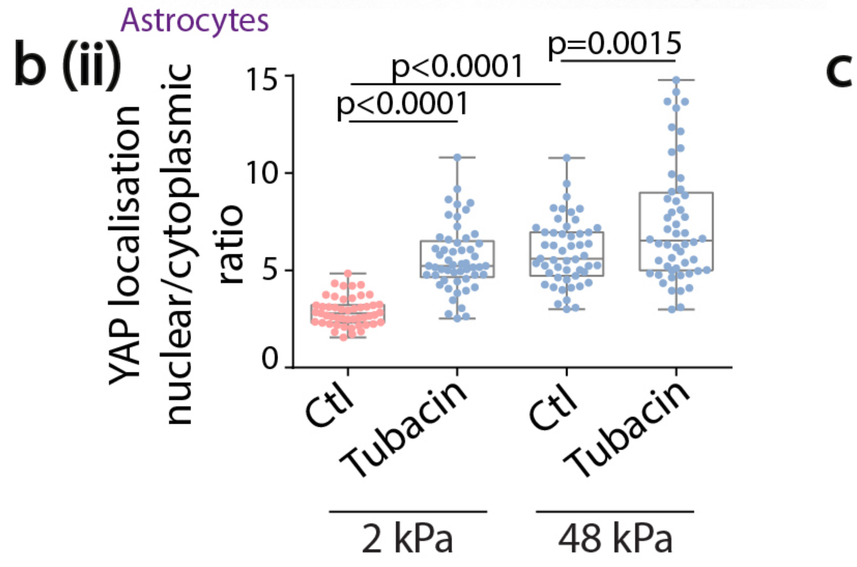

HUVECs

c (ii)

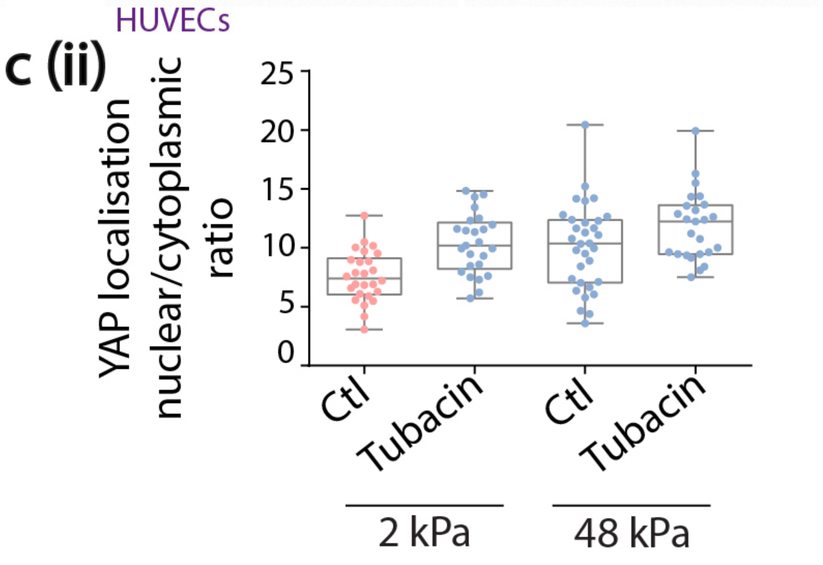

d (i)

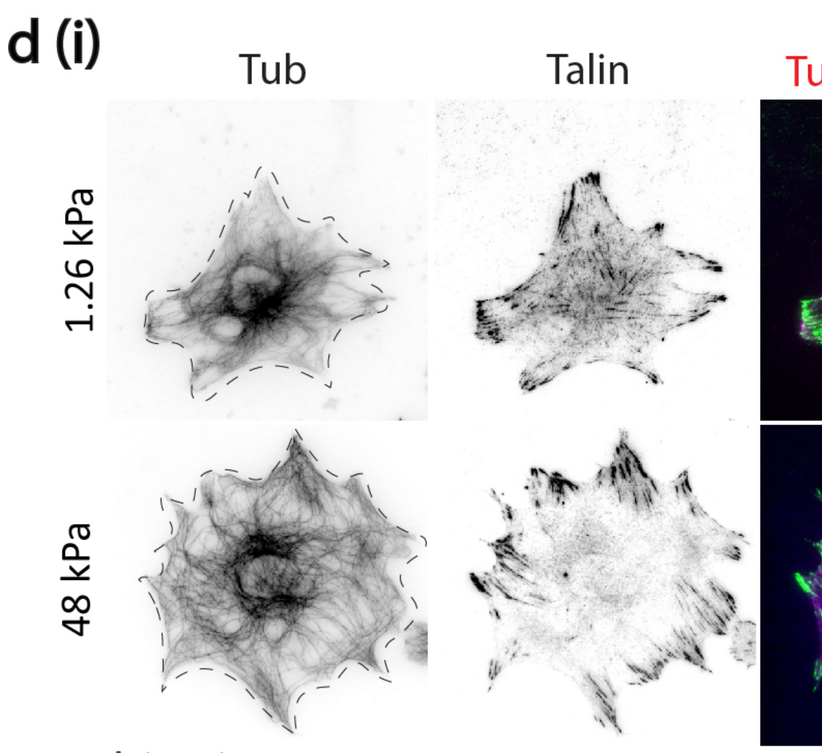

Astrocytes

d (ii)

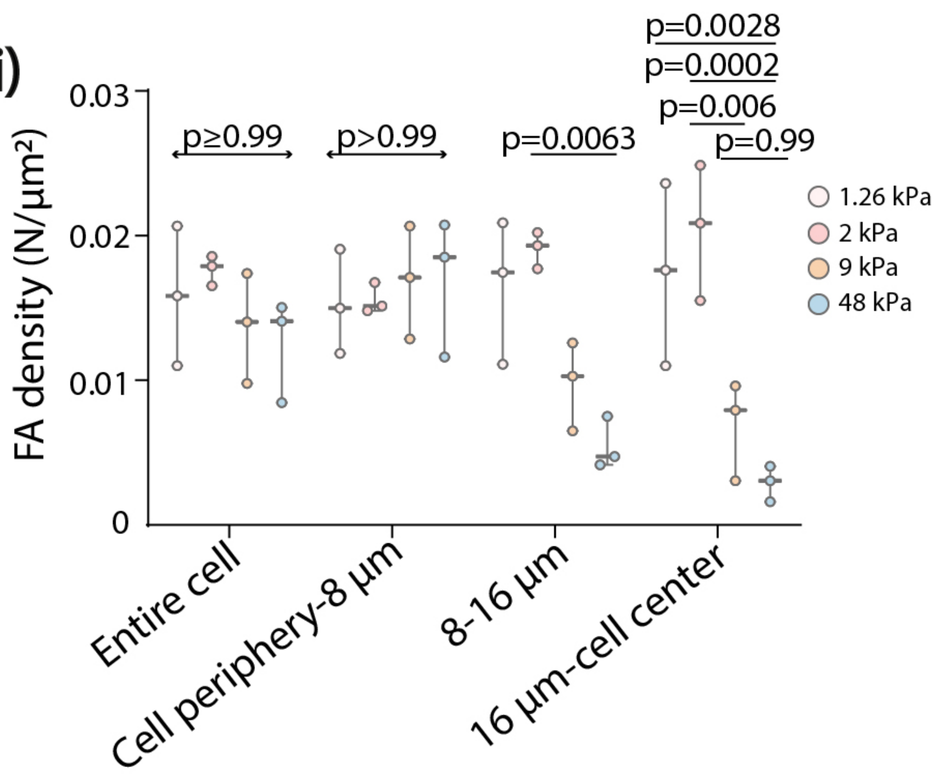

e (i)

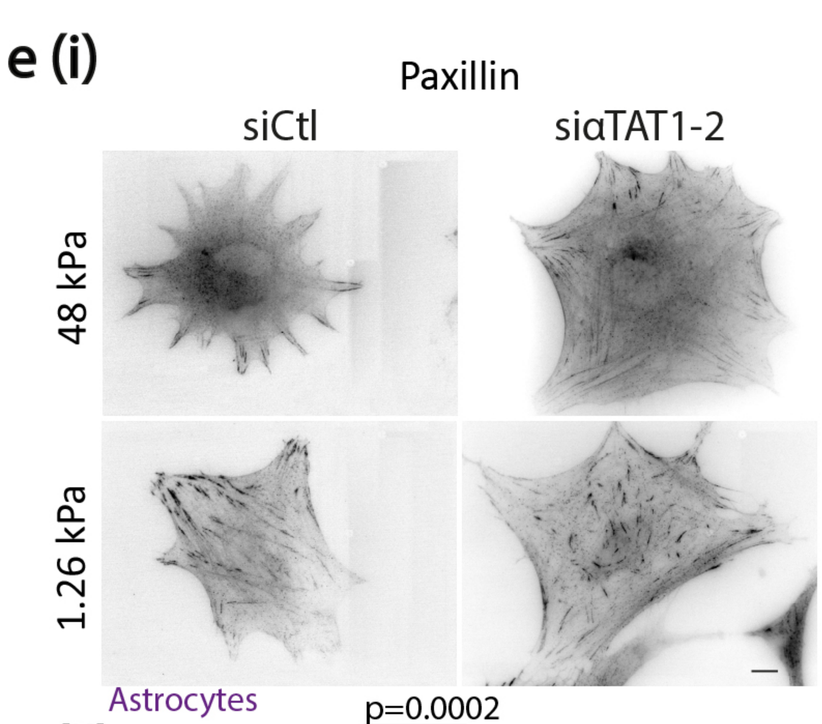

Astrocytes

e (ii)

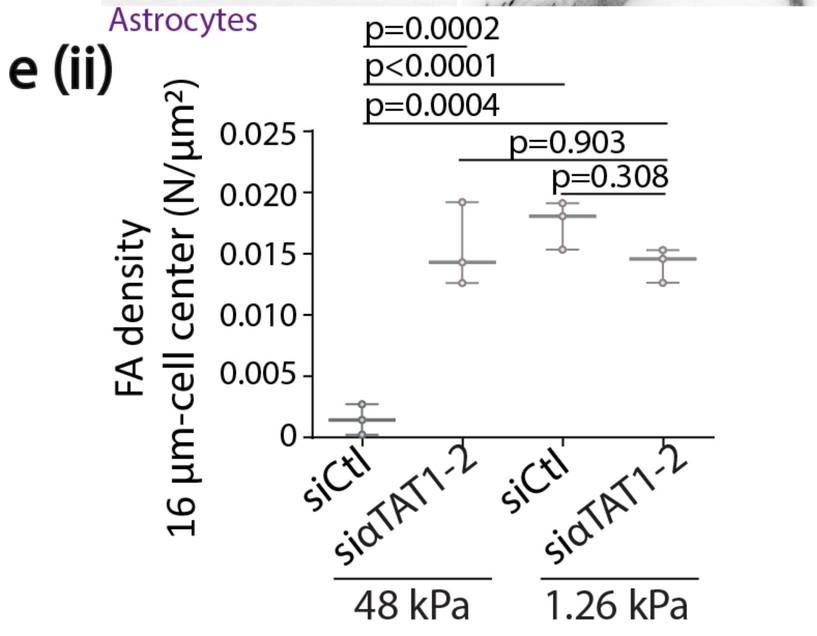

f (i)

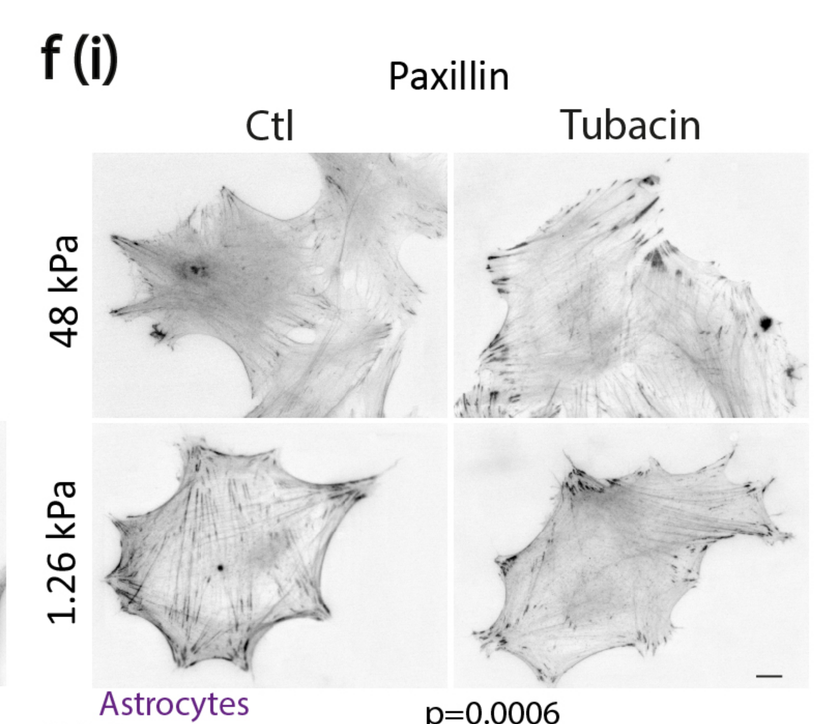

Astrocytes

f (ii)

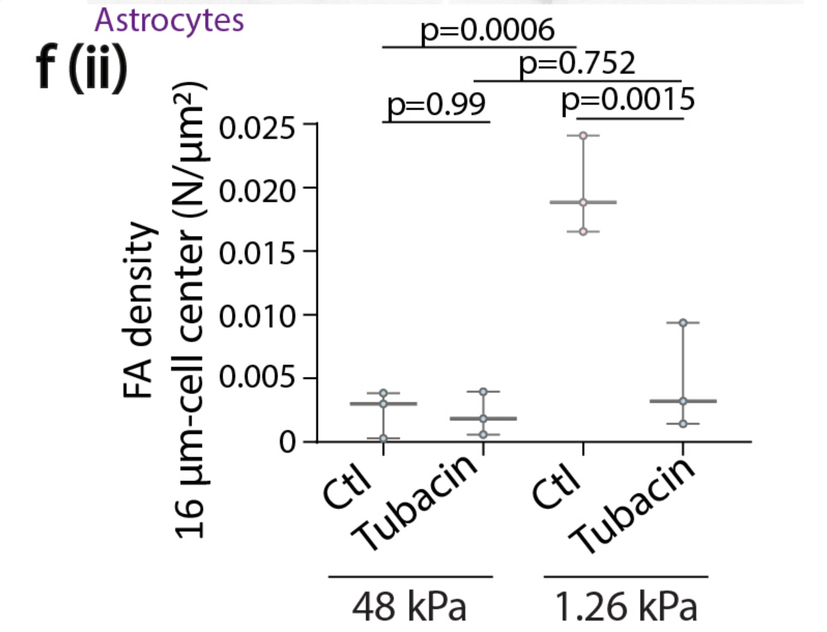

g

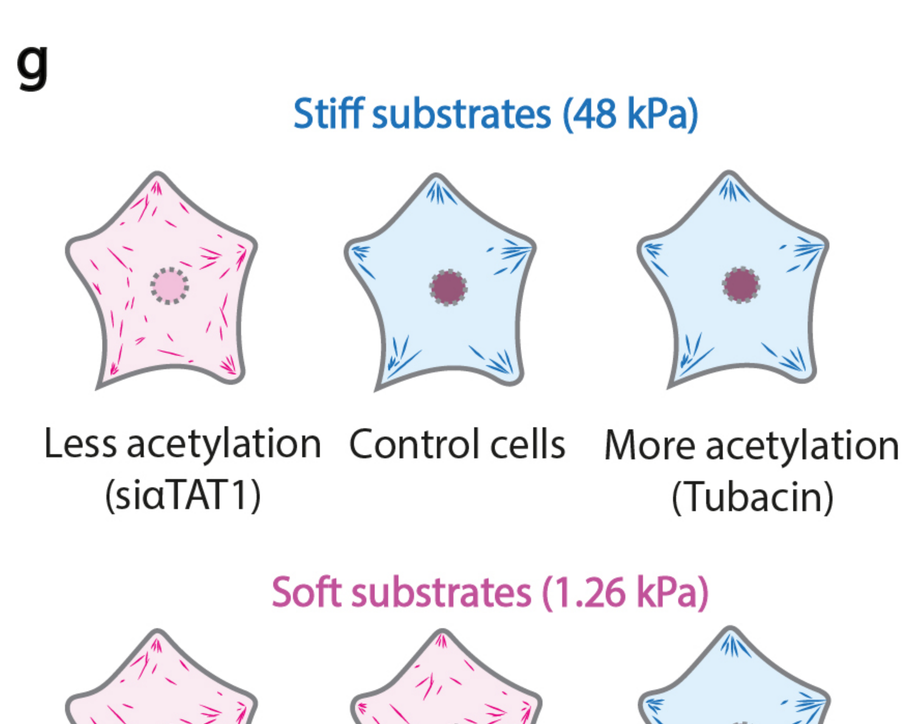

Figure 3

a (i)

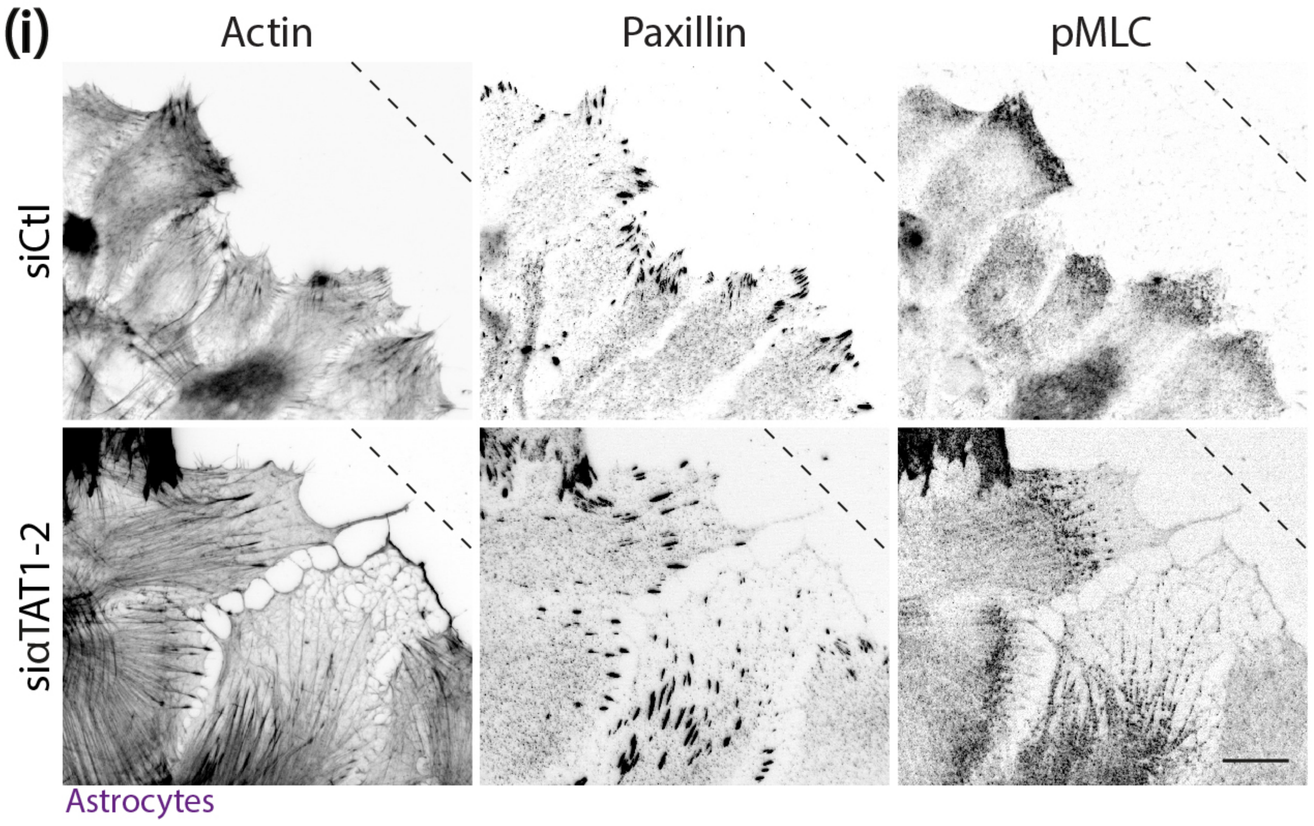

a (ii)

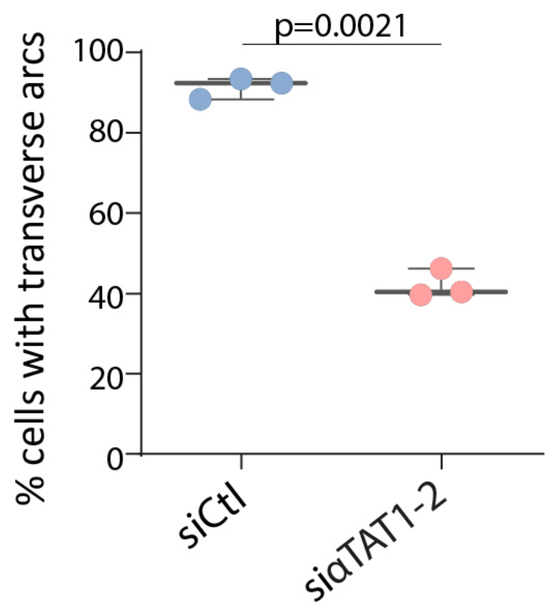

b

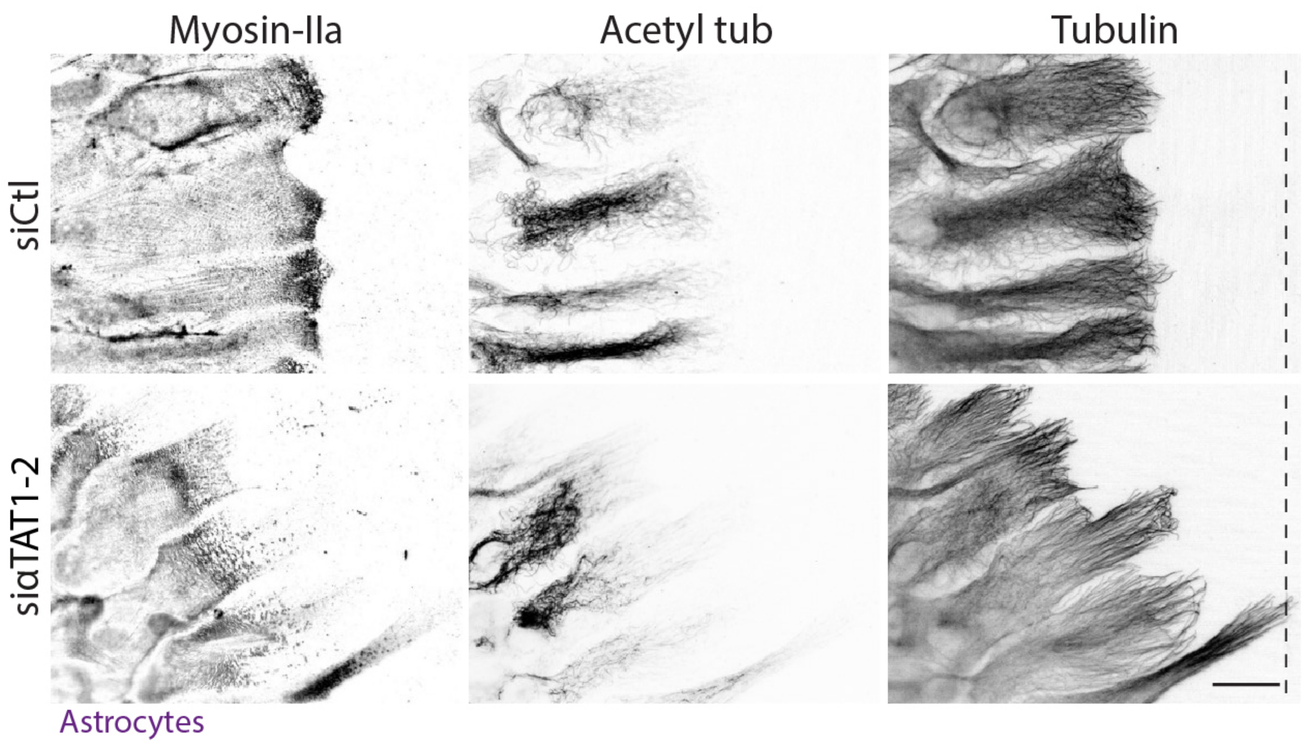

c

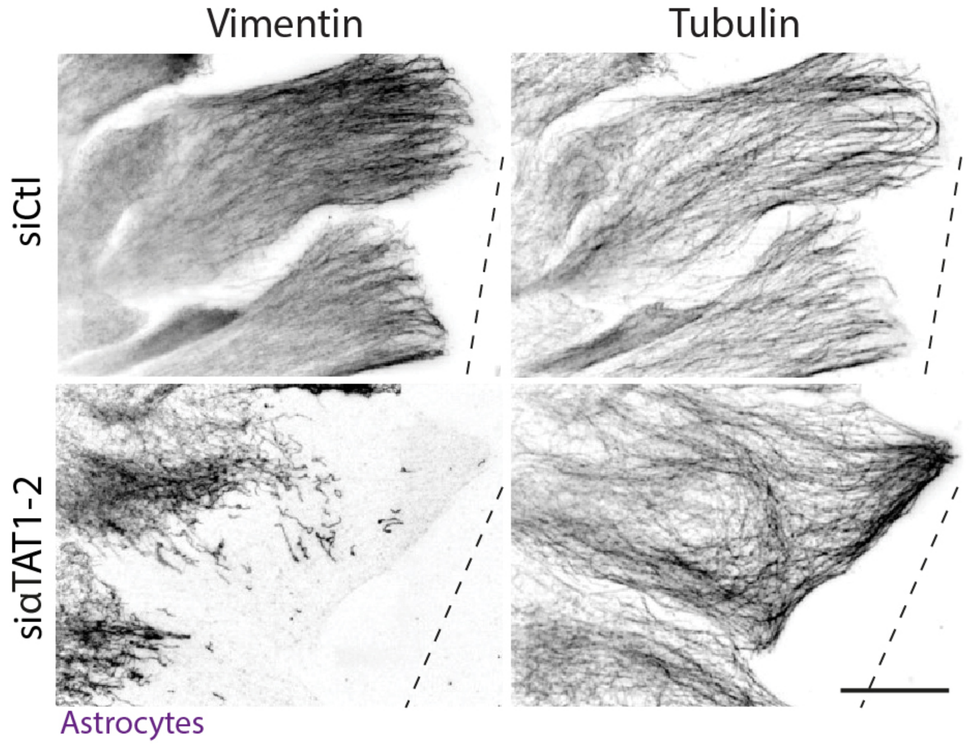

d

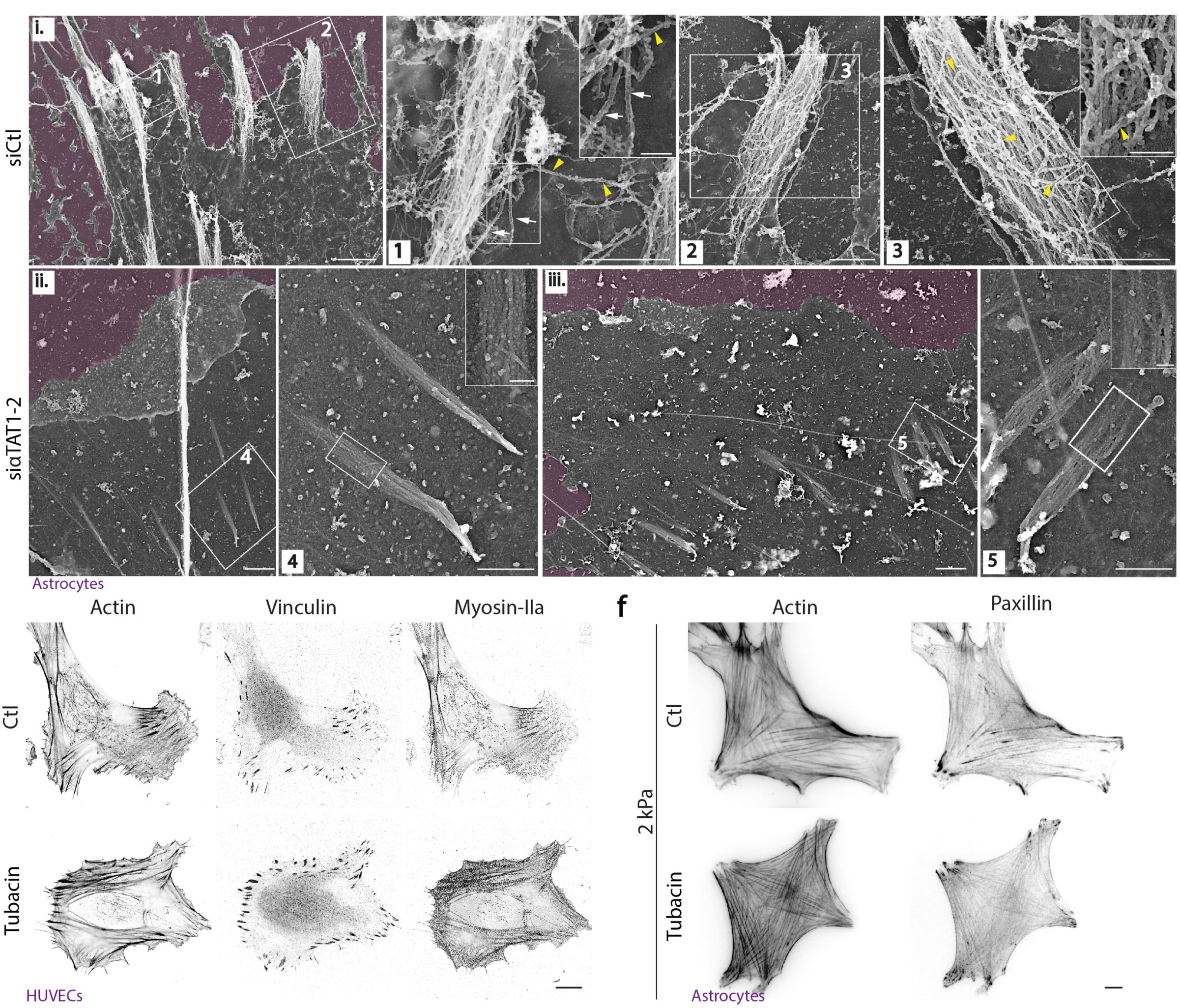

e

f

Figure 4

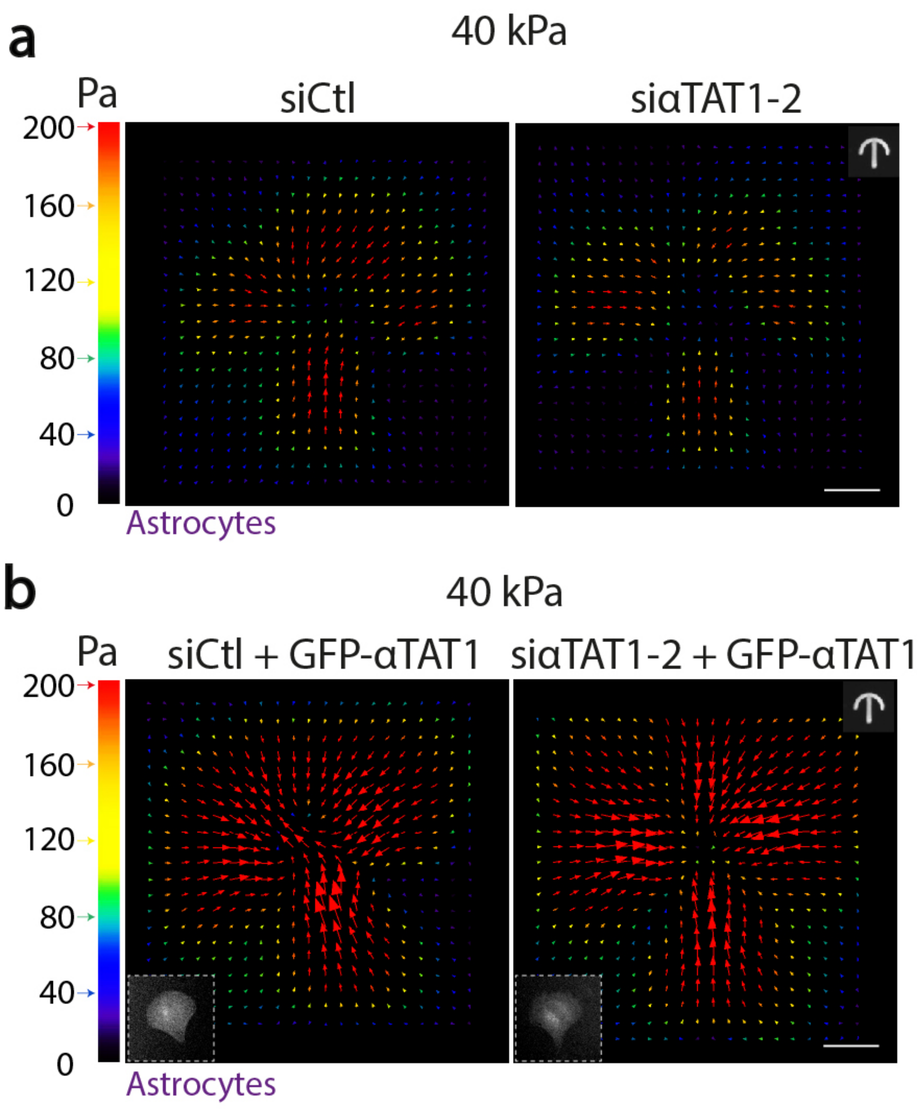
a
40 kPa
Pa
siCtl
siαTAT1-2
200
160
120
80
40
0
Astrocytes
b
40 kPa
Pa
siCtl + GFP-αTAT1
siαTAT1-2 + GFP-αTAT1
200
160
120
80
40
0
Astrocytes

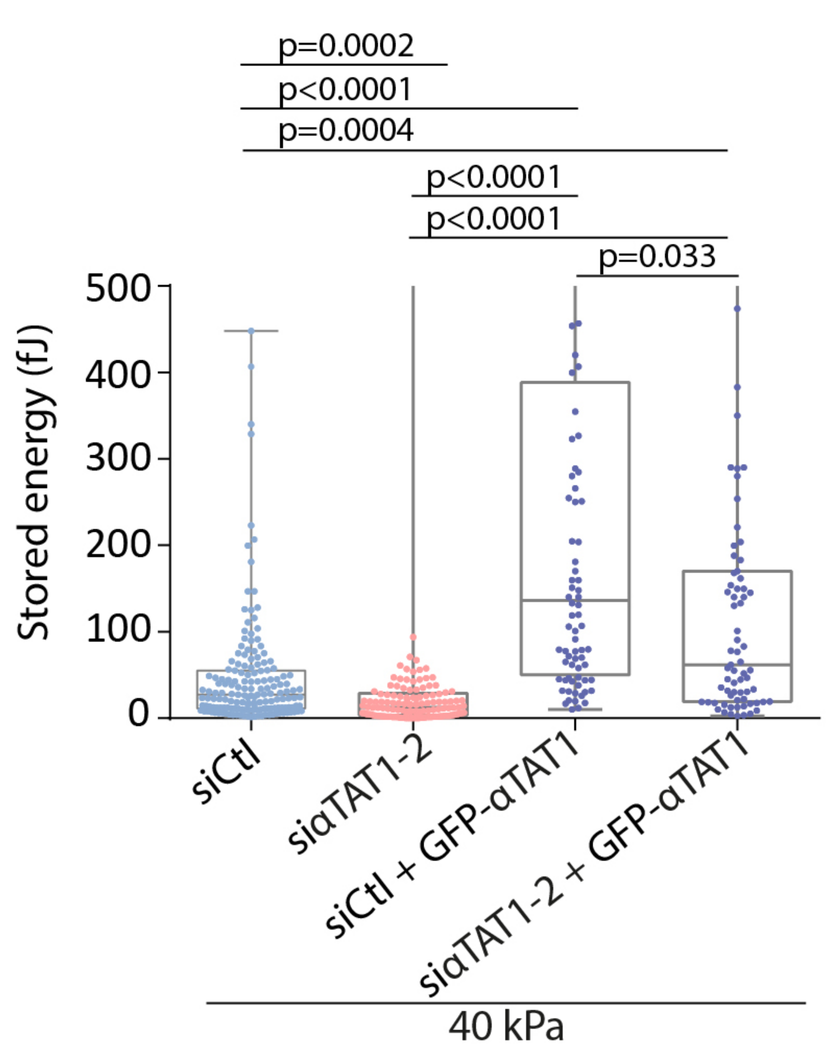
p=0.0002
p<0.0001
p=0.0004
p<0.0001
p<0.0001
p=0.033
Stored energy (fJ)
500
400
300
200
100
0
siCtl
siαTAT1-2
siCtl + GFP-αTAT1
siαTAT1-2 + GFP-αTAT1
40 kPa

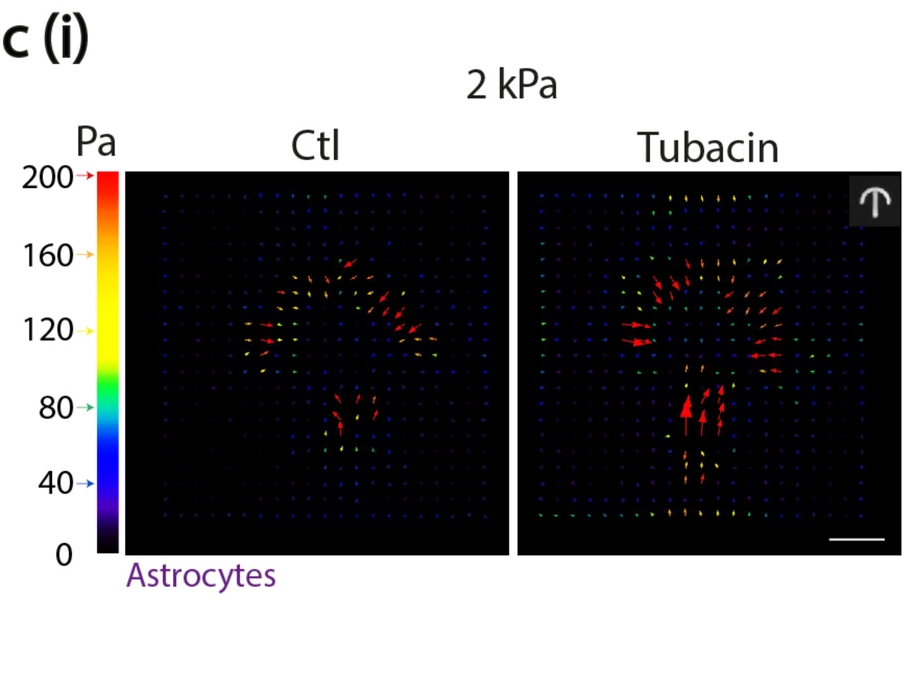
c (i)
2 kPa
Pa
Ctl
Tubacin
200
160
120
80
40
0
Astrocytes

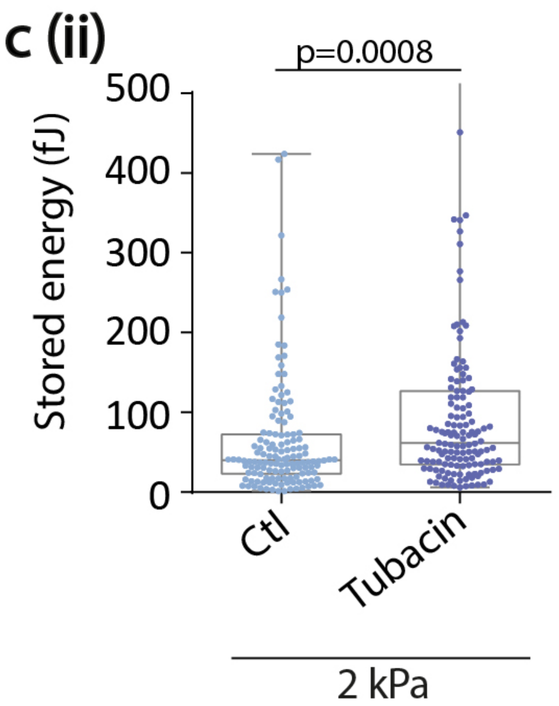
c (ii)
p=0.0008
Stored energy (fJ)
500
400
300
200
100
0
Ctl
Tubacin
2 kPa

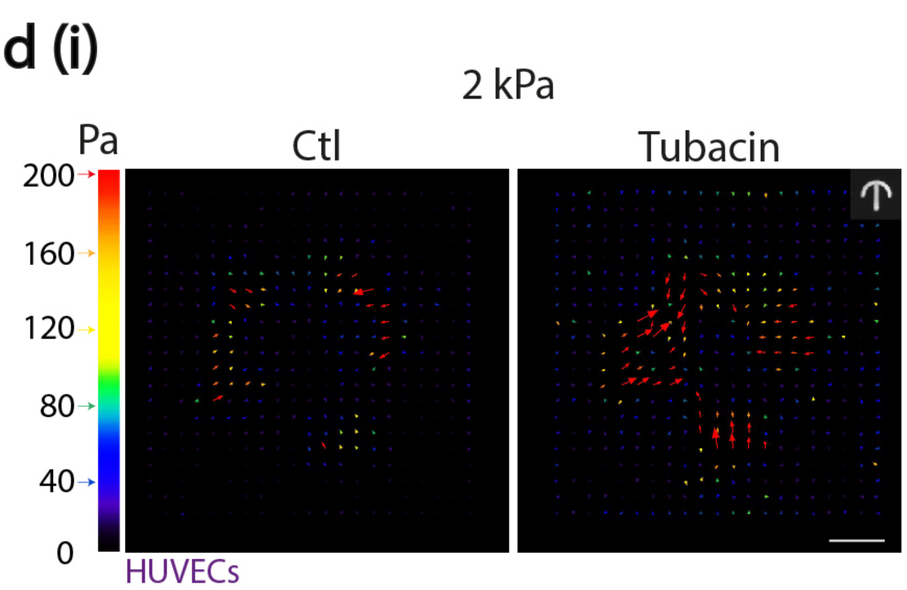
d (i)
2 kPa
Pa
Ctl
Tubacin
200
160
120
80
40
0
HUVECs

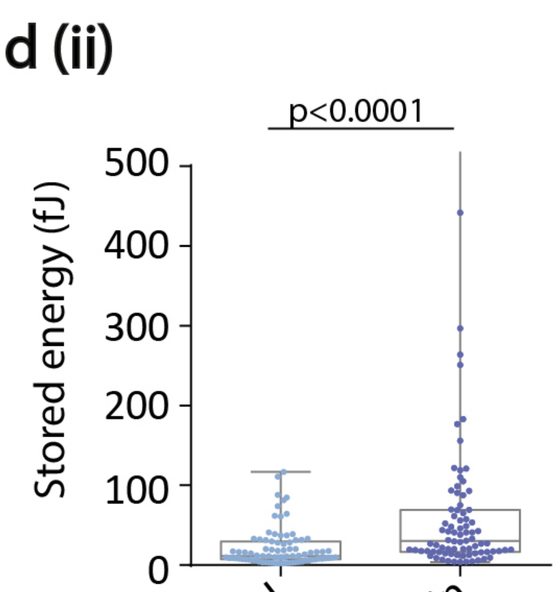
d (ii)
p<0.0001
Stored energy (fJ)
500
400
300
200
100
0
Ctl
Tubacin
2 kPa

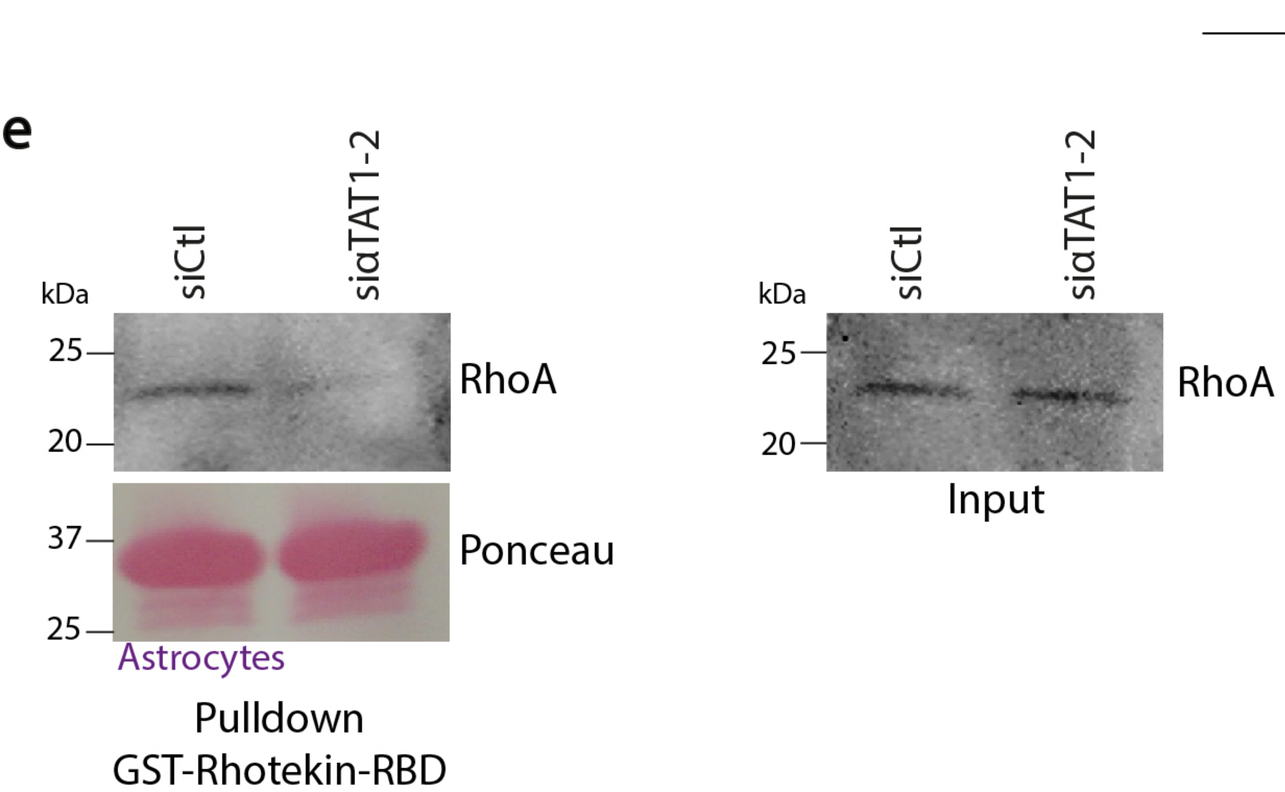
e
siCtl
siαTAT1-2
kDa
25
20
RhoA
37
25
Ponceau
Astrocytes
Pulldown
GST-Rhotekin-RBD
siCtl
siαTAT1-2
kDa
25
20
RhoA
Input

Figure 5

a (i)

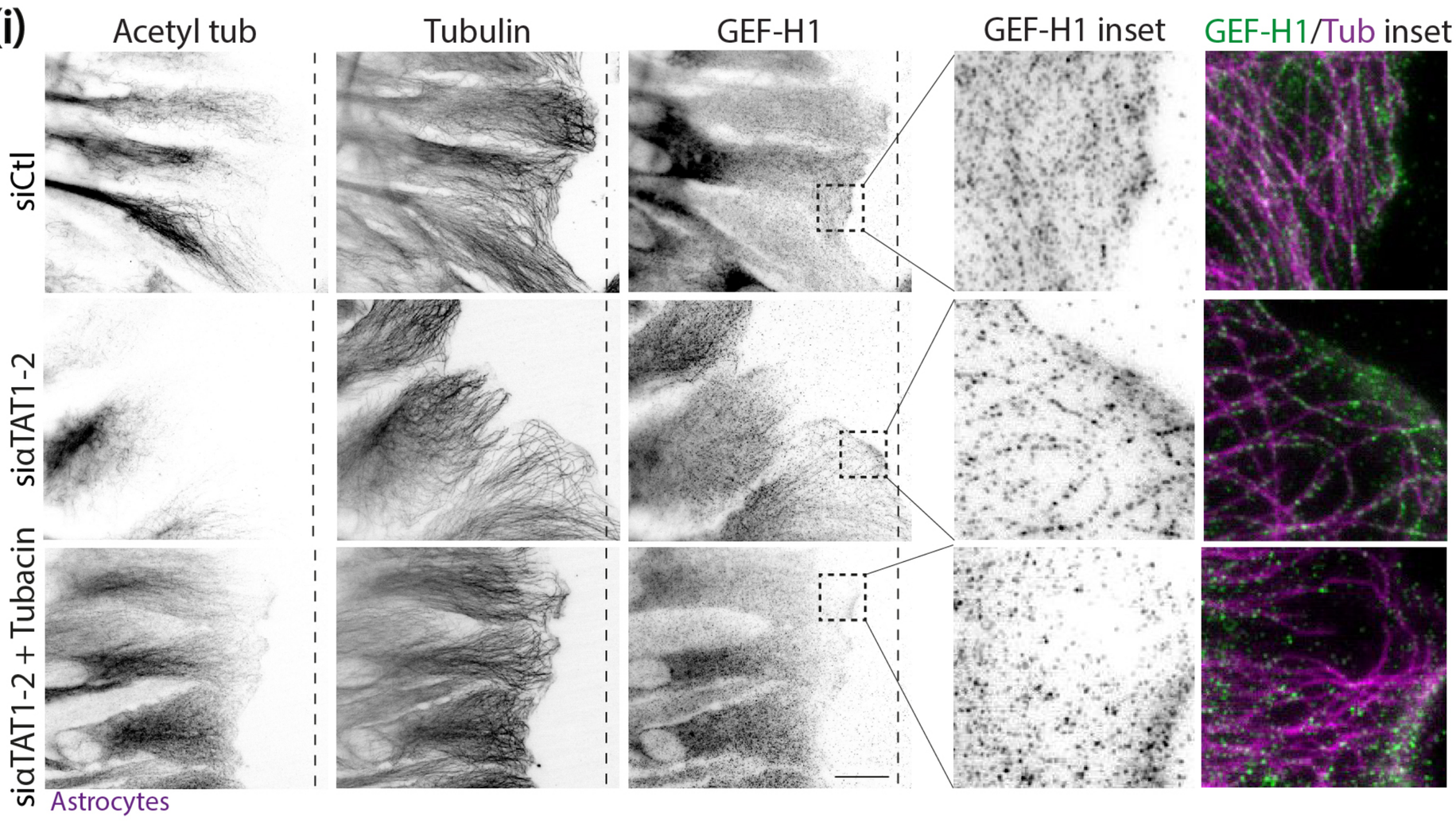

a (ii)

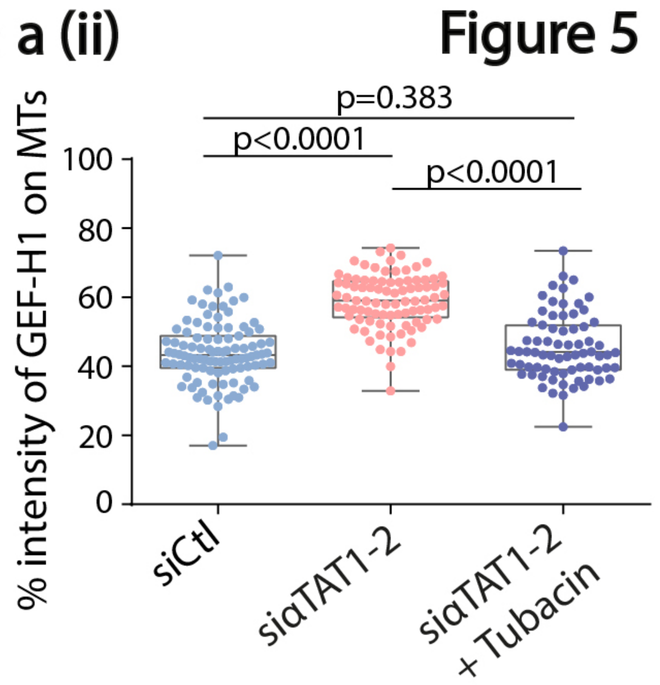

b (i)

b (ii)

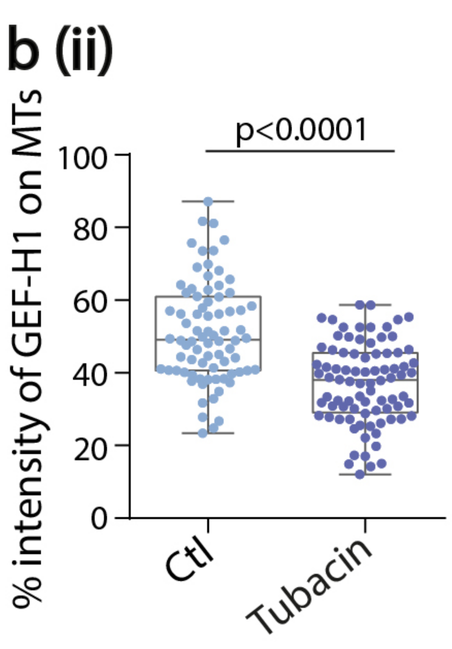

c

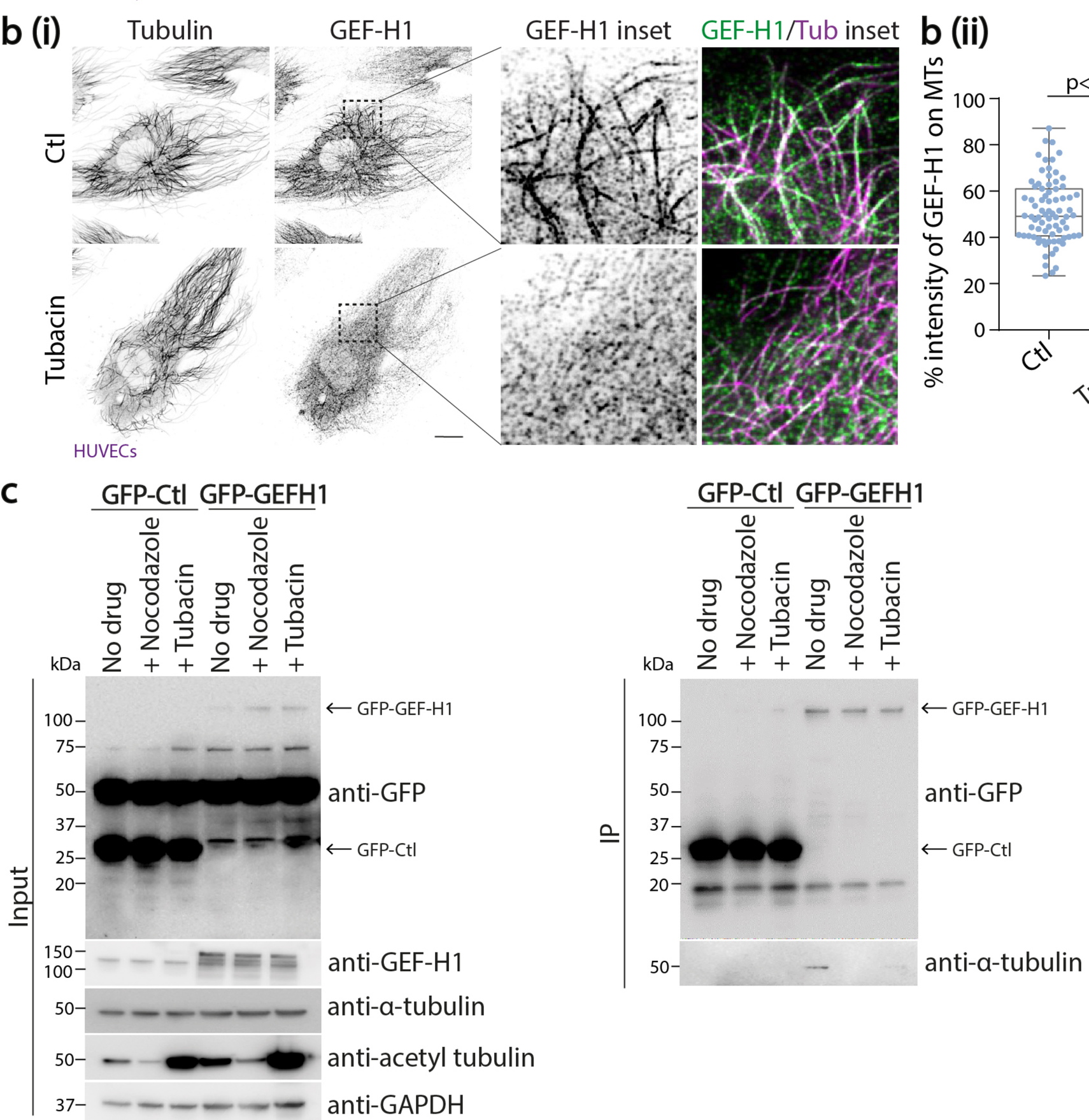

d (i)

d (ii)

Figure 6

a

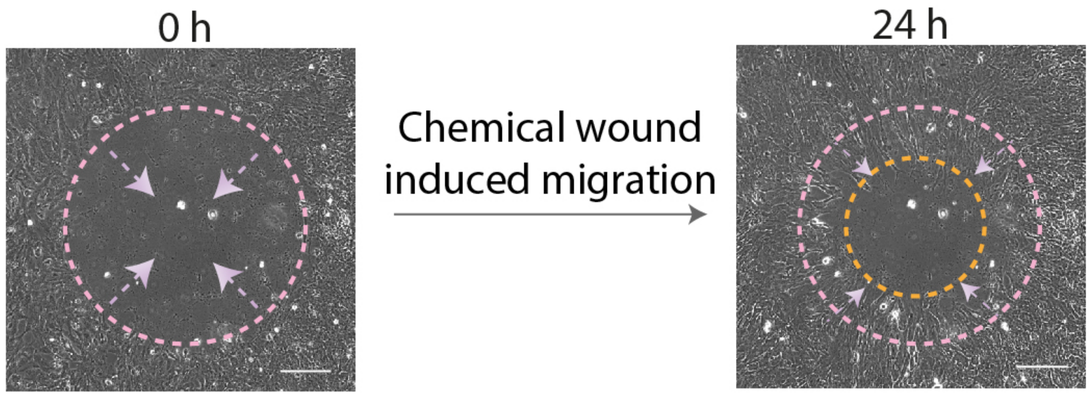

b (i)

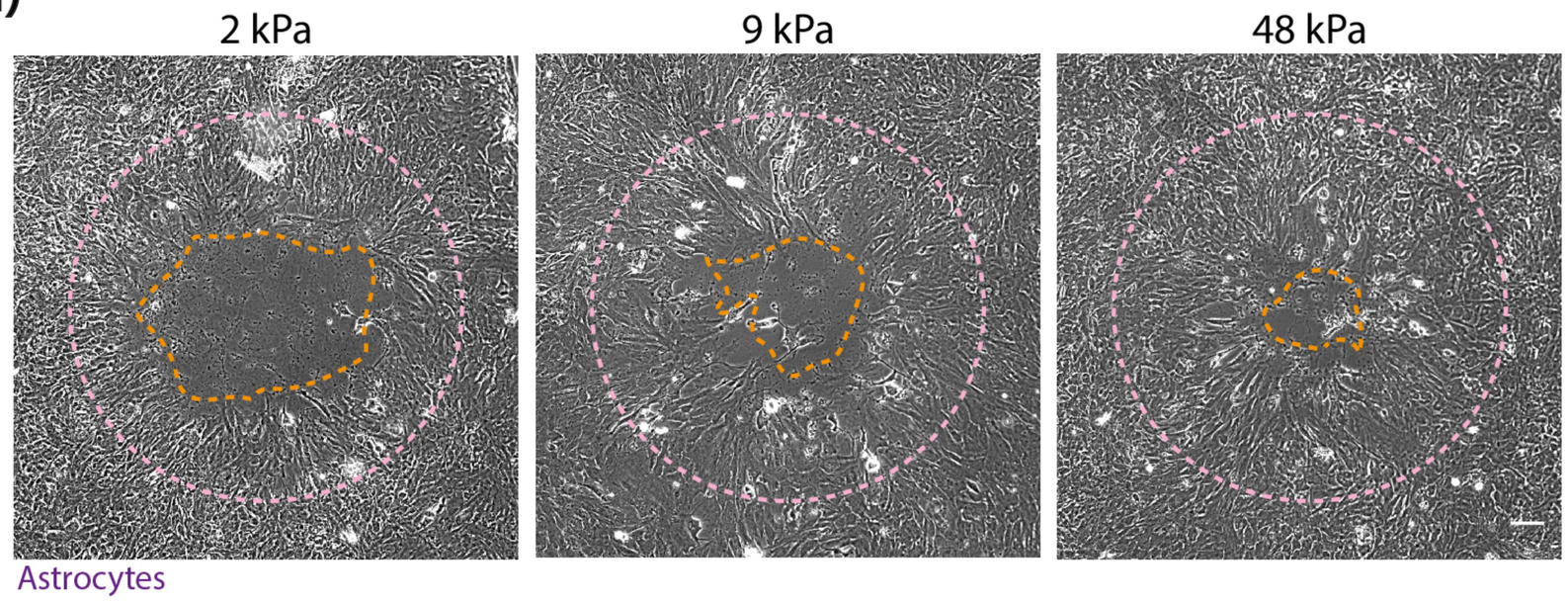

b (ii)

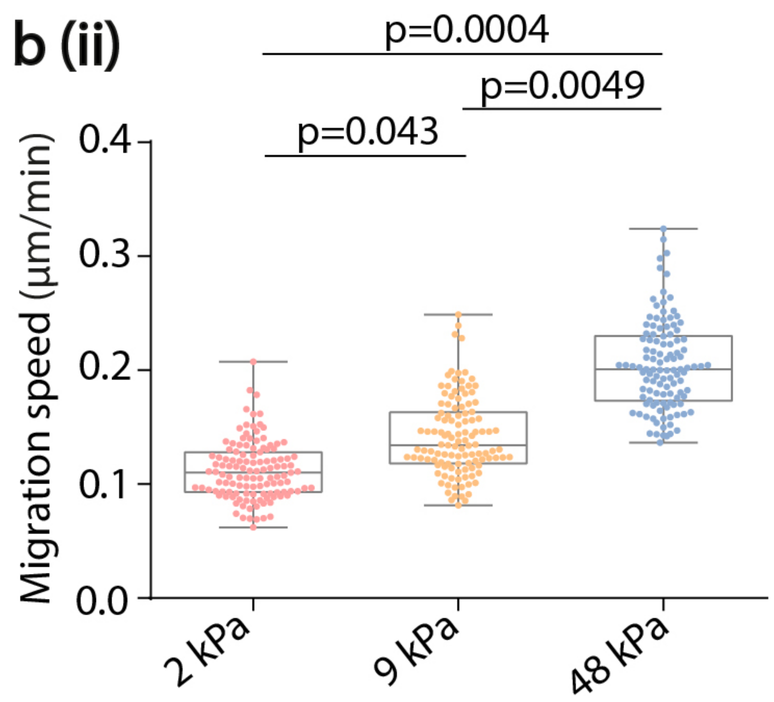

c (i)

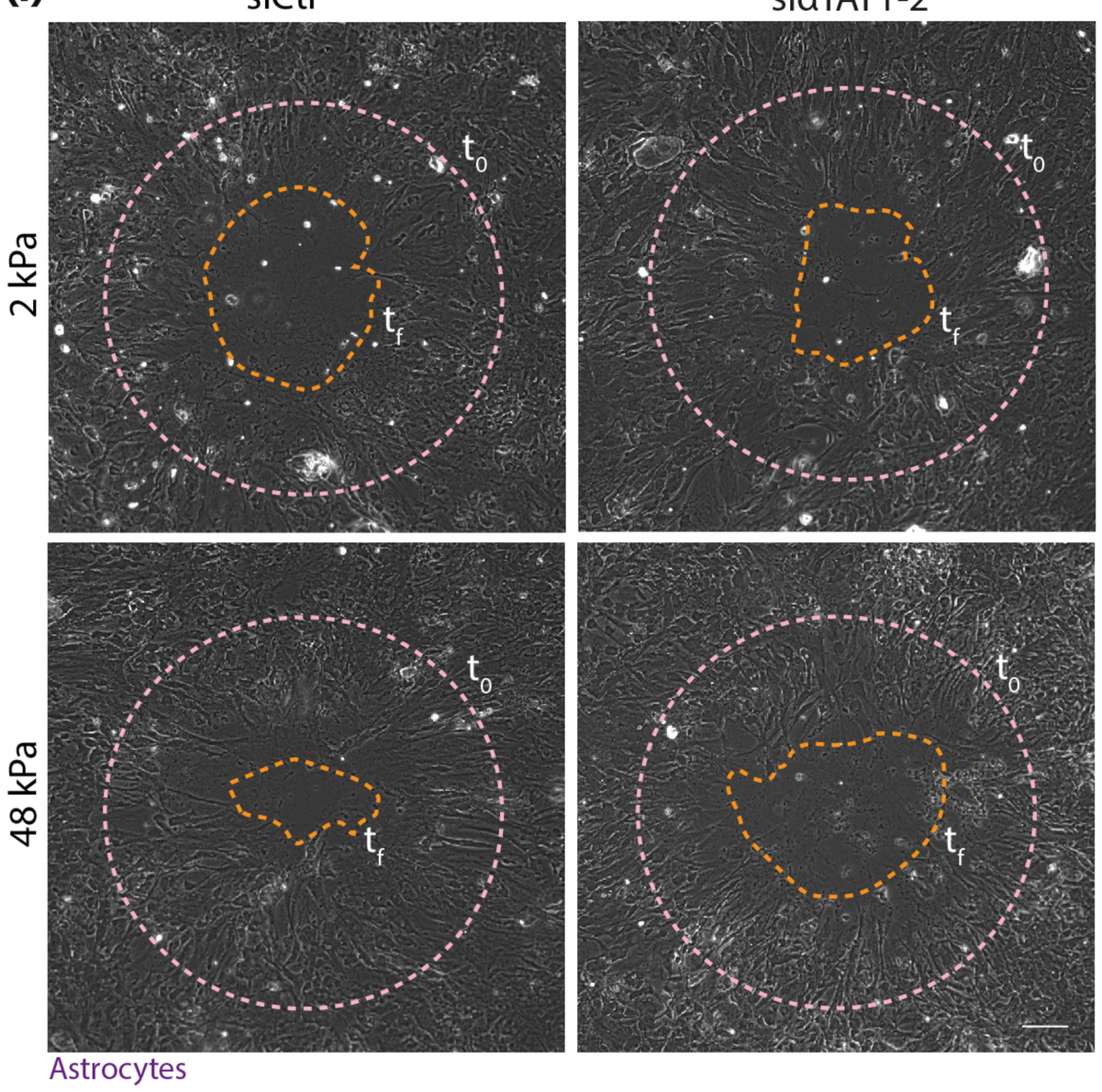

c (ii)

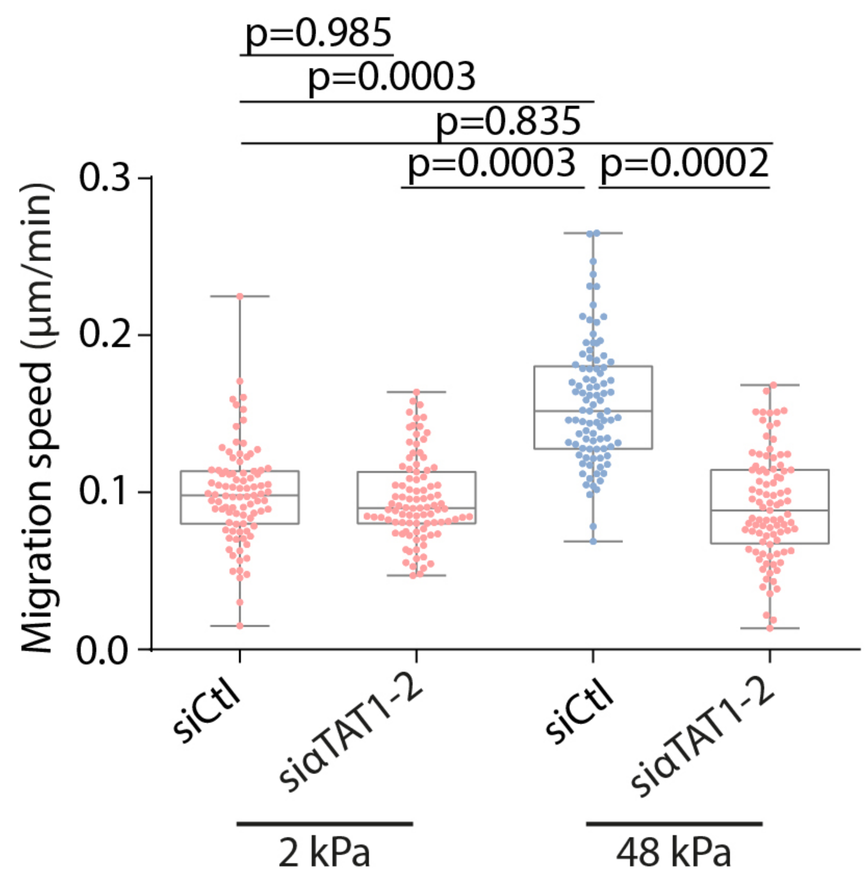

d

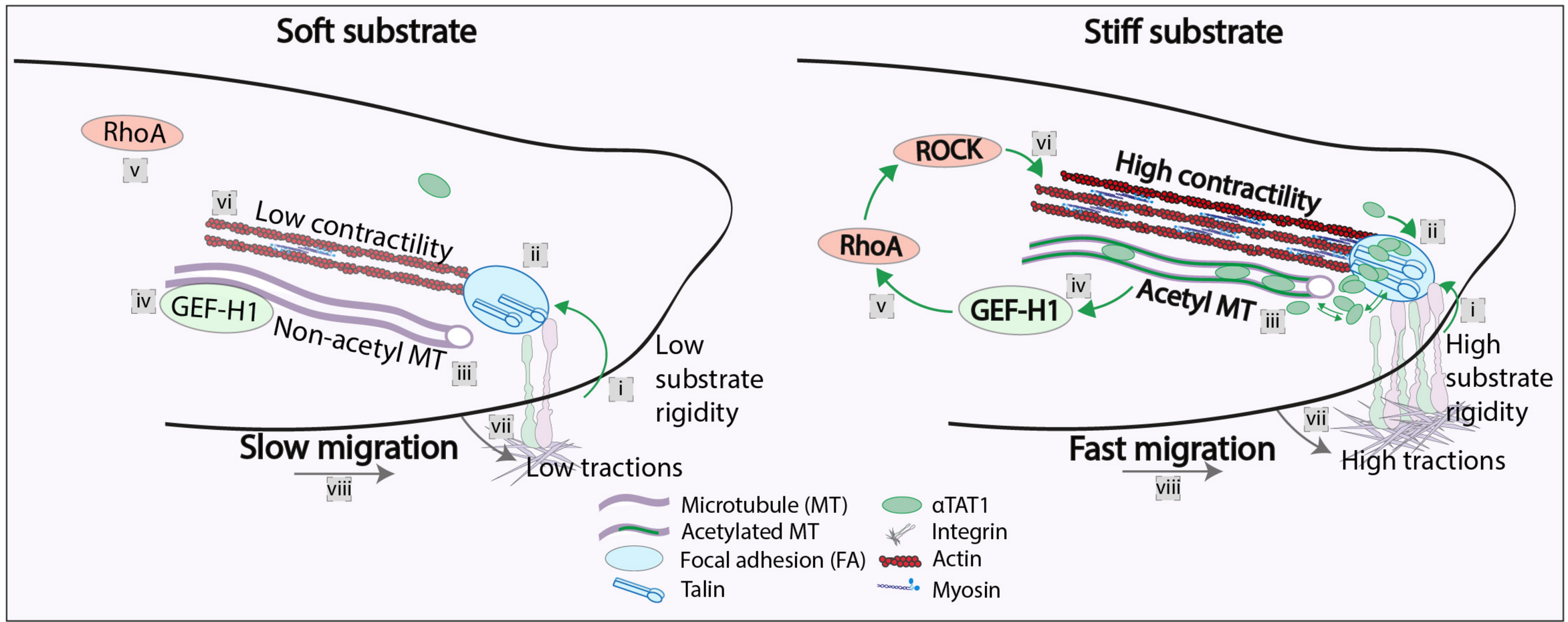

Extended Data Figure 1

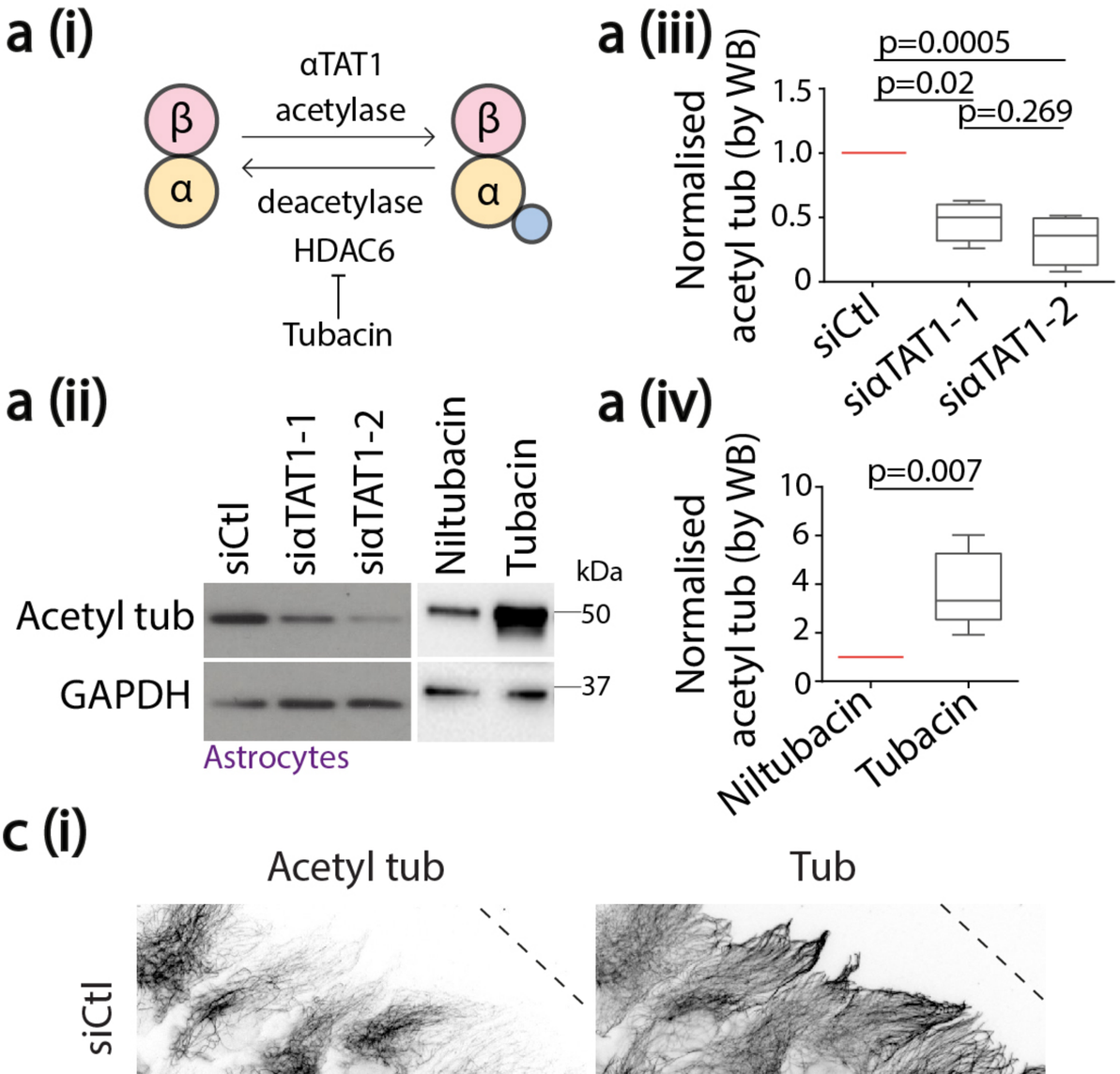

a (i)
RGD Ctl
RGD Peptide
Tub/acetyl tub/DAPI
Astrocytes
a (ii)
p=0.043
Ratio of acetyl tub/tub (immunofluorescence)
RGD Ctl
cRGD Peptide
b (i)
Ctl
MnCl2
Tub/acetyl tub/Paxillin
Astrocytes
b (ii)
p<0.0001
Ratio of acetyl tub/tub (immunofluorescence)
Ctl
MnCl2
c (i)
siCtl
siβ1
kDa
β1 integrin
Acetyl tub
GAPDH
150
50
37
Astrocytes
c (ii)
p=0.0015
Normalised β1 integrin (by western blot)
siCtl
siβ1 integrin
c (iii)
p=0.0097
Normalised acetyl tub (by western blot)
siCtl
siβ1 integrin
d (i)
siCtl
siβ1 integrin
Tub/acetyl tub//DAPI
Astrocytes
d (ii)
p<0.0001
Ratio of acetyl tub/tub (immunofluorescence)
siCtl
siβ1 integrin
e (i)
Ctl
Src kin 1
PF-562271 (FAK Inh)
Tub/acetyl tub/Paxillin
Astrocytes
e (ii)
Ratio of acetyl tub/tub (immunofluorescence)
Ctl
Src kin 1
PF-562271 (FAK Inh)
f (i)
Ctl
Src kin 1
kDa
Acetyl tub
GAPDH
50
37
48 kPa
f (ii)
p=0.0129
Normalised acetyl tub (by western blot)
Ctl
Src kin 1
48 kPa
g
#peptides/100 aa
Only in GFP-Ctl
log10(p-value)
log2(fold change GFP-αTAT1/GFP-Ctl)
ATAT1
Focal adhesion enriched
HSPA9
HSPA8
RPS3A
A1B
CLTC
RPL4
PPKAR2A
HAZ
RPL9
YWHAB
TLN1
TGB1
RPS15
CTNNB1
SCARB2
GIT2
ARHGEF7
#peptides/100 aa
Only in GFP-αTAT1
h
Normalised Talin levels (by pulldown)
p=0.0036
GST alone
GST-αTAT1
GST-PD
i
Normalised Talin levels (by pulldown)
p=0.0075
GFP Ctl
GFP-αTAT1
GFP-IP
j (i)
siCtl
siTalin1
kDa
Talin
GAPDH
250
37
Astrocytes
j (ii)
p=0.0007
Normalised Talin (by western blot)
siCtl
siTalin1
k
GFP-αTAT1 (TIRF)
Epifluorescence
Inset
Astrocytes
l
GFP-αTAT1 (TIRF)
mCherry-Vinculin
Ctl
+ Nocodazole
Astrocytes

Extended Data Figure 2

Extended Data Figure 3

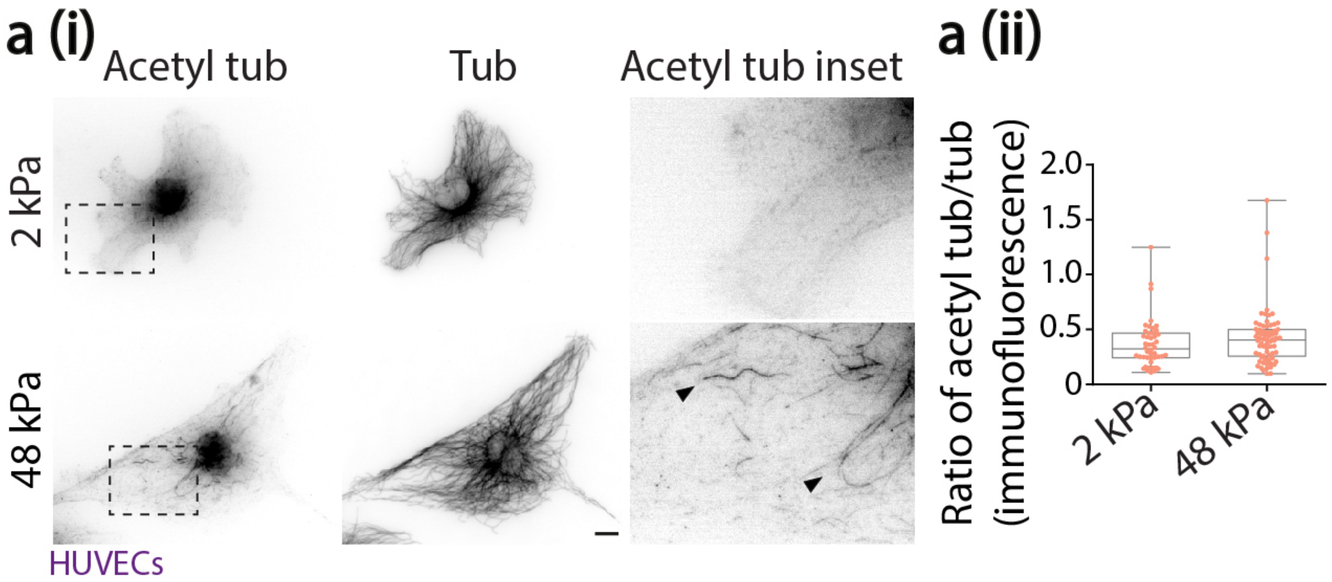

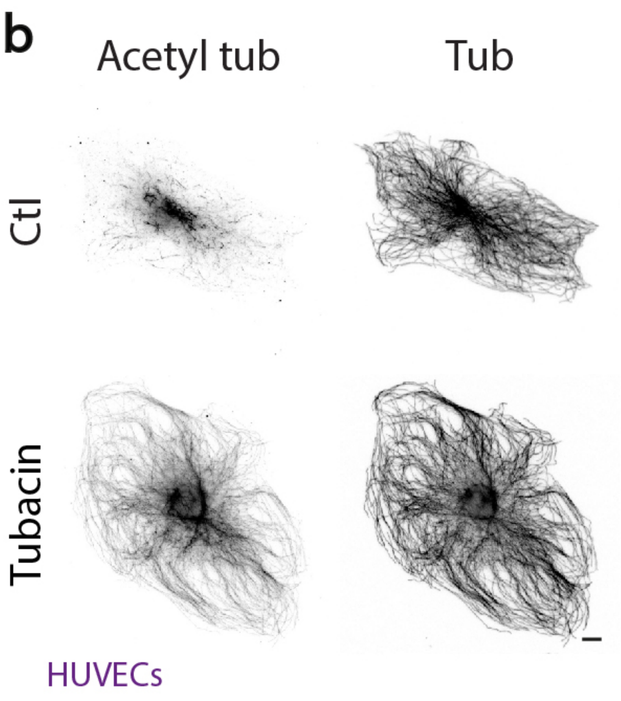

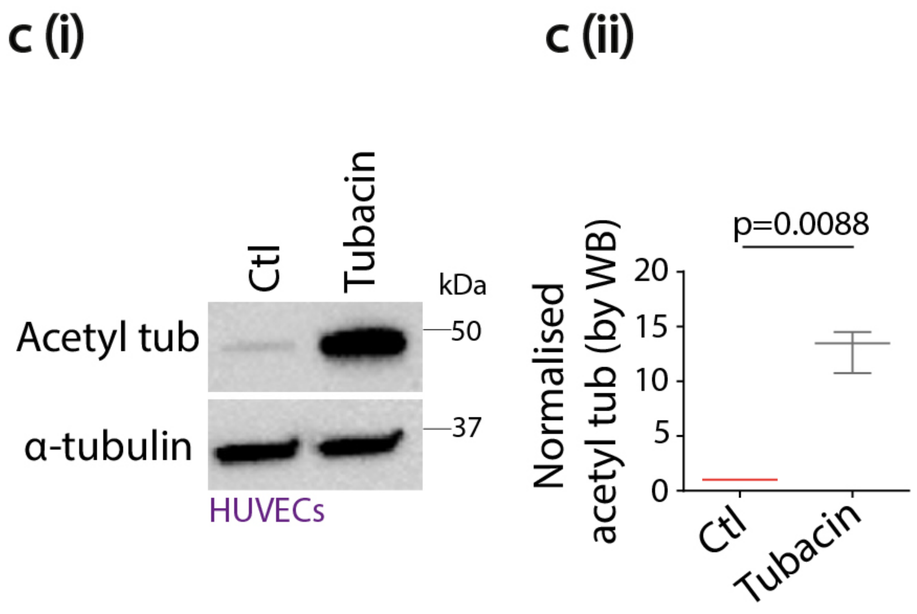

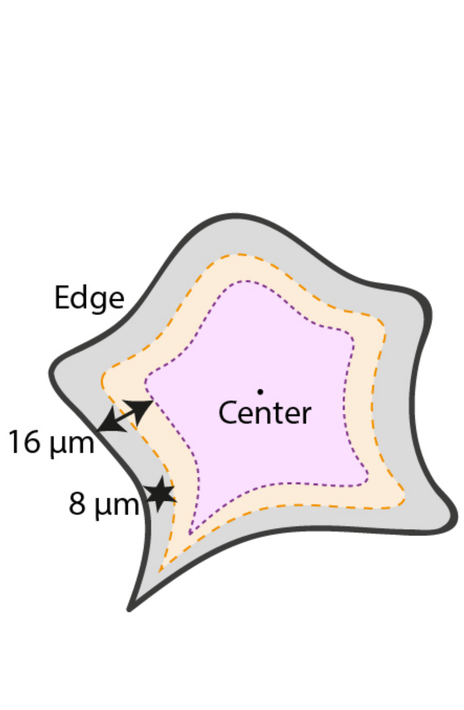

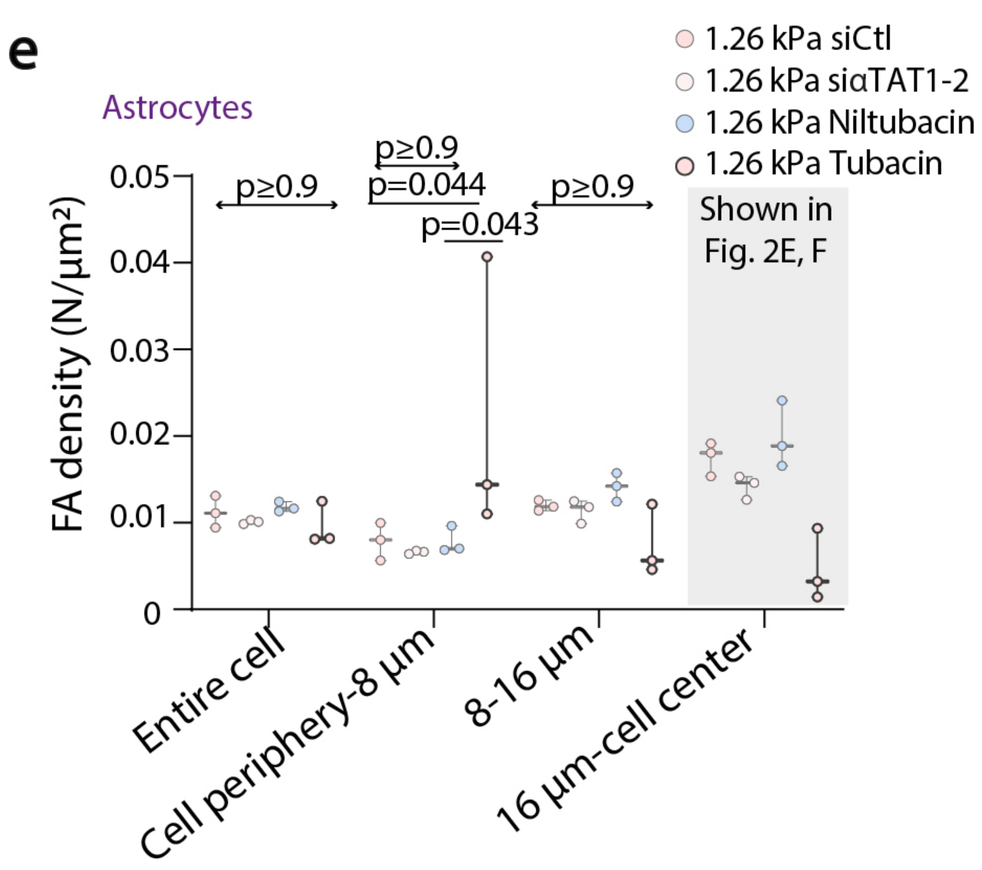

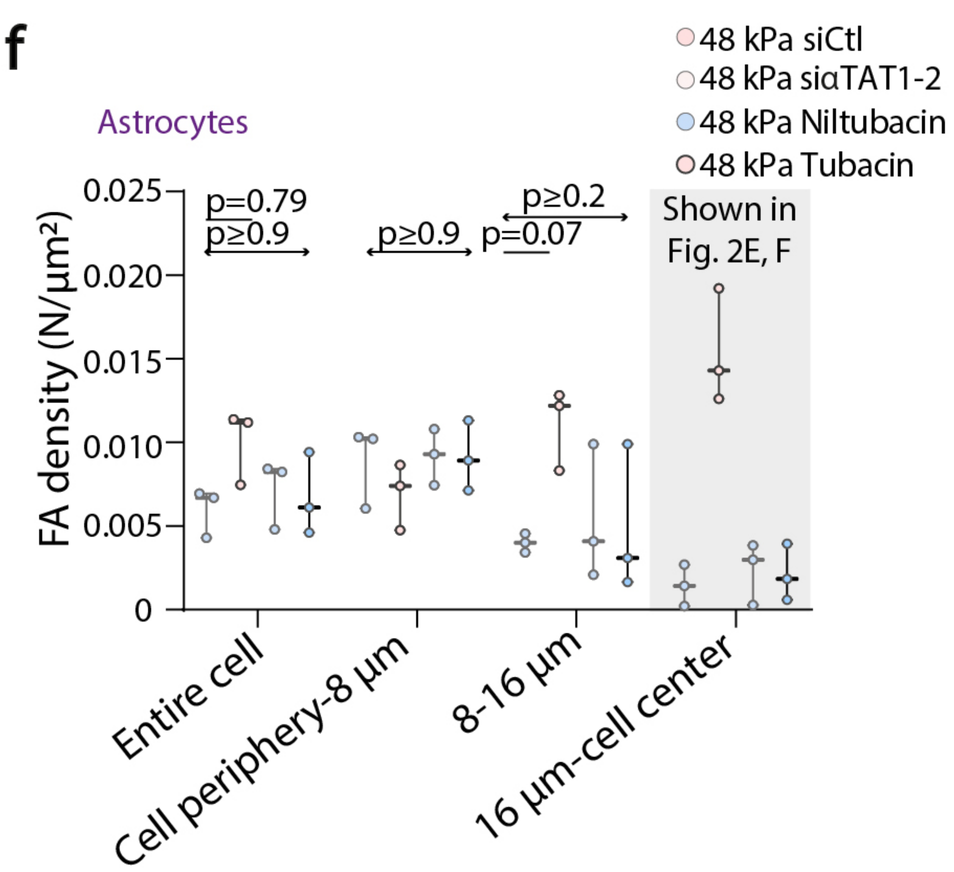

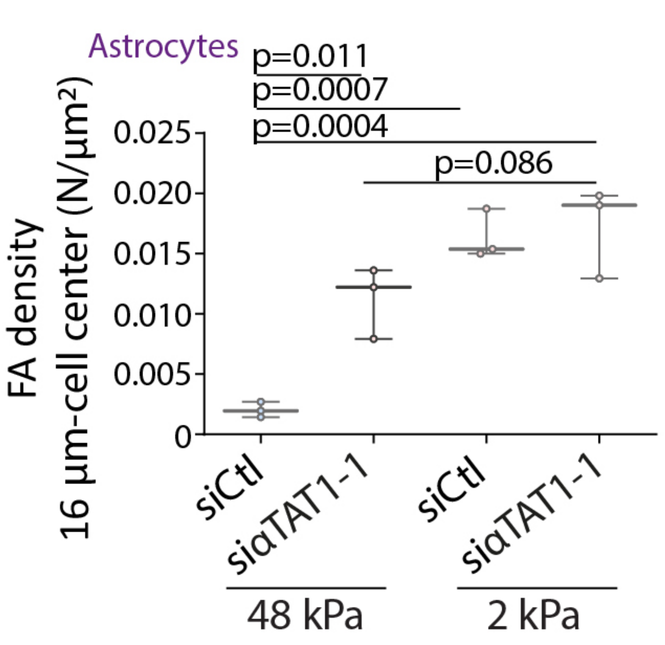

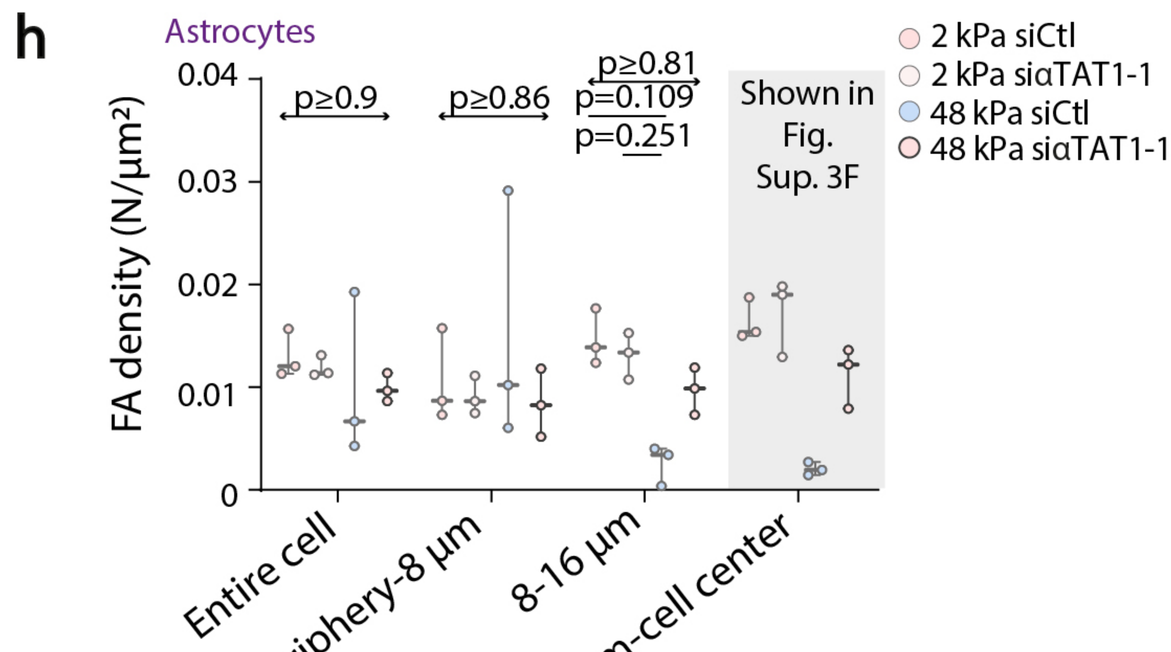

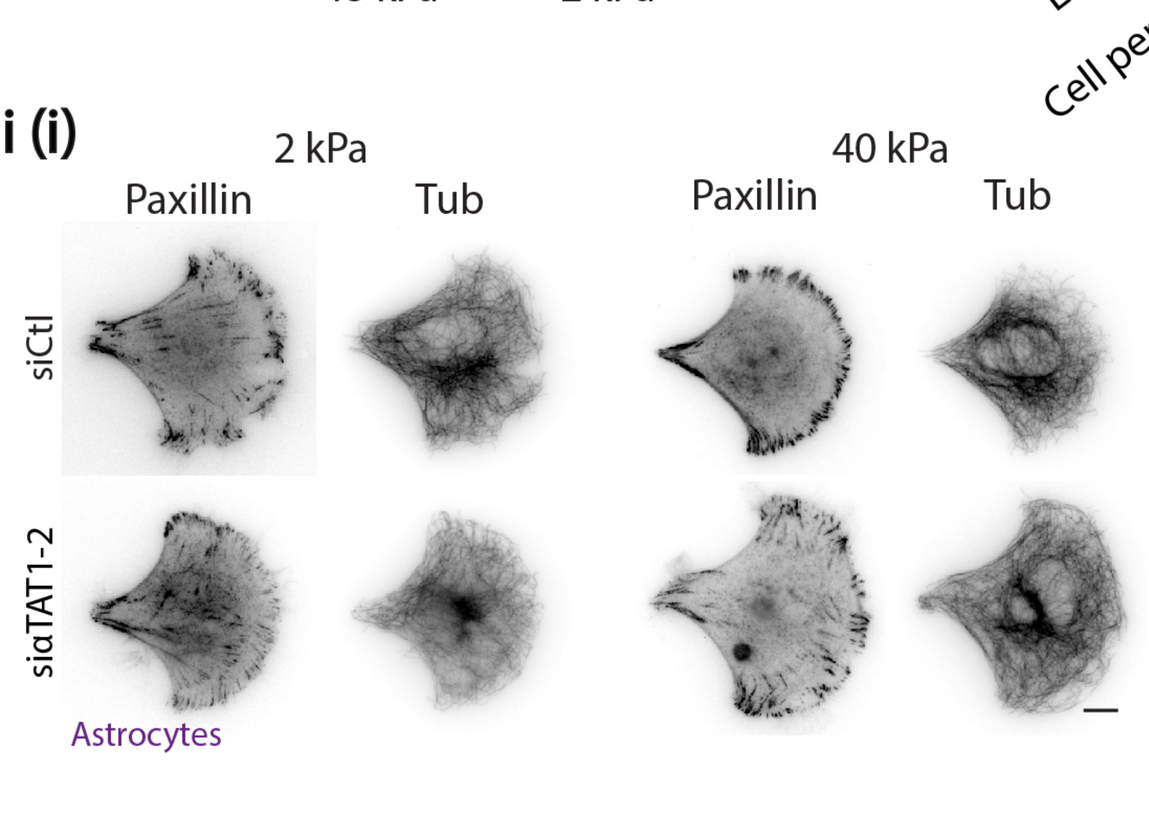

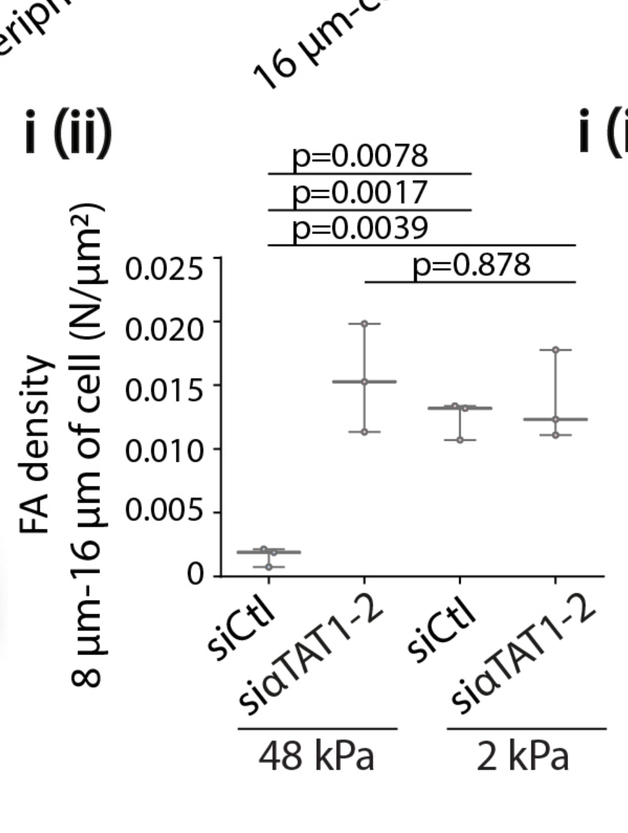

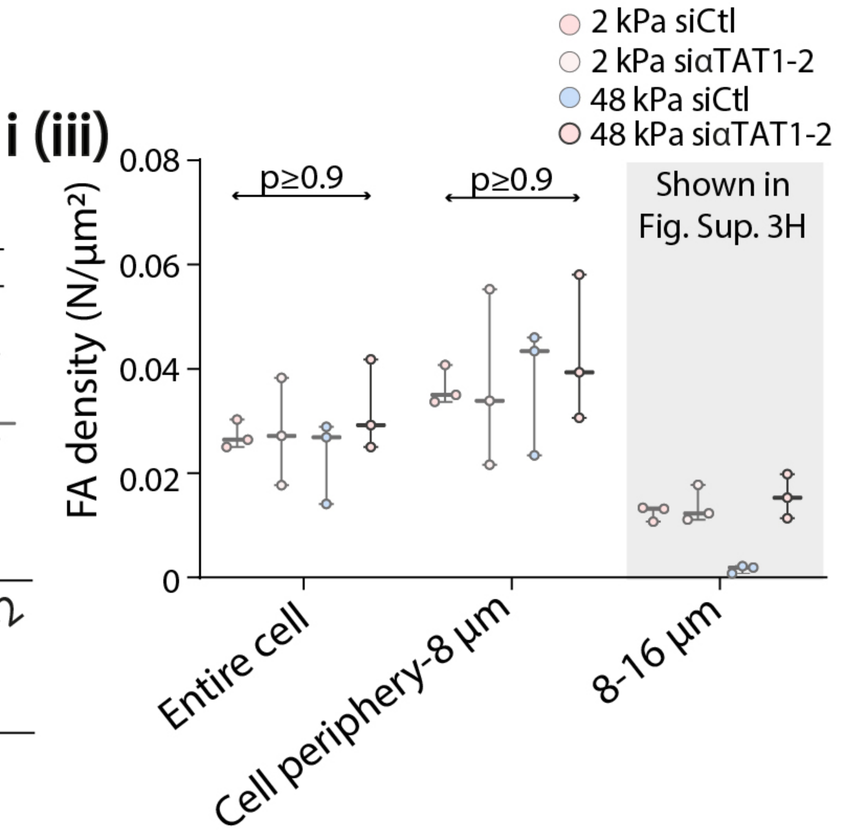

Extended Data Figure 4

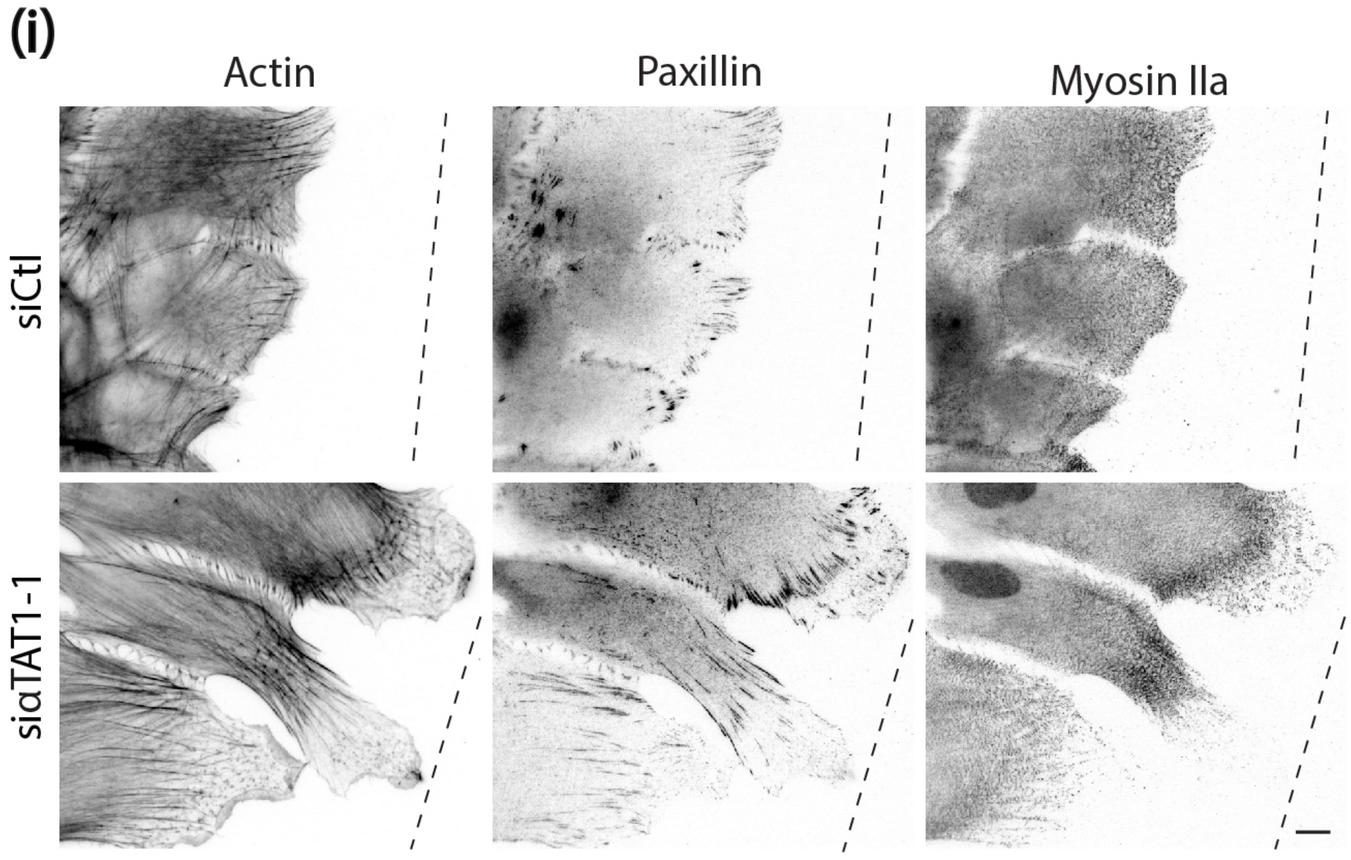

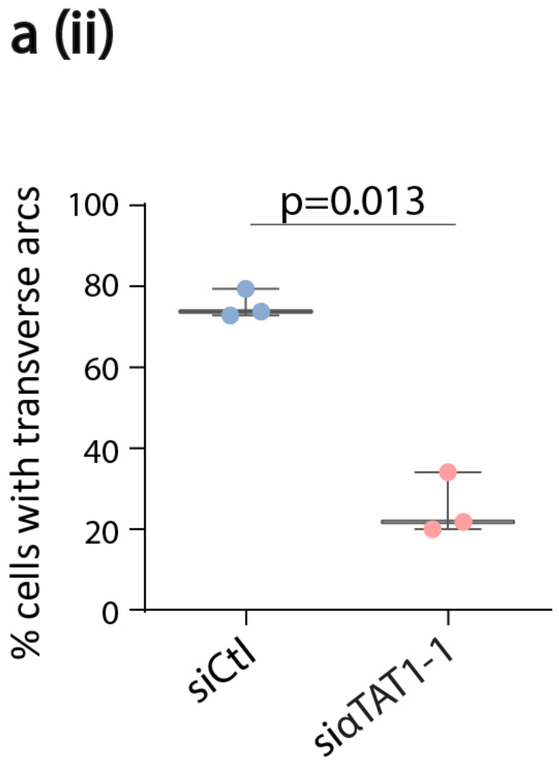

Extended Data Figure 5